BRUECKNER-HARTREE-FOCK METHODS FOR INVESTIGATING HEAVY-ION REACTIONS

by

Keith A. Sage

Department of Physics
Duke University

Date: 5/20/78

Approved:

R Y Cusson
Ronald Y. Cusson, Supervisor

E G. Bilpuch

Frank DeLucia

J. A. Aher.

A dissertation submitted in partial fulfillment of the requirements for the degree of Doctor of Philosophy in the Department of Physics in the Graduate School of Duke University

1978

E

ABSTRACT

(Nuclear Physics)

BRUECKNER-HARTREE-FOCK METHODS FOR

INVESTIGATING HEAVY-ION REACTIONS

by

Keith A. Sage

Department of Physics
Duke University

Date: 5/22/78

Approved:

R Y Cusson
Ronald Y. Cusson, Supervisor

E G Bilpuch

Frank DeLucia

J. A.Ither

An abstract of a dissertation submitted in partial fulfillment of the requirements for the degree of Doctor of Philosophy in the Department of Physics in the Graduate School of Duke University

1978

BRUECKNER-HARTREE-FOCK METHODS FOR

INVESTIGATING HEAVY-ION REACTIONS

by

Keith A. Sage

Brueckner-Hartree-Fock techniques are applied to the calculation of the heavy-ion interaction potential for six reactions involving combinations of ^{4}He, ^{12}C, ^{14}C, and ^{16}O. The K-matrix model for the Hamiltonian is developed and its parametrisation discussed. A self-consistent method for calculating the spin-orbit interaction is introduced and tested by fitting the nuclear properties over a wide range of nuclei. The cluster potential energy for each reaction studied is found first in an adiabatic approximation and then by using a new overlap technique in a sudden approximation. The formalism for this overlap method, taken from the work of Lowdin, is discussed in detail. The results of the overlap calculation point out the importance of shell effects in the heavy-ion potential. Comparison of the calculated adiabatic and sudden cluster potentials with the work of other authors is discussed.

The use of the adiabatic and sudden potentials as the real part of the optical potential is discussed in detail. Attempts to fit experimental data for $^{12}C + {}^{4}He$ elastic scattering meet with little success, but it is shown that the $^{16}O + {}^{16}O$ adiabatic potential should be useful in the optical model fitting of $^{16}O + {}^{16}O$ elastic scattering data. The heavy-ion optical potentials obtained here are compared with the optical potentials calculated by other authors.

ACKNOWLEDGEMENTS

I would like to express my appreciation to Professor E. G. Bilpuch of the Triangle Universities Nuclear Laboratory for the financial and logistical support which the Laboratory has provided me over the past four years. I also thank M. Bailey of TUNL for her cheerful assistance with the figures in the thesis. I would like to thank the TUNL community in general for the friendship extended to a theorist lost in a sea of experimentalists.

I am grateful to Professor R. Y. Cusson for suggesting this topic and guiding it to completion. My sincere thanks go to Professor L. C. Biedenharn, whose invaluable advice and support was greatly appreciated. I acknowledge with pleasure the assistance of Dr. R. Kent Smith of Duke and the support provided by Ms. Nan Simon.

I am indebted to my typists, Mrs. Maggie Catron and Mrs. Jerry Oakes, for the excellent job done in typing the manuscript with little advance notice.

Finally, I would like to thank my wife, Chris, whose love and patience have made the completion of this work possible.

This research was supported in part by a grant to TUNL from the U.S. Department of Energy.

K. A. S.

CONTENTS

LIST OF FIGURES

LIST OF TABLES

BRUECKNER-HARTREE-FOCK METHOD

FOR INVESTIGATING

HEAVY-ION REACTIONS

CHAPTER I

INTRODUCTION

The explosive proliferation of papers dealing with heavy-ion reactions which has occurred in the literature recently reveals the increase in interest in the topic. The range of various models applied to explain data obtained in heavy-ion scattering is as broad as the field of nuclear physics itself, stretching from semi-classical calculations which involve hundreds of partial waves to intricate many-body theories that include mesonic degrees of freedom. In the last decade many topical conferences on heavy-ion theory have been held throughout the world. The present work is a consideration of only one of the many methods for investigating heavy-ion collisions--the Brueckner-Hartree-Fock method.

While the concept of protons and neutrons as independent particles in the nucleus has existed for many years, the independent-particle model was first legitimized with a consistent theoretical framework in the shell model of Mayer (1948) and Haxel, Jensen and Suess (1949). Earlier, Hartree had successfully calculated the electronic energy levels of many-electron atoms using a self-consistent field method (Hartree, 1928), and the exchange effect in such systems was considered by Slater (1930) and by Fock (1930). These techniques were quickly applied to the independent-particle model of nuclear physics in the calculation of nuclear binding energies, single particle spectra and other properties. However, the environments of electrons in the atom and nucleons in the nucleus differ in a fundamental way: the nucleon experiences a strong repulsive force whenever it approaches within 0.5 fm of

another nucleon. In a series of papers with other co-workers (see the references in the article by Bethe mentioned below), Brueckner developed a method, based on the multiple scattering theory of Watson, which accounts for the hard core of the nucleon-nucleon interaction in a statistical approximation. The use of Brueckner's techniques in a Hartree-Fock calculation (known as BHF theory) has been the subject of countless studies. The paper on nuclear many-body theory by Bethe (1956) and the review article by Kohler (1975) serve as good introductions to early and later developments in BHF theory.

In the calculation described in the following chapters, Brueckner's method is applied to the collision of two heavy ions with A_1, $A_2 \lesssim 16$. Chapter II contains a discussion of the effective two-body interaction and its parameterization. Two refinements to the earlier work of Cusson, Hilko, and Kolb (1976) (which forms the basis for the present work) are discussed in Chapter III. In sections A and B of Chapter IV, the adiabatic cluster potential is defined, and technical aspects of the calculation are presented in Section C; results of the calculation for several heavy-ion systems are discussed in Section D. The calculation of a cluster potential in a sudden or overlap approximation is developed in the first three sections of Chapter V; the results of this calculation are discussed in Section D. Finally in Chapter VI, the use of the cluster potentials obtained in chapters IV and V in an optical model is considered; the chapter ends with a comparison of deep folding potentials with the shallow potentials calculated in this work.

CHAPTER II

DISCUSSION OF THE K-MATRIX MODEL

A. Introduction

The model interaction described in this section had its beginning in the single-particle K-matrix model of Meldner (1969); refinements of the model by Kolb, Cusson and Harvey (1973), by Trivedi (1974), and by Cusson, et al. (1976) have led to its use in the present form, first by Cusson, Hilko and Kolb (1976) (hereinafter known as CHK) and in the present work. Because the development and parameterisation of this model interaction is not the purpose of the research described here, only a brief summary of the K-matrix is given for the sake of completeness. It is important to understand just how the present knowledge of nuclear physics enters into such a realistic interaction; the aim of this chapter is to show the influence of experimental information and physical intuition on the form and parameterisation of the model.

The basic features of the K-matrix can be examined in the limiting case of spin- and isospin-saturated nuclear matter. Although the reaction matrix employed in these calculations is of single-particle form, a two-body reaction matrix is written below for generality. Non-interacting neutron- and proton-matter is assumed, where the states are labelled by k_τ, the linear momentum, and where τ is an isospin label. The uniform densities of the interpenetrating proton and neutron fluids are given by the Fermi gas expression:

$$\rho_\tau = \frac{1}{3\pi^2} k_{F\tau}^3 \qquad \tau = \begin{cases} +1 & \text{protons} \\ -1 & \text{neutrons} \end{cases} \qquad (1)$$

If the isospin dependence is ignored temporarily, the total density becomes,

$$\rho = \frac{2}{3\pi^2} k_F^3$$

and the total energy per nucleon E/A is given as

$$E/A = \frac{3}{5}\frac{\hbar^2}{2M}k_F^2 + \frac{3}{2k_F^3}\frac{1}{(4\pi^2)}\int d^3k_1 \int d^3k_2 \langle \vec{k}_1\vec{k}_2|K([n])|\vec{k}_1\vec{k}_2\rangle \quad (2)$$

The K-matrix is assumed to depend upon the nucleon density through the occupation number (density) functional (n) = $n_{k_1}, n_{k_2}, \ldots, n_{k_F}$, where n_k is the four-fold degenerate occupation number of state k. Because the matrix elements of K are assumed to be Galilean invariant and antisymmetrised, the reaction matrix is a function of the difference $|\vec{k}_1 - \vec{k}_2|$, and can be expanded in momentum-space in the multipole form:

$$K(|\vec{k}_1 - \vec{k}_2|, [n]) = \sum_{L=0}^{\infty}\sum_{M=-L}^{+L} K_L(k_1, k_2, [n])\, Y_L^M(\hat{k}_1)\, Y_L^{M*}(\hat{k}_2) \quad (3)$$

Since the momentum space distribution is spherically symmetric, only the L = 0 term of K contributes to the integral in eq (2).* If it is further assumed that the reaction matrix $K(k_1, k_2, n)$ is a smooth analytic function of the two momenta k_1 and k_2, then K may be written in the symmetric, separable form

$$K \approx K_0(k_1, k_2, [n]) = \sum_{\lambda\mu} G_{\lambda\mu}([n])\, f_\lambda(k_1)\, f_\mu(k_2) \quad (4)$$

where the density-dependence of $G_{\lambda\mu}([n])$ and the momentum dependence of f_λ are to be specified below. It is through the functional forms for these factors in Eq. (4) that the nuclear physics contained in the model is exhibited.

Replacing $\langle k_1 k_2|K|k_1 k_2\rangle$ in Eq. (1) with its approximate form, Eq. (4), and defining the useful integral

$$F_\lambda(k_F) = \int_0^{k_F} k^2 f_\lambda(k)\, dk = \int_0^{\infty} k^2 f_\lambda(k)\, n(k)\, dk \quad (5)$$

yields the total energy per nucleon,

$$E/A = \frac{3}{5}\frac{\hbar^2}{2M}k_F^2 + \frac{3}{2k_F^2}\sum_{\lambda\mu} G_{\lambda\mu}([n])\, F_\lambda(k_F)\, F_\mu(k_F) \quad (6)$$

---

*This assumption is also valid for the calculation of cluster-cluster potentials, for although that system may be deformed in coordinate space, it is nearly spherical in momentum space.

By performing an occupation number variation using Eq. (6) with a Lagrange multiplier ε_λ (which can be identified as the single particle energy), included to satisfy the orthonormality constraint, the single particle energies are found to be

$$\varepsilon_\alpha = \frac{\hbar^2}{2m} k_\alpha^2 + \sum_{\lambda\mu} G_{\lambda\mu}([n])\, f_\lambda(k_\alpha)\, F_\mu(k_F) + \frac{1}{2}\frac{1}{k_\alpha^2} \sum_{\lambda\mu} \left[\frac{\delta}{\delta n_\alpha} G_{\lambda\mu}([n])\right] F_\lambda(k_F)\, F_\mu(k_F) \tag{7}$$

The first two terms can be identified as the single particle kinetic energy,

$$t_\alpha = \frac{\hbar^2}{2m} k_\alpha^2 \tag{8}$$

and the single particle nuclear potential

$$v_\alpha = \sum_{\lambda\mu} G_{\lambda\mu}([n])\, f_\lambda(k_\alpha)\, F_\mu(k_F) \tag{9}$$

The last term in Eq. (7) is identified as the Brueckner rearrangement potential,

$$\Delta_B(k_\alpha) = \frac{1}{2k_\alpha^2} \sum_{\lambda\mu} \left[\frac{\delta}{\delta n_\alpha} G_{\lambda\mu}([n])\right] F_\lambda(k_F)\, F_\mu(k_F) \tag{10}$$

It now remains to determine the functional form for $G_{\lambda\mu}([n])$ and f_λ (and, hence, for F_λ) based on our knowledge of the nuclear force.

In an approach similar to that taken by Bethe (1971), the reaction matrix is assumed to be separable into long- and short-range parts. The long-range term is attractive and, in this model, momentum dependent; hence, it is non-local in coordinate space. The short-range part of the K-matrix is the highly renormalized repulsive term in the nucleon-nucleon interaction and will, along with the rearrangement potential, provide the saturation required of the nuclear potential. The short-range term will be discussed first.

Because of the short range of this part of the nuclear potential, it should be local in coordinate space and independent of momentum $\vec{k}$; therefore, $f_{\lambda=1}(\vec{k}) = 1$. Furthermore, if the short-range potential (with its repulsive core) is to prevent compression of the nucleus to densities exceeding the nuclear matter value, this term must be density-dependent; that is,

$$G_{11} = G_{11}(k_1, k_2, [n]) \sim G_{11}(k_F) \qquad (11)$$

Simple, quadratic forms of $G_{11}(k_F)$ have been suggested but the momentum dependence of this model must be more general in order that the Brueckner rearrangement term $\Delta_B(k)$ have the proper momentum dependence, as determined using Eq. (10). This can be done by using the following form for $G_{11}(k_F)$:

$$G_{11}(k_F) = G_{11}^{1} + G_{11}^{0} \int_0^{k_F} k^2 g(k) n(k)\, dk \qquad (12)$$

Inserting Eq. (12) into Eq. (10) yields the momentum dependence of $\Delta_B(k)$:

$$\Delta_B(k, k_F) = \frac{G_{11}^{0}}{2} g(k) \frac{k_F^6}{9} \qquad (13)$$

The form of g(k) is to be determined from consideration of two limiting cases involving rearrangement terms. In the first case, a zero-range (particle-hole) two-body interaction of the form

$$\langle ij | K | \alpha a \rangle = \delta_{i\alpha} \delta_{ja} \qquad (14)$$

is used to calculate the rearrangement diagram due to Pauli effects. The result is Real $(\Delta_\alpha) \sim n_\alpha$, i.e. a step function. An analytic calculation of the same diagram using a Yukawa form for the interaction gives a smoothly decreasing function of k as the other limiting case for $\Delta(k)$. It is assumed that a realistic expression should lie between these limits, and the function shown below was chosen for g(k):

$$g(k) = \sum_{n=0}^{4} \frac{z^n}{n!} e^{-z} \qquad z = \frac{9}{2} \frac{k^2}{k_0^2} \qquad (15)$$

This expression is a rounded step function (Fermi function), whose sole parameter, k_0, is determined from experimental information (Brandow, 1969) to be $k_0 \sim 1$ fm^{-1}. This value was varied, by Cusson, et al. (1976) along with other parameters of the model (discussed later) to obtain good agreement of the single-particle properties and total binding energies with experimental values for several spherical, closed-shell nuclei (Cusson, et al., 1976).

As previously mentioned, the long-range part of the reaction matrix is to be momentum dependent. Furthermore, it should be weaker than the repulsive core of the short-range term; for this reason, G_{12} is taken to be independent of $[n]$, and G_{22} is neglected entirely. The momentum dependence of the long-range term is contained in the function $f_2(k)$ which has the form

$$f_2(k) = \frac{1}{1+(ak)^2} \tag{16}$$

The choice of parameters in the model, including a in Eq. (16) above, will be discussed following the examination of isospin effects, the transformation to finite nuclei, and the other terms in the Hamiltonian.

B. Isospin, Finite Nuclei and All the Rest

This section begins with a discussion of the effects of introducing isospin into the nuclear matter Hamiltonian. The nuclear fluid is assumed to consist of neutron and proton matter as in Eq. (1). The two-body reaction matrix becomes

$$K^{\tau\tau'}(k_1^\tau, k_2^{\tau'}, [n]) = \sum_{\lambda\mu=1}^{2} G_{\lambda\mu}([n])\, h_{\lambda\mu}^{\tau\tau'} f_\lambda(k_1^\tau) f_\mu(k_2^{\tau'}) \tag{17}$$

where the isospin mixing matrix $h_{\lambda\mu}^{\tau\tau'}$ is

$$h_{\lambda\mu}^{\tau\tau'} = \frac{1}{2}\begin{bmatrix} 1 - t_{\lambda\mu}^0 & 1 + t_{\lambda\mu}^0 \\ 1 + t_{\lambda\mu}^0 & 1 - t_{\lambda\mu}^0 \end{bmatrix} \tag{18}$$

The parameter $t_{\lambda\mu}^0$ will be discussed below. The short-range and Brueckner

rearrangment potentials are now derived from

$$G_{11}([n]) = G_{11}^{1} + \frac{G_{11}^{0}}{2} \sum_{\tau''} \int_{0}^{k_{F\tau''}} k^2 g(k) n(k) dk \qquad (19)$$

Performing the occupation number variation as in Eq. (7) yields

$$\begin{aligned} \varepsilon(k_\tau, k_F^P, k_F^N) &= \frac{\hbar^2}{2m} k_\tau^2 + G_{11}([n]) \sum_{\tau'} h_{11}^{\tau\tau'} \frac{1}{3} k_{F\tau'}^3 \\ &+ G_{12} \sum_{\tau'} h_{12}^{\tau\tau'} \int_0^{k_{F\tau'}} k^2 f_2(k) n(k) dk + \frac{G_{12}}{1+(a k_\tau)^2} \sum_{\tau'} h_{12}^{\tau\tau'} \frac{k_{F\tau'}^3}{3} \qquad (20) \\ &+ \frac{1}{2} G_{11}^{0} g(k_\tau) \sum_{\tau'\tau''} h_{11}^{\tau'\tau''} k_{F\tau'}^3 k_{F\tau''}^3 \end{aligned}$$

The first term in this expression is the single particle kinetic energy, the sum of the second and third terms is small for values of ρ_τ less than the nuclear matter equilibrium value of $\rho_e = \frac{1}{3\pi^2} k_{Fe}^3$ (~ 0.08 nucleons/fm^3), and both terms are local in coordinate space. These two density-dependent parts of the single particle potential are responsible for saturation in the nucleus. Because the combination becomes strongly repulsive for $\rho_\tau > \rho_e$, their presence in H will be important in the calculation of the ion-ion interaction in the 'sudden' approximation, i.e. when the two colliding clusters strongly overlap, and little rearrangement can occur. This point will be discussed in Chapter V.

The fourth term in Eq. (20) is the long-range momentum- and density-dependent attractive nuclear potential. The last term is the Brueckner potential, which is non-local due to the momentum dependence of $g(k_\tau)$. In the adiabatic approximation discussed in Chapter IV, the rearrangement term Δ_B provides the nucleons sufficient opportunity to rearrange so that there is no sudden increase in density above ρ_e, and consequently, the adiabatic potential has no repulsive core at small ion-ion separations.

Because the K-matrix described above has been derived using the properties of (infinite) nuclear matter, the question arises: What correction must be applied to the single particle Hamiltonian in order to transform to the

more interesting case of finite nuclei? This question can be re-stated as follows: In which terms of Eq.(20) will the surface of a nucleus become important? These questions are answered by considering the single particle Hamiltonian which is obtained from Eq.(20) by replacing $\vec{k}_\tau$ with its coordinate space representation $\frac{1}{i}\vec{\nabla}_\tau$ and by replacing $k_{F\tau}^3$ with $3\pi^2\rho_\tau(r)$. The replacement

$$k_{F\tau}^3 \longrightarrow 3\pi^2\rho_\tau(\vec{r}) \tag{21}$$

is the usual Thomas-Fermi approximation and is valid when the nucleon density $\rho_\tau(\vec{r})$ varies slowly with r. Appropriate corrections should be applied to those terms of Eq.(20) whose range is greater than $1/k_F$. In particular, the previous condition does not hold in the nuclear surface, and it is in this region that corrections to the long-range attractive term of the single particle potential are necessary.

The necessary correction terms consist of a series of higher order derivatives of $\rho(r)$, which may be summed to yield the space-averaged, or smeared, density (Kolb, Cusson and Harvey, 1973)

$$\bar{\rho}_{\tau\xi}(\vec{r}) = e^{-(\xi k_{op}^2)} = \frac{1}{(2\xi\sqrt{\pi})^3}\int d^3r' \, e^{-|\vec{r}-\vec{r}'|^2/4\xi^2}\,\rho_\tau(\vec{r}') \tag{22}$$

This correction is applied only to the attractive nuclear potential so that this term of the single particle Hamiltonian is:

$$\pi^2 G_{12}\left(h_{12}^{\tau p}\,\bar{\rho}_{p\xi}(\vec{r}) + h_{12}^{\tau n}\,\bar{\rho}_{n\xi}(\vec{r})\right)\Big/\left(1+(a k_{op})^2\right) \tag{23}$$

where the mixed density (in parenthesis) is written explicitly.

Now that the transformation to finite nuclei has been sketched, the remaining terms of the single particle Hamiltonian, the Coulomb energy, the pairing energy, and the spin-orbit energy will be examined. The first two are discussed briefly here, while Chapter III is devoted to the spin-orbit potential. The latter differs considerably from that used in previous calculations in that it is now fully self-consistent.

Only a short description of the Coulomb and pairing terms are given here; further details can be found in (Trivedi, 1974), (Cusson, et al., 1976) and CHK. The Coulomb energy is divided into direct and exchange contributions as shown below.

$$V_{C,\text{direct}}(\vec{x}) = e^2 \int d^3x' \frac{\rho_p(x')}{|x-x'|} \quad ; \quad V_{C,\text{exch}}(\vec{x}) = -e^2 \frac{\rho_p(\vec{x},\vec{x}')}{|\vec{x}-\vec{x}'|} \qquad (24)$$

The direct term is calculated using Gaussian integration techniques applied to the problem by Kolb and Cusson (1972), and the exchange term is approximated by a method developed by these two workers. The error in the exchange term is about 5%, or 2 MeV in the Pb region.

Although the pairing energy plays a minor role in the mass region of interest, careful attention must be given to this term for the case of a highly deformed, fissioning compound system, e.q. the reaction $^{12}C + {}^{12}C \rightleftharpoons {}^{24}Mg$ or $^{16}O + {}^{16}O \rightleftharpoons {}^{32}S$. Further discussion of the pairing parameters will be given in Chapter IV. The pairing (BCS) energy is calculated with the expression (Trivedi, 1974):

$$\mathcal{E}^{\tau}_{BCS} = -\frac{1}{2} \sum_{\lambda} u^{\tau}_{\lambda} v^{\tau}_{\lambda} n^{\tau}_{\lambda} \Delta^{\tau}_{\lambda} \quad , \{\lambda\} = \text{occupied states} \qquad (25)$$

where $$v^{\tau}_{\lambda} = \frac{1}{2}\left(1 - (\varepsilon^{\tau}_{\lambda} - \varepsilon_{F\tau})/((\varepsilon^{\tau}_{\lambda} - \varepsilon_{F\tau})^2 + \Delta^2(\varepsilon^{\tau}_{\lambda}))^{1/2}\right) \; ; \; (u^{\tau}_{\lambda})^2 = 1 - (v^{\tau}_{\lambda})^2 \qquad (26)$$

$(v^{\tau}_{\lambda})^2$ is the occupation probability for the state λ ; $(u^{\tau}_{\lambda})^2$ is the non-occupation probability for the same state. The $\varepsilon^{\tau}_{\lambda}$ are single particle energy eigenvalues obtained by solving the single particle Schrodinger equation:

$$h\psi^{\tau}_{\lambda} = \varepsilon^{\tau}_{\lambda} \psi^{\tau}_{\lambda}$$

$\varepsilon_{F\tau}$ gives the level of the Fermi sea for nucleons of kind τ. The energy-dependent pairing gap $\Delta(\varepsilon^{\tau}_{\lambda})$ has a Gaussian form:

$$\Delta(\varepsilon^{\tau}_{\lambda}) = \Delta_0 \exp\left(-(\varepsilon^{\tau}_{\lambda} - \varepsilon_{F\tau})/D_0\right) \qquad (27)$$

and the constants Δ_0 and D_0 are included in Table I with the other parameters. The value of D_0 shown in the table was chosen so that ε_{BCS} vanishes for spherical nuclei such as ^{16}O. It should be noted that the pairing contribution to h is the only term which is not self-consistent.

C. Parametrisation

Table I contains an enumeration of the important parameters of the model for the values used in the present calculations. A detailed description of the choices made for most of the parameters is given in Cusson, et al. (1976). The origin of each value in Table I is discussed briefly below, so that the input from experimental and previous theoretical results can be shown.

The three reaction matrix parameters G^0_{11}, G^0_{22}, and G_{12} are determined using the properties of nuclear matter, specifically the equilibrium Fermi momentum and the binding energy per nucleon. These two quantities are also included in the table for completeness. In addition, these results yield a value of 150 MeV for the compressibility of nuclear matter, where

$$K = k_F^2 \frac{\partial^2 (E/A)}{\partial k_F^2} \Big|_{k_F = k_{Fe}} \qquad (28)$$

Experimental evidence concerning the momentum dependence of the rearrangement energy gives a value of $k_0 \approx 1$ fm^{-1} for the cutoff momentum in g(k) (see Eq.15). The values of the isospin matrix parameters $t^0_{\lambda\mu}$ are chosen by requiring that the neutron-neutron repulsive interaction equal the neutron-proton repulsive interaction, that the neutron-proton attractive force be twice the neutron-neutron or proton-proton attractive term, and that the symmetry energy term (B_{sym} in the table, obtained by expanding the binding energy per nucleon for nuclear matter (Cusson, et al, 1976)) have a realistic value.

TABLE I

INPUT PARAMETERS FOR THE K-MATRIX

PARAMETER	VALUE USED IN K-MATRIX
G^o_{11}	157.15 MeV - fm^3
G^1_{11}	114.66 MeV - fm^6
G_{12}	-183.7 MeV - fm^3
k_o	1.1549 fm^{-1}
t^o_{11}	0.20382
t^o_{12}	0.5
a	0.4 fm
β	0.35 fm
V_{so}	175 MeV. fm^5
Δ^*_o	0.12, 6.0 MeV
D_o	12.0 MeV
$+E_b$	16.4 MeV
$+k_{Fe}$	1.36 fm^{-1}
K	150 MeV
$+B_{sym}$	66 MeV

* Δ_o= 0.12 MeV for $\alpha+\alpha$, $^{12}C+\alpha$ And $^{16}O+\alpha$; Δ_o = 6.0 MeV for ^{14}C α, $^{12}C + ^{12}C$ And $^{16}O + ^{16}O$.

+These values are taken from properties of nuclear matter.

The non-locality or diffuseness a is chosen initially as a = 0.5 from the energy dependence of the optical model potential. This value was adjusted by Cusson, et al. (1976) to the value shown in the Table. The smearing parameter was determined as ζ = 0.35 fm by comparing the calculated rms charge radius to values found in fits to elastic electron scattering data (see Cusson, et al., 1976). The spin-orbit strength V_{SO} is chosen to give good spin-orbit splitting in both ^{16}O and ^{208}Pb. This term is discussed in greater detail in Chapter III.

Finally there are the BCS pairing parameters; as mentioned previously, $D_0 = 12.0/\sqrt{A}$ MeV is chosen to give no pairing energy for ^{16}O (and other spherical nuclei). The choice of Δ_0 can influence the shape of the potential energy surface, so that care must be used in the choice of Δ_0. As noted in Table I, Δ_0 = 0.1 MeV for $\alpha+\alpha$, $^{12}C + \alpha$, and $^{16}O + \alpha$, while Δ_0 = 6.0 for $^{14}C + \alpha$, $^{12}C + ^{12}C$ and $^{16}O + ^{16}O$. The smaller value of Δ_0 gives a deformed ^{8}Be compound system, spherical ^{16}O and deformed ^{20}Ne. The case of $^{14}C + \alpha$ is discussed in Section D of Chapter IV.

CHAPTER III

SELF-CONSISTENT SPIN-ORBIT INTERACTION AND SURFACE SYMMETRY POTENTIAL

A. Historical Development

In this chapter, the necessity of including in the single-particle potential a spin-orbit term in addition to the one-body phenomenological spin-orbit interaction of the shell model is demonstrated, and the form and parameterisation of this term is given. The possibility of including a surface symmetry potential is examined also. The nature and applicability of such a term in the single-particle potential is discussed in the last section of the chapter.

In previous calculations (Trivedi, 1974; Kolb, Cusson and Harvey, 1973; Cusson, 1976; CHK, 1976)with K-Matrix models similar to that described here, the contribution of the spin-orbit interaction to the Hamiltonian was calculated using the usual phenomenological form:

$$V^{\tau}_{\vec{l}\cdot\vec{\sigma}}(r) = V_{so} \sum_{\tau'} h^{\tau\tau'}_{12}\, \vec{\sigma}\cdot(\vec{\nabla}\rho_{\tau'} \times \vec{k}_{op}) + \text{Hermitian conjugate} \qquad (29)$$

In the case of spherical nuclei (Trivedi, 1974) this reduces to the familar Thomas expression:

$$V^{\tau}_{\vec{l}\cdot\vec{\sigma}}(r) = V_{so} \sum_{\tau'} \vec{l}\cdot\vec{\sigma}\, \frac{1}{r}\frac{\partial}{\partial r}\left(h^{\tau\tau'}_{12}\rho_{\tau'}(r)\right) \qquad (30)$$

In the references mentioned in the preceeding paragraph, the spin-orbit contribution was determined using either Eq.(29) or Eq.(30) in a non-self-consistent manner. Trivedi (1974) and Kolb, Cusson and Harvey (1973) mention

unsuccessful attempts to obtain the spin-orbit interaction in the context of the realistic K-matrix model; that is, the expansion, Eq. (4) in Chapter II, would have contained a term which could be related to the one-body spin-orbit potential of the shell model (Mayer and Jensen, 1955). Had these efforts been successful, the result would have been a self-consistent calculation of the spin-orbit potential. While the authors mentioned above were forced to sacrifice self-consistency for a usable, phenomenological spin-orbit interaction, the present work contains a self-consistent form for $V_{\vec{\rho}\cdot\vec{\sigma}}^{\tau}$, following the methods of Brink and Vautherin (1972) and Vautherin (1973).

Brink and Vautherin (1972--hereinafter known as BV) have performed a Brueckner-Hartree-Fock calculation for spherical nuclei using the Skyrme force as an effective interaction. Applying a variational principle to the nucleon-, spin-, and kinetic energy-density-dependent expression for the total energy, they obtain a central, single-particle potential which contains the following term for nucleons with isospin label τ (Eq.22a of BV):

$$-\frac{1}{2}W_0\left(\operatorname{div}\vec{J}+\operatorname{div}\vec{J}_\tau\right) \tag{31}$$

where $\vec{J}=\vec{J}_p+\vec{J}_n$ and where $\vec{J}_\tau$, the spin-density (or, more accurately, the spin-orbit density), is given by (Eq.(11) of BV):

$$\vec{J}_\tau=(-i)\sum_{j\sigma\sigma'}\phi_j^*(\vec{r},\sigma,\tau)\left[\vec{\nabla}\phi_j(\vec{r},\sigma',\tau)\times\langle\sigma|\vec{\sigma}|\sigma'\rangle\right] \tag{32}$$

The contribution of Eq.(31) to the total energy is in addition to the one-body spin-orbit potential used by BV.

Vautherin (1973) has extended this work to the case of deformed nuclei by requiring only axial symmetry of the Hartree-Fock wavefunctions. In this deformed calculation, Eq.(32) again gives the form of the spin-orbit density, where the wavefunctions ϕ_j now depend upon the cylindrical coordinates $\mathbf{r}=(r,z,\varphi)$.

Calculations for both spherical and deformed nuclei, incorporating the BV self-consistent spin-orbit potential in the single particle Hamiltonian, are described in this study. In the next sections, the necessity of including a term similar to Eq.(31) in the single particle potential is suggested, and the parameterisation of the spin-orbit potential is presented. Also included in Section C is a comparison of previous work with the present calculation.

B. Self-consistent Spin-orbit Potential

In view of the unsuccessful attempts by Trivedi (1974) and by Kolb, Cusson and Harvey (1973) to obtain an effective spin-orbit potential via Meldner's K-matrix model, this approach has been abandoned in favor of the method of Brink and Vautherin. In their calculation, BV use as an effective interaction, the zero-range Skyrme force (Skyrme, 1956 and Skyrme, 1959) and derive expressions for the central nuclear potential and the spin-orbit contribution to the single-particle potential. Neglecting a small term in $\vec{J}_\tau(\vec{r})$, BV obtain the usual form of the one-body spin-orbit potential:

$$V^\tau_{\vec{l}\cdot\vec{\sigma}} = -\frac{i}{2} W_0 \vec{\nabla} \rho^\tau_{mixed} \cdot (\vec{\nabla} \times \vec{\sigma}) \tag{33}$$

where

$$\rho^\tau_{mixed} = \rho + \rho_\tau \tag{34}$$

This expression is identical to Eq.(29), used in the spherical and deformed calculations, provided the proper choice of the isospin mixing parameters is made. A discussion of the isospin-dependent density-mixing matrix is given in the next section.

The major difference between the BV calculation of the spin-orbit contribution to the total energy, and previous work is that BV have included a scalar spin-orbit density dependent term, Eq.(31), in the central nuclear potential. This term occurs naturally in the BV derivation of the central

potential and is not a result of the choice of the Skyrme force as the nucleon-nucleon interaction. (Since the appendices in BV give an excellent presentation of this derivation, it is not repeated here.) Consequently, one must conclude that all Hartree-Fock calculations must contain a term of the form Eq. (31) in the central part of the nuclear Hamiltonian, and furthermore, that the strength W_0 in the central term must be the same as the spin-orbit strength in a term like Eq. (33). The former conclusion is justified by improved agreement with experiment of the calculated rms charge radii, spin-orbit splittings, and total binding energy for spherical nuclei, as discussed in the next section.

As mentioned above, the strength parameter W_0 occurs in both the one-body $V_{\vec{q}\cdot\vec{\sigma}}$ and in the BV scalar contribution due to the spin-orbit density. While it is possible to introduce a different parameter for the strength in Eq. (32) (thereby obtaining still another adjustable quantity in the Hamiltonian), there is no physical basis for such a difference. Hence, the same number is used for both the spin-orbit and div $\vec{J}$ parts of the total Hamiltonian. The exact forms of these potentials are given below:

$$V^{\tau}_{\vec{q}\cdot\vec{\sigma}} = V_{so} \sum_{\tau'} \eta_{\tau\tau'}\, \vec{\sigma}\cdot(\vec{\nabla}\rho_{\tau'} \times \vec{k}_{op}) + \text{herm. conj.} \qquad (35)$$

$$V^{\tau}_{SCALAR} = -V_{so} \sum_{\tau'} \operatorname{div}(\eta_{\tau\tau'}\, \vec{J}_{\tau'}) \qquad (36)$$

The isospin-dependent density mixing matrix is given by

$$\eta_{\tau\tau'} = \frac{1}{2} \begin{bmatrix} 1-\tau_s & 1+\tau_s \\ 1+\tau_s & 1-\tau_s \end{bmatrix} \qquad (37)$$

where both τ_s and V_{SO} are chosen to obtain good agreement with experiment for the binding energies, single particle spectra and rms charge radii for ^{16}O, ^{40}Ca, ^{48}Ca, and ^{208}Pb. In order that Eq.(36) agree with the BV spin-orbit density dependent term Eq.(32), one should set $\tau_s = -1/3$ (because $V_{SO} \approx 3\cdot W_0$).

This gives the contribution due to protons as

$$V^{\tau}_{SCALAR} = -V_{so}\,\vec{\nabla}\cdot\left(2\vec{J}_p + \vec{J}_N\right) \qquad (38a)$$

and for neutrons as

$$V^{N}_{SCALAR} = -V_{so}\,\vec{\nabla}\cdot\left(\vec{J}_p + 2\vec{J}_N\right) \qquad (38b)$$

The effect of $\tau = +1/3$, which gives the mixed spin-orbit densities $2\vec{J}_n + \vec{J}_p$ for protons and $2\vec{J}_p + \vec{J}_n$ for neutrons, has also been considered. It is shown in the next section that, except for $N \neq Z$ nuclei, the sign of τ_s has very little effect on the single particle spectra, rms charge radii and total binding energies of the nuclei under consideration. The value of $\tau_s = +1/3$ is used in the calculations presented in Chapters IV and V because somewhat better agreement with experimental results is obtained compared to the results for $\tau_s = -1/3$.

C. Parameterisation of Spin-orbit Potential And Comparison With Previous Work

As mentioned above, $\tau_s = +1/3$ was chosen on the basis of an improvement in the properties of spherical closed shell nuclei. Further evidence to support this choice (and, in general, the inclusion of the div $\vec{J}$ term) comes from the great improvement obtained for the total binding energy of ^{12}C, calculated using the deformed model to be discussed in the next chapter. While $E_{tot} \simeq 82$ MeV in CHK, the use of a self-consistent spin-orbit interaction ($\tau_s = +1/3$ and $V_{SO} = 175$ MeV-fm^5) gives a total binding energy, $E_{tot}(^{12}C) = 92.23$ MeV. Comparing these results with the experimental binding energy, $E_{exp} = 92.17$ MeV, shows that the div $\vec{J}$ term can lead to significant

corrections when added to the Hamiltonian.

The tables given below contain a comparison of the present work with several other studies for the (doubly magic) nuclei ^{16}O, ^{40}Ca, ^{208}Pb and (closed proton shell) ^{48}Ca. From the numbers in Table II, the single particle spectra for ^{16}O, ^{40}Ca and ^{48}Ca are seen to agree with experimental values at least as well as those calculated by Cusson, et al. (1976), and in particular, the spin-orbit splittings are quite similar. It is this similarity which eliminates the task of determining the "best value" of V_{SO}; rather than pursue an unnecessary search for a new V_{SO} the value used by Cusson et al. is retained. This is justifiable provided the other properties of the nuclei included in the study either improve upon or agree with those of Cusson et al.

Table III is a comparison of the total binding energy of various even-even nuclei, calculated using the self-consistent spin-orbit term, with results obtained by other researchers. For the case of ^4He, there is a slight improvement over the results of Cusson et al. (1976), but the alpha-particle remains under-bound considerably. This problem with $E_{tot}(^4He)$ extends into the calculation in the deformed basis, and as noted in Chapter IV, causes problems in the cluster potentials for reactions involving the alpha-particle (see also the comment in CHK).

In the case of ^{16}O, the inclusion of the spin-orbit density dependent interaction, Eq.(32), results in even more over-binding than that obtained by Cusson, et al. However, the total energy obtained here is still considerably better than the value of BV, and is within 2% of the experimental quantity. Negele (1972) has a value of $E_b(^{16}O)$ which is very close to $E_b^{exp}(^{16}O)$. Results for the two isotopes of calcium, ^{40}Ca and ^{48}Ca also show some improvement over previous work. For example, the total binding energy of ^{40}Ca is 344.4 MeV (for both values of τ_s). This is closer to the experimental value of

TABLE II

SINGLE-PARTICLE SPECTRA

	State	EP (MeV) Calc.	EP (MeV) Exp.	EP (MeV) Cusson, et al.	En (MeV) Calc.	En (MeV) Exp.	En (MeV) Cusson, et al.
^{16}O	1s1/2	-28.97	-40±8	-28.99	-32.11	----	-32.11
	1p3/2	-16.34	-18.4	-16.33	-19.61	-21.8	-19.59
	1p1/2	-10.40	-12.1	-10.46	-13.69	-15.7	-13.73
	1d3/2	-3.36	-0.6	-3.36	-6.61	-4.14	-6.60
	2s1/2	-0.47	-0.1	-0.58	-3.57	-3.63	-3.63
^{40}Ca	1s1/2	-33.62	-50±11	-33.82	-40.36		-40.55
	1p3/2	-24.01	{-34±6}	-24.15	-30.83		-30.99
	1p1/2	-20.38		-20.34	-27.31		-27.28
	1d5/2	-13.92	----	-13.96	-20.80		-20.86
	2s1/2	-8.44	-10.9	-8.76	-15.50	-18.1	-15.84
	1d3/2	-7.51	-8.3	-7.38	-14.48	-15.6	-14.36
	1f7/2	-2.70	-1.4	-2.66	-9.51	-8.36	-9.48
	2p3/2				-5.07	-6.2	-5.42
	2p1/2				-2.89		-3.01
	1f5/2				-1.22		-1.07
^{48}Ca	1s1/2	-40.98	-55±9	-40.42	-39.17		-39.15
	1p3/2	-31.35	{-35±7}	-30.64	-29.12		-29.20
	1p1/2	-28.64		-27.71	-26.45		-26.35
	1d5/2	-21.63	----	-20.81	-19.65		-19.60
	2s1/2	-15.93	-15.3	-15.52	-15.66	-12.55	-16.05
	1d3/2	-15.06	-15.7	-15.14	-14.12	-12.52	-14.18
	1f7/2	-10.06	-9.6	-9.99	-9.41	-9.94	-9.35
	2p3/2	-4.26	-1.9	-4.72	-5.58	-5.14	-6.42
	2p1/2	-2.43	-0.0	-2.50	-3.85	-3.11	-4.01
	1f5/2	-2.07		-1.79	-1.45		-1.79

TABLE III

BINDING ENERGIES (in MeV)

NUCLEUS	PRESENT WORK $T_z = \frac{1}{3}$	PRESENT WORK $T_z = -\frac{1}{3}$	EXP	CUSSON et al.	BV	NEGELE
^{4}He	—	27.04	28.3	26.7	—	—
^{16}O	129.9	129.9	127.6	128.6	131.52	127.8
^{40}Ca	344.43	344.42	342.6	347.2	345.6	352.8
^{48}Ca	422.17	424.75	416.0	410.5	428.64	—
^{208}Pb	—	1643.13	1636.4	1637.0	1641.12	1680.6

342.6 MeV than BV, Negele (1972) and Cusson, et al.

In a comparison of the numbers in Table IV with the calculations of other workers, the usefulness of the spin-orbit-density dependent term in the model becomes apparent. The table is a list of the rms charge radii for several nuclei. Good agreement with the experimental value for r_{ch} should indicate the possibility of successfully fitting electron scattering data using the density distributions calculated here. (However, no attempts are made to fit electron scattering data; that is not the purpose of this calculation.) The data in Table IV show that although the value of r_{ch} for ^{48}Ca from Cusson, et al. (1976) is in better agreement with experiment, the present values for the other nuclei in the table are closer to the experimental numbers than those of Cusson, et al. BV also have this same blend of relative success and failure in predicting r_{ch}. Negele's results are very similar to the present work.

Finally this section closes with comments on two remarks in the discussion by Cusson, et al. (1976); they suggest that the disagreement between theory and experiment for the quantity $\Delta E = E_{tot}(^{48}Ca) - E_{tot}(^{40}Ca)$ (their value is 12% smaller than the experimental value) can be reconciled by including a spin-orbit contribution in the Brueckner rearrangement potential Δ_B. Using the results of the present calculation, $\Delta E \sim 6\%$ larger than the experimental value. This difference (due mainly to the 6 MeV overbinding of ^{48}Ca) shows that the remark by Cusson, et al. is partly valid: an additional spin-orbit contribution in the Hamiltonian is useful, although it enters as part of the central nuclear potential rather than the rearrangement potential.

The second remark by Cusson, et al. is the statement that the disagreement between theoretical and experimental values of the rms charge radius difference, $\Delta r_{ch} = r_{ch}(^{40}Ca) - r_{ch}(^{48}Ca)$ can be resolved by including

TABLE IV

RMS CHARGE RADII (in fermi)

NUCLEUS	PRESENT WORK $T_3 = +\frac{1}{3}$	PRESENT WORK $T_3 = -\frac{1}{3}$	EXP	CUSSON et al.	BV	NEGELE
^{4}He	____	2.097	1.71	2.09	____	____
^{16}O	2.790	2.790	2.73	2.795	2.68	2.79
^{40}Ca	3.501	3.500	3.49	3.489	3.41	3.50
^{48}Ca	3.511	3,525	3,48	3,551	3,46	____
^{208}Pb	____	5,492	5,50	5,533	5,44	5,49

a surface-symmetry term in the nuclear potential. The numbers in Table IV indicate that, while $r_{ch}(^{48}Ca)$ is still greater than the ^{40}Ca value (whereas the opposite is true experimentally), the discrepancy is much smaller than the difference of Cusson, et al. These results are also significantly better than those of BV. The improvement is obtained by adding only the div $\vec{J}$ type term to the nuclear Hamiltonian; there is no new surface energy included. In the last section of the chapter, it is further demonstrated that the surface-symmetry term is not necessary, at least for even-even nuclei.

D. Surface-symmetry Potential

The motivation for including a surface-symmetry potential in the calculation of heavy-ion potentials comes from the usual expansion of the binding energy, in which there is a contribution taken to be proportional to the surface area of the nucleus:

$$E_s = a_s A^{2/3}\left(1 - K\left(\frac{N-Z}{A}\right)^2\right) \qquad (39)$$

The first term in Eq.(39) is the surface tension correction to account for the finite size of the nucleus, while the term containing $(N - Z)^2/A^2$ is included to account for the stability of neutron rich nuclei. (See, for example, Nix, 1972,)

An expression of the form of Eq.(39) is useful in a simple model, but the question to be considered is: how can this be implemented in a density-dependent realistic model? For the first term in Eq.(39), the answer is rather easy. A density-dependent function which peaks in the nuclear surface, vanishes in the interior and also vanishes outside the surface has the necessary form. The curve in Fig. 1a show a typical density profile (e.g. for ^{16}O); Figure 1b is a sketch of the function $\frac{1}{\rho}(\nabla\rho)^2$, which possesses the requisite characteristics of the surface energy term $a_s A^{2/3}$.

Figure 1 (a.) Typical Fermi-Dirac density distribution $\rho(r)$ vs. r.

(b.) Graph of the surface-peaked function $\frac{1}{\rho}(\nabla\rho)^2$ vs. r.

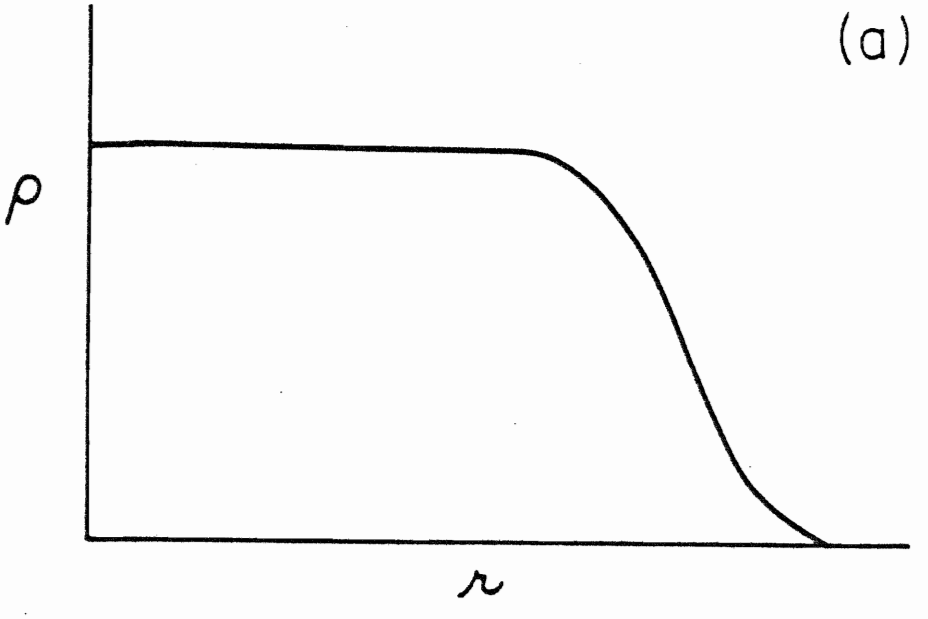
(a)
ρ
r

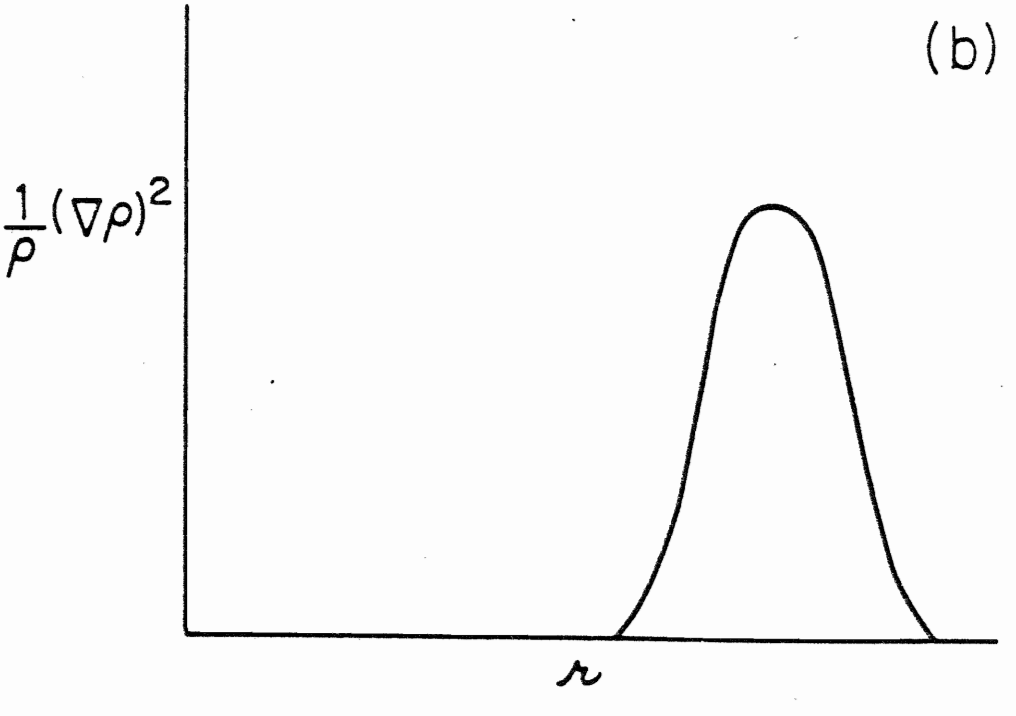
(b)
$\frac{1}{\rho}(\nabla\rho)^2$
r

The form of the second term in Eq.(39), the surface symmetry energy E^{τ}_{sym}, will be either a function of the differences of the neutron and proton nucleon densities, or will involve a mixed expression in the two densities. In fact, Cusson (1976) has shown that this functional form could be:

$$E^{\tau}_{sym} = g^{0}_{s} \frac{1}{\rho_{\tau}} (\vec{\nabla}\rho_{\tau} \cdot \vec{\nabla}\rho_{-\tau}) \qquad (40)$$

Combining this with the surface energy results in the realistic analog of Eq.(39):

$$V^{\tau}_{s} = -g^{0}_{s} \left[\frac{1}{\rho_{\tau}} (\vec{\nabla}\rho_{\tau})^{2} \right] + g^{s}_{s} \left[\frac{1}{\rho_{\tau}} \vec{\nabla}\rho_{\tau} \cdot \vec{\nabla}\rho_{-\tau} \right] \qquad (41)$$

The use of this term is investigated in a series of calculations which are described below.

First, the consequences of including only the first term in Eq.(41) in the nuclear Hamiltonian are explored. Table V presents these results under case I, where $g^{0}_{s} \neq 0$ and $g^{s}_{s} = 0$. The only quantities which have been improved relative to the calculation without surface corrections are the rms charge radii of ^{48}Ca and ^{40}Ca. Case I gives a Δr_{ch} which agrees well with the electron scattering experimental results; however, every other nuclear property calculated is worse. Specifically, the problem of over-binding is much worse for all nuclei in the table. In addition, r_{ch} for ^{208}Pb is much too low. To give this correction a fair chance to improve the binding energies, different nuclear matter parameters were varied while g^{0}_{s} remained fixed; these attempts lead to even worse results than case I. It is clear that the use of the g^{0}_{s} term alone is not profitable.

Before a contribution like Eq.(41) could be rejected, the outcome of including the surface-symmetry energy, i.e., $g^{0}_{s} = 0$ and $g^{s}_{s} \neq 0$ must be considered. These results are given in case II in Table V. It was hoped, a

TABLE V

SURFACE SYMMETRY POTENTIAL

NUCLEUS		CASE I $g_s^0 \neq 0, g_s^1 = 0$	CASE II $g_s^0 = 0, g_s^1 \neq 0$	CASE III $g_s^0 \neq 0, g_s^1 \neq 0$
^{16}O	E_{tot} (MeV)	129.92	140.99	141.01
	r_{ch} (fm)	2.79	2.80	2.80
^{40}Ca	E_{tot}	344.50	365.47	365.52
	r_{ch}	3.50	3.54	3.54
^{48}Ca	E_{tot}	423.71	445.27	446.42
	r_{ch}	3.49	3.57	3.55
^{208}Pb	E_{tot}	1653.54	1698.13	1705.7
	r_{ch}	5.47	5.60	5.59

priori, that the symmetry effects in this term could alleviate the binding energy problem in ^{208}Pb. The data in Table IV show that this is not the case. All of the relevant quantities have poor values relative to experiment and to the results with no surface corrections. Finally, as seen for case III, $g_s^0 \neq 0$ and $g_s^s \neq 0$, in the table, no combination of the two terms in Eq.(41) could improve on the results obtained with only the self-consistent spin-orbit corrections and no surface energy terms added to the Hamiltonian. For the sake of completeness, calculations using various combinations of div $\vec{J}$, g_s^0 and g_s^s terms, as well as calculations with changes in the nuclear matter parameters were performed; the conclusion that div $\vec{J}$ alone provides a fairly useful global model still holds.

CHAPTER IV

CALCULATION OF THE ADIABATIC POTENTIAL

A. Introductory Comments

In this chapter, results of the calculation of ion-ion or cluster potentials for several reactions using the K-matrix model and refinements discussed in Chapters II and III are presented. The potentials described in this chapter are quasi-static or adiabatic and correspond to head-on (angular momentum L = 0) collisions between the two ions.

The cluster potentials displayed in Section D are obtained using a constrained, deformed Brueckner-Hartree-Fock self-consistent iterative scheme in which polarization of the emerging fragments as well as fusion into a compound system is allowed. The constraints are discussed in greater detail in Section C, where a step-by-step description of the iterative process is given. The calculation proceeds in a deformed, single oscillator basis, with a special energy-selection algorithm used to minimize the number of basis states while maintaining good convergence of the total energy. The total wave-function of the ion-ion system is calculated as a single Slater determinant; therefore, Pauli corrections are included at all stages of the calculation. Finally, the basis employed has axial symmetry about the z-axis of the system; while the two clusters need not be identical, each must possess axial symmetry.

Before a derivation of the form of the cluster potential and the enumeration of the procedure for calculating the cluster potential (Sections B and C, respectively), the term "adiabatic" should be defined in the context of this work. Usually this term occurs in the phrase

"adiabatic approximation"; in the adiabatic approximation, one assumes that there is some division of the total energy of the system into two parts, according to the characteristic time scale associated with the coordinates describing two different types of motion of the system. The Born-Oppenheimer approximation is an example of an adiabatic approximation: the motion of the electrons in their molecular orbits is assumed to be much more rapid than the relative motion of the nuclei (in the diatomic molecule, for example); the nuclei are considered to be fixed in position as far as the calculation of the electronic energy levels is concerned (Slater, 1963).

This picture of the diatomic molecule can also be applied to the calculation described in this chapter, except that rather than consider two nuclei which move slowly with respect to orbiting electrons, here the centers-of-mass of the clusters are regarded as stationary relative to the motion of their constituent nucleons. In the adiabatic calculation discussed below, the stabilization of the total energy is required at each separation R of the two centers-of-mass. In this way, one obtains the lowest energy configuration consistent with the constraint and initial density distribution chosen for that separation. (See Section C for details of the constraint potential and initial densities, and Section D for comments on the effects of these choices.) Eisenberg and Greiner (1970) state this succinctly as: "...the nuclear orbits are rearranged in energetically favored positions at every instant during the collision."

The critical test to be applied to the adiabatic approximation made here is: Would the adiabatic cluster potential provide a useful description of experimentally measured quantities? This question really should read: Are there any experimental situations in nuclear physics to which a Born-Oppenheimer type of model might apply? For a partial answer,

one may look to the low-energy (in the center-of-mass) elastic scattering of two heavy ions (Villars, 1977). When the relative kinetic energy of the two ions is not too large, the centers of mass of the two clusters converge slowly, and the ions have time to polarise (rearrange) as demanded by the nuclear and Coulomb forces present. Another example is the reverse process, the fission of a heavy nucleus into two fragments which separate with low relative kinetic energy. In both cases, much of the relevant dynamical information is contained in the instantaneous total energy and the sequence of shapes of the fragments along the scattering or fission path.

The present calculation provides just this type of information. A complete curve of the potential energy is obtained by calculating the instantaneous energy at each cluster separation R in an adiabatic approximation, i.e., the potential curves shown in Section D represent quasi-static processes. The deformation parameters of each fragment in a reaction can likewise be extracted as a function of R. In the case of low-energy elastic scattering of two heavy-ions, it must be noted that the adiabatic potential has one obvious flaw: only central collisions ($L = 0$) are considered. However, Fliessbach (1971) has commented that $L \neq 0$ collisions lead to only a weak L-dependence in the potential. Hence, the adiabatic cluster potentials shown in Section D should be useful in describing some types of experimental data.

Having considered what types of reactions are amenable to description by these adiabatic potentials, one should also examine those situations where the adiabatic approximation is no longer valid. There are two obvious candidates. First, in the case of high energy scattering, the nucleons have no time to rearrange into the lowest energy configuration, i.e., the characteristic time of the fragment separation coordinate is

(at least) comparable to the orbiting time of individual nucleons. This problem is discussed in more detail in Chapter V. Secondly, the adiabatic approximation fails in reactions in which damping occurs (Villars, 1977). This damping is manifested as a transfer, or loss, of energy from the entrance channel into other channels or degrees of freedom (Swiatecki and Bjornholm, 1972). An example of such a process is a reaction in which two heavy ions begin to fuse together, but the system de-excites by neutron evaporation rather break-up into the original fragments. If consideration is restricted to low-energy reactions in which damping is not important, it may be possible to interpret the experimental data using the adiabatic cluster potentials described below.

B. Definition of Cluster Potential .

In this section, the definition of the cluster potential is given, and problems associated with removal of the spurious center-of-mass kinetic energy are examined. The Hamiltonian for the $A = A_1 + A_2$ particle system is given by

$$H_{TOT} = \sum_{i=1}^{A} \frac{p_i^2}{2M} + \frac{1}{2} \sum_{i \neq j} K_{ij}([n]) \qquad (42)$$

The potential energy is written as a two-body K-matrix for generality. $[n]$ is the occupation number functional. Removing the kinetic energy of the center of mass, defined as

$$T_{CM} = |\vec{P}_T|^2 / 2AM \qquad (43)$$

where $\vec{P}_T = \sum_{i=1}^{A} p_i$ yields the Hamiltonian for the motion relative to the center of mass,

$$H_{Rel} = H_{TOT} - T_{CM} \qquad (44)$$

The kinetic energy term T_{cm} has both one- and two-body terms. In the Appendix, it is shown that the direct part of the two-body term vanishes identically because $\langle \vec{P}_T \rangle = 0$ for the states used in this calculation. The two-body exchange term is assumed to be small and is neglected (Cusson, Hilko and Kolb, 1976). The one-body term which remains is given by

$$T_{CM} \approx \frac{1}{A} \sum_{i=1}^{A} \frac{P_i^2}{2m} \tag{45}$$

The relative motion Hamiltonian becomes

$$H_{rel} = \left(1 - \frac{1}{A}\right) \sum_{i=1}^{A} \frac{P_i^2}{2m} + \frac{1}{2} \sum_{i \neq j=1}^{A} K_{ij}([n]) \tag{46}$$

Because only binary clusters are considered in these calculations, the relative motion Hamiltonian Eq. (46) can be re-cast as

$$H_{rel} = T_{cl} + V_{cl} \tag{47}$$

Equation (47) defines the cluster potential V_{cl} in terms of H_{cl} and T_{cl},

$$V_{cl} = H_{rel} - T_{cl} \tag{48}$$

The cluster kinetic energy T_{cl} is defined as

$$T_{cl} = \frac{1}{2} \mu m \left| \vec{V}_{A_1} - \vec{V}_{A_2} \right|^2 \tag{49}$$

where $\vec{V}_{A_1}$ = total velocity of cluster A_1, and $\vec{V}_{A_2}$ = total velocity of cluster A_2. The reduced mass number μ is

$$\mu = \frac{A_1 A_2}{(A_1 + A_2)} \tag{50}$$

Consider the operator T_{cl}. First,

$$\vec{V}_{A_1} = \sum_{i=1}^{A_1} \dot{\vec{r}}_i \quad ; \quad \vec{V}_{A_2} = \sum_{j=1}^{A_2} \dot{\vec{r}}_j \tag{51}$$

so that

$$\Delta\vec{V} = \vec{V}_{A_1} - \vec{V}_{A_2} = \sum_{k=1}^{A} \alpha_k \dot{\vec{r}}_k \quad ; \quad \alpha_k = \begin{cases} +1 & k \le A_1 \\ -1 & A_1 < k \le A \end{cases} \tag{52}$$

The cluster kinetic energy $\frac{1}{2}\mu m|\Delta V|^2$ is not symmetric under the exchange of particles between the two clusters. It can be shown that only the symmetrical part of the operator T_{cl} can contribute to $\langle V_{cl} \rangle$ for the antisymmetrized states used here (CHK, 1976). Furthermore, the symmetrical term in T_{cl}, T^S_{cl} has direct and exchange components; the exchange term is neglected in this calculation (see Cusson, Hilko and Kolb, 1976), so that the relative motion kinetic energy is approximately

$$T_{cl} \approx \frac{1}{A} \sum_{i=1}^{A} \frac{p_i^2}{2m} \tag{53}$$

that is, $T_{cl} \approx T_{cm}$. The cluster potential energy is then defined in terms of the <u>total</u> Hamiltonian by

$$V_{cl} = H_{Rel} - T_{CM} \approx H_{TOT} - 2T_{CM} \tag{54}$$

This is the form of V_{cl} used in the calculation of the adiabatic potentials shown in Section D.

As mentioned above, the definition of V_{cl} is predicated upon the assumption of <u>binary</u> fragments; hence, the description of the interaction in a given system A_1, A_2 is a function of a single coordinate, the cluster-cluster separation. This separation is defined for this work using the total mass quadrupole moment, Q_{2T} (calculated with respect to the center of mass):

$$R = \sqrt{Q_{2T}/2\mu} \tag{55}$$

where $Q_{2T} = \sum_{i=1}^{A} \langle i | 2z^2 - y^2 - x^2 | i \rangle_{CM}$. This choice of R is similar to that of other authors (Mosel, 1972), (Wilets, Goldburg, Lewis, 1970). This definition is employed because for well-separated spherical clusters, R is simply the distance between the centers of mass, and for binary fission or for two fragments in fusion, the total energy depends (in part) upon the elongation and hence, the quadrupole moment, of the compound system. The coordinate defined above was chosen instead of the simple center-center separation distance because in the latter there is no consideration of the polarisation of the fragments. Also, one notes from its definition that R is a one-body operator for the total system and is unchanged by the antisymmetrisation between the clusters of the total wave-function. Any coordinate which lacks this property may change drastically as the two clusters strongly overlap, thereby introducing a spurious change in energy of a fusing system. Finally, R = 0 does not imply that the centers of the two converging clusters are superposed, leading to a doubling of the central density; rather, R = 0 implies that $Q_{2T} = 0$, i.e., the compound system of the completely fused fragments is spherical. Thus, the definition of R given above is in accord with the adiabatic nature of the potential, V_{cl}.

The removal of the kinetic energy $T_{cm} + T_{cl}$ from the total energy H_{tot} to obtain V_{cl} requires further examination. Several authors (Dreizler, et al., 1974), (Brink and Stancu, 1975), (Zint, Mosel, 1975), (Zint, Mosel, 1976) have suggested empirical methods for removing the spurious center-of-mass and relative motion kinetic energies, and have had varying degrees of success with their methods. The prescription given above for removing the cluster kinetic energy is based on the presence of two clusters in the fusing system. This assumption does not hold when the system has completely fused; in this case, the coordinate describing the separation of the clusters R is no longer an independent degree of freedom.

Consequently, the fusion of binary fragments into the compound system effectively removes one degree of freedom from the problem, apparently making the subtraction of T_{cl} in Eq. (48) unnecessary. The potentials V_{cl} are too deep by T_{cl} in the regions of V_{cl} corresponding to a completely fused system. By the equipartition of energy theorem, each degree of freedom should have approximately the same kinetic energy, so that $T_{cl} \approx T_{cm} \approx 15$ MeV (in the ground state of the system) gives the amount by which V_{cl} should be too deep. This number could be smaller for a compound system which does not completely fuse into a spherical ground state. Further comments on this subject can be found in Section D; the results presented there appear to support a graduated removal of T_{cl} only in the case of the lightest system studied here, $^{8}Be \rightleftharpoons \alpha + \alpha$. In spite of the ambiguity as to how much of T_{cl} should be removed, the full amount is subtracted to obtain V_{cl}; this simple method is preferred to the ad hoc methods of graduated removal mentioned previously. It should be noted that further consideration of the spurious kinetic energy problem must be given before V_{cl} is used in Schrödinger's equation. (See Chapter VI for further discussion.)

Finally, the figures in Section D show that the cluster potentials give the correct value of E_{tot} for $R \longrightarrow \infty$, i.e., just the binding energies of the two fragments plus the Coulomb energy of two point charges. This indicates that the method for removing the spurious kinetic energy is adequate, at least for large R.

C. Basis Selection, Constraints and Iterative Procedure

This section is concerned with technical aspects of the calculation of the adiabatic cluster potential and begins with a discussion of the selection of the basis.

Basis and basis-cutoff algorithm.

As mentioned previously, the calculation of the ion-ion potential is done using a deformed single oscillator basis. The oscillator basis is used because the momentum space representation of the states has the same functional form as the coordinate space representation. This simplifies the calculation of the momentum-dependent parts of the Hamiltonian. According to CHK, if a two-center oscillator basis were used, the problem of calculating non-local matrix elements of H_{tot} becomes costly in computing time. The basis states are chosen to be deformed oscillator states described by the functions

$$\Psi^{l_z}_{n_z n_r}(r,z,\phi) = \Phi^{\mu}_{n_r}(\eta)\,\psi_{n_z}(\zeta)\,\frac{e^{i l_z \phi}}{\sqrt{2\pi}}, \qquad (56)$$

multiplied by a two-component spinor $\chi^{\sigma_z}_{\frac{1}{2}}$; this product is coupled to the total angular momentum $j_z = l_z + \frac{1}{2}\sigma_z$. The arguments of the functions above are

$$\eta = \frac{r^2}{b_r^2}\,, \quad \zeta = \frac{z}{b_z}\,, \quad \mu = |l_z| \qquad (57)$$

where b_r and b_z are the r- and z-direction oscillator length paremeters, respectively. The determination of b_z and b_r will be discussed below. The two quantum numbers n_z and n_r represent the number of nodes in the z- and r-dependent parts of $\Psi^{l_z}_{n_z n_r}$, respectively. The two functions comprising the total wave-function are

$$\Phi^{\mu}_{n_r}(\eta) = \left[\frac{n_r!\,2}{(n_r+\mu)!}\right]^{\frac{1}{2}} \frac{\eta^{\mu/2}}{b_r}\, e^{-\frac{1}{2}\eta}\, L^{\mu}_{n_r}(\eta) \qquad (58)$$

$$\psi_{n_z}(\zeta) = \left[\sqrt{\pi}\,2^{n_z} n_z!\, b_z\right]^{-\frac{1}{2}} e^{-\frac{1}{2}\zeta^2} H_{n_z}(\zeta) \qquad (59)$$

where $L^{\mu}_{n_r}(\eta)$ is the associated Laguerre polynomial, and $H_{n_z}(\zeta)$ is the Hermite polynomial.

The negative values of $K = j_z$ are not included in the calculation explicitly, because both the j_z and the $-j_z$ states are occupied in the even-even nuclei in the reactions studied here.

The basis parameters b_z and b_r can be determined once the initial density distribution is chosen. The goal in the selection of these parameters is to minimize the basis size and to obtain good convergence of E_{tot}, simultaneously. If one assumes that the choice of an initial density distribution gives half-density radii $R_{\frac{1}{2}}$ and $Z_{\frac{1}{2}}$ in the r- and z-directions, one can choose an angular momentum cutoff, ℓ_{zc} as:

$$\ell_{zc} = k_{Fa} R_{\frac{1}{2}} \tag{60}$$

where k_{Fa} is the momentum of the highest occupied state and $k_{Fa} \sim 1$ fm^{-1} (see CHK for details). This cutoff establishes an upper bound on the range of values of $K = j_z$. CHK have found that $\ell_{zc} \approx R_{\frac{1}{2}} + 1$ gives good convergence for $^{16}O + {}^{16}O \rightleftharpoons {}^{32}S$.

For the deformed oscillator basis, the phase space occupied by the basis states is an ellipsoidal volume. One of the axes of the ellipse has a half-length equal to the wave-number cutoff k_c; the other axes of the ellipse have half-lengths equal to the spatial cutoffs z_c and r_c. CHK have found that the following coordinate-space cutoffs

$$\begin{aligned} z_c &= \sqrt{2}\,(Z_{\frac{1}{2}} + 1.8\ \text{fm}) \\ r_c &= \sqrt{2}\,(R_{\frac{1}{2}} + 1.8\ \text{fm}) \end{aligned} \tag{61}$$

give a basis of sufficient size to accommodate $^{16}O + {}^{16}O$ at large separations, while insuring accurate calculation of the total energy. The 1.8 fm in the above expressions is added to account for the surface diffuseness expected in the nucleus, and the $\sqrt{2}$ factor is included to fit the ellipsoidal volume of the basis phase space into the rectangular phase space of a true nucleus. Because the momentum space in a spatially-deformed nucleus

is nearly spherical, only one momentum cutoff, k_c, is given. In the present work, $k_c = 2.2$ fm^{-1}. Larger values of k_c would increase the basis size and may not improve the accuracy of the total energy calculation significantly. Calculations with $k_c = 2.9$ fm^{-1} for $^{16}O + ^{16}O$ show no marked improvement in E_{tot}.

An oscillator with momentum cutoff k_c and spatial cutoff z_c has an oscillator parameter $b_z = \sqrt{z_c/k_c}$; likewise, $b_r = \sqrt{r_c/k_c}$. The characteristic oscillator frequencies ω_z and ω_r are obtained from these parameters as

$$\omega_z = \frac{\hbar}{m b_z^2} \quad ; \quad \omega_r = \frac{\hbar}{m b_r^2} \tag{62}$$

The kinetic energy of a particle in the basis state (n_z, n_r, μ) has the expectation value

$$T(n_z, n_r, \mu) = \frac{1}{2}\left[\hbar\omega_r(2n_r + \mu + 1) + \hbar\omega_z(n_z + \tfrac{1}{2})\right] \tag{63}$$

Recall that $\mu = |\ell_z|$. The energy-selection algorithm requires that this expectation value not exceed the kinetic energy of the state of highest momentum k_c, i.e.,

$$T(n_z, n_r, \mu) \leq \frac{\hbar^2 k_c^2}{2m} \approx 100 \text{ MeV} \tag{64}$$

For a given $\ell_z \leq \ell_{zc}$, the above condition determines a set of pairs of basis quantum numbers (n_z, n_r) ; because $j_z = \ell_z + \frac{1}{2}\sigma_z$, the energy-selection algorithm in Eqs. (60) - (64) limits the allowed values of n_z and n_r for each $K = j_z$, and thereby minimizes the size of the basis for each reaction studied.

Because of the axial symmetry imposed in the calculation, K is a good quantum number; hence, the matrix representing h_{eff} is diagonal in K and can be calculated and diagonalized in blocks labeled by K. The

largest block occurs for $K = \frac{1}{2}$ and for the calculations described here, is of order less than fifty-six. Thus, no more than fifty-six basis states are needed at once. For a typical basis size, consider $^{16}O + ^{16}O$ at R $\approx$ 10 fm; CHK have found that a basis with fixed parameters ω_z = 6.7 MeV, ω_r = 12.5 MeV and having max (n_z) = 12 and max (n_r) = 3 yields a total energy accurate to 0.2 MeV.

Constraint potentials.

In the calculation of the quasi-static cluster potential, the ion-ion system must be constrained to remain in a chosen configuration throughout the iterative process; otherwise, the system will fuse completely or separate into two clusters, depending upon which results in the lowest total energy. The desired configuration is maintained by adding a constraint potential to the relative single particle Hamiltonian to obtain the effective single particle Hamiltonian actually used in the constrained iterations:

$$\hat{h}^{\tau}_{eff} = \hat{h}^{\tau}_{rel} - \lambda_q v_q(\vec{k}, \vec{r})$$

Recall that the relative motion single particle Hamiltonian is:

$$\hat{h}^{\tau}_{rel} = \sum_{i=1}^{A} \left[\frac{p_i^2}{2m}\left(1 - \frac{1}{A}\right) + v_N^{\tau}(i) + \Delta_B^{\tau}(i) + v_{l\cdot\sigma}^{\tau}(i) + v_{coul}^{\tau}(i) + v_{pair}^{\tau}(i) \right] \quad (65)$$

as given in Chapter II. The spin-orbit density dependent term is included in $v_N^{\tau}(i)$, the central nuclear potential. The constraint potential (with strength λ_q) is momentum- and position-dependent:

$$v_q(\vec{k}, \vec{r}) = \exp\left(-c^2 k_{op}^2\right) \rho_q(\vec{r}) \quad (66)$$

CHK have chosen c $\approx$1 fm to allow damping of the constraint potential. This damping prevents v_q from affecting the high momentum components of

h^{τ}_{rel}, and v_q therefore does not change the saturation properties built into the K-matrix.

The spatial dependence of the constraint, given by $\rho_q(\vec{r})$ must also avoid an influence on the saturation properties of h^{τ}_{rel}. This is done by choosing $\rho_q(\vec{r})$ to be the initial density $\rho_o(\vec{r})$, less its spherical average (Cusson, Hilko and Kolb; 1976). That is,

$$\rho_q(r, \cos\theta) = \rho_o(r, \cos\theta) - \frac{1}{2}\int_{-1}^{1} d(\cos\theta)\, \rho_o(r, \cos\theta) \tag{67}$$

CHK point out that, since the volume integral of Eq. (67) vanishes, only quadrupole and higher moments are non-zero. (This is the reason for the subscript 'q'.) The rms radius of the system is only slightly affected by this function. The potential $v_q(r)$ is essentially of quadrupole form, although higher moments are present; these are of importance in maintaining the neck shape in the initial density when the two clusters begin to overlap significantly.

CHK report that for some initial density distributions, the constraint potential $\lambda_q v_q(\vec{k}, \vec{r})$ is an unstable perturbation, and the desired configuration cannot be maintained. An example is an initial density distribution whose separation puts it near the top of the Coulomb barrier (for instance, see $^{16}O + {}^{16}O$ in Chapter IV, Section D). At this separation, known as the strong absorption radius, the nuclear interaction and Coulomb forces are comparable, and the system could proceed toward separation (in order to lower the Coulomb energy) or fuse (thereby increasing the nuclear binding energy). CHK avoid this instability by adjusting the strength λ_q in the constraint potential after each iteration. Further stability is achieved by including only part of the density ρ^{τ}_i from the i^{th} iteration as input to the Hamiltonian for the $(i+1)^{st}$ iteration,

$$\rho^{\uparrow}_{i+1} = f\,\rho^{\uparrow}_{i} + (1-f)\,\rho^{\uparrow}_{i-1} \qquad (68)$$

The fraction f is also readjusted after each iteration, in a manner designed to maintain the initial shape of the system. CHK give a detailed description of the two methods of stabilizing the iterations. In nearly all of the calculations performed here, fewer than twenty-five iterations are necessary to provide the desired convergence of the total energy.

Finally, a second constraint potential is included in the form of a dipole constraint,

$$v_d(z) = \lambda_d z \qquad (69)$$

This potential is needed to prevent the density distribution from wandering up or down the z-axis during the iterations. The strength λ_d is adjusted after each iteration. The dipole potential is not necessary in the case of identical ions; however, it is included to allow the calculation of the cluster potential for density distributions which are not symmetric about the center of mass of the total system, for example, $^{16}O + {}^{4}He$.

Initial density distribution.

The initial density distribution, $\rho_o(r)$, chosen as the starting density for the iterative scheme described in the next section, is important since the constraint potential is calculated from $\rho_o(r)$. Because the shape of the constraint is held constant for each iteration while its strength is adjusted, the initial density affects the final density distribution through the constraint potential.

For scattering problems such as those discussed here, two types of initial density distributions are necessary. The initial distribution must be able to describe a system made up of two fusing fragments (or, the compound system which will scission into two fragments), as well as well-

separated fragments which do not overlap strongly. Furthermore, these two types of distributions must be chosen so that when a change is made from one type to the other (as in obtaining the complete cluster potential for two separated fragments which fuse), the cluster potential does not have an unphysical discontinuity at the change-over separation distance. The change from one deformed cluster to two well-defined, slightly overlapping clusters occurs at the half-density overlap radius, $R_{\frac{1}{2}}$. $R_{\frac{1}{2}}$ is the separation between clusters at which the total density of cluster A_1 plus cluster A_2 becomes larger than the interior equilibrium density of either cluster. A brief description of only the single cluster initial density distribution is given below because the two-cluster distribution is just a superposition of two one-cluster distributions, with a shift to give the desired separation between clusters.

The initial density of the single cluster is obtained by folding a step-function density distribution with a Gaussian smearing function (this is discussed in greater detail in CHK):

$$\rho_o(\vec{r}) = \rho_o' \int_V d^3r' \exp\left(|\vec{r}-\vec{r}'|^2/d^2\right) \qquad (70)$$

where $\rho_o' = 0.155$ nucleons/fm^{-3}, and d = 1.24 fm. The volume V is the volume enclosed by a contour described by $r = \sqrt{x^2 + y^2} = r(z)$; the choice of the form of the z-dependence of the radial cylindrical coordinate r(z) therefore determines the initial density distribution. This functional form must be chosen so that the normalization condition,

$$2\pi\rho_o' \int_{z_-}^{z_+} dz \int_0^{r(z)} dr' r' = A_1 + A_2 = A \qquad (71)$$

is satisfied; $z_\pm$ are the appropriate upper and lower integration limits, respectively. The Gaussian smearing function is not included in Eq. (71) because it has no effect on the normalization. Eq. (71) is then the norm-

alization condition,

$$\int_V d^3r\, \rho(r) = A \tag{72}$$

CHK have chosen the following form for r(z):

$$\left(\frac{r}{s}\right)^2 = \exp\left(-\sqrt{\frac{5}{4\pi}}\beta_0\right)\left(1 - x + x\left|\frac{z - z_0}{s}\right|^{\alpha}\right)\left(1 - \left(\frac{z}{s}\right)^2\right) \tag{73}$$

The quantities which determine r(z) and hence the initial density are: β_0, the input quadrupole deformation parameter of the contour; the necking parameter x, where x = 0 for no neck in the density contour and $x \geq 1$ for two distinct fragments; z_0/s, the mass ratio parameter; and the neck-length parameter, α. For the light nuclei used in this work (A_1, $A_2 \leq 16$), $\alpha = \frac{2}{3}$ gives the desired short neck, leading to spherical fragments at scission. s is the scale factor obtained from the normalization condition Eq. (71).

The mass ratio parameter is chosen such that the ratio of the volumes of the two barely touching hemispheres in Figure 2 equals the ratio of the masses of the two fragments. The contour is obtained by setting x = 1 and ignoring the scale factor for the moment (s = 1). The ratio of the volumes can be seen from Figure 2 to be

$$\frac{\frac{4\pi}{6}(1 - z_0)^3}{\frac{4\pi}{6}(1 + z_0)^3} = \frac{(1 - z_0)^3}{(1 + z_0)^3} \tag{74}$$

hence, the condition which determines z_0 becomes

$$\frac{A_1}{A_2} = \frac{(1 - z_0)^3}{(1 + z_0)^3}$$

which is rearranged to give

$$z_0 = \left[\left(\frac{A_1}{A_2}\right)^{\frac{1}{3}} - 1\right] \Big/ \left[\left(\frac{A_1}{A_2}\right)^{\frac{1}{3}} + 1\right] \tag{75}$$

Figure 2. Half-density contours used to calculate the mass-asymmetry parameter, z_o. The scale at the right is appropriate for the half-density contours in the $^{12}C + \alpha$ system.

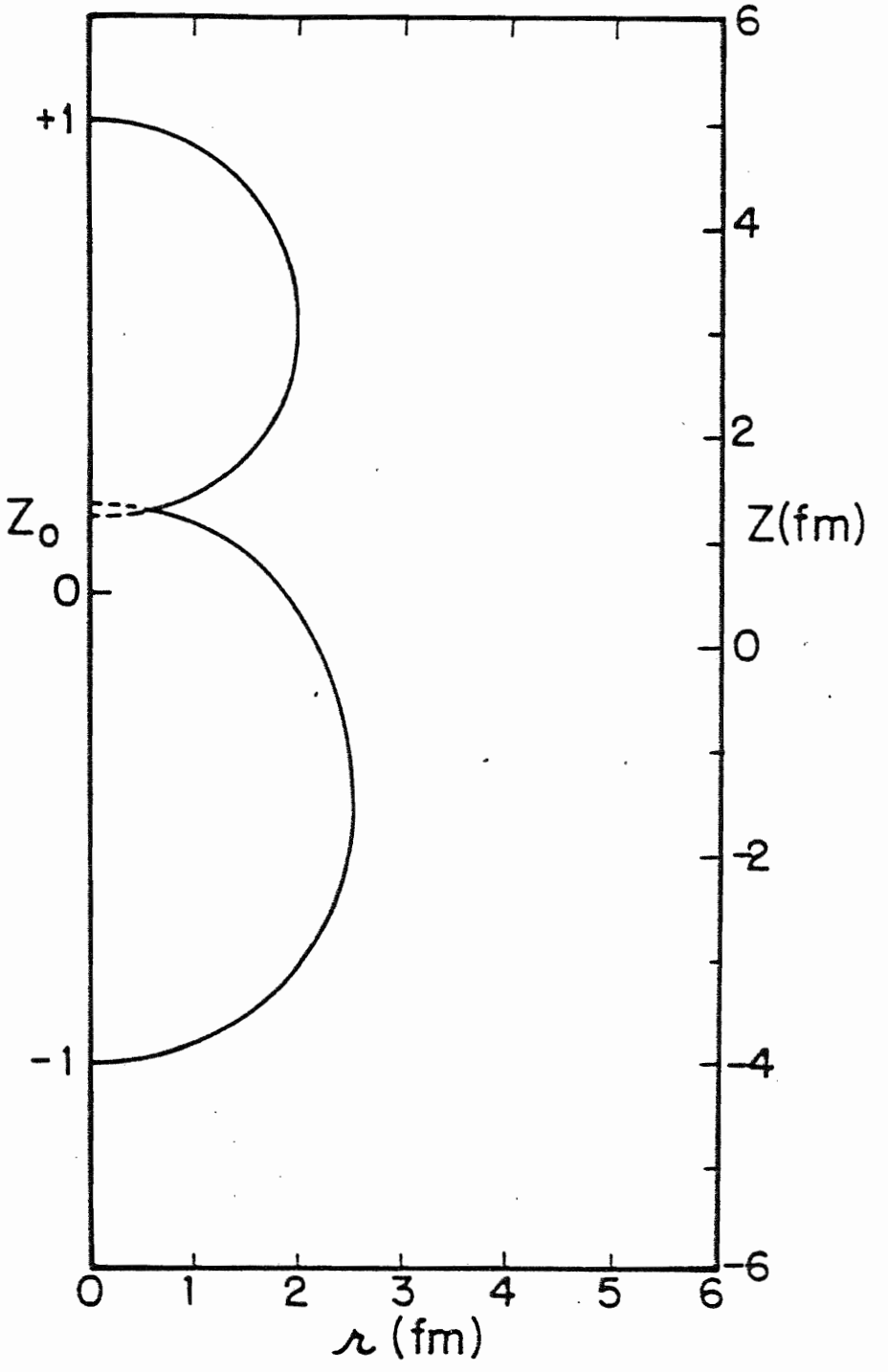
+1
Z_0
0
-1
6
4
2
0
-2
-4
-6
Z(fm)
0
1
2
3
4
5
6
r (fm)

After z_0 is found, the scale factor s is chosen to satisfy the normalization condition.

By choosing different values for the set (β_0, z_0, x), various initial density distributions are obtained. For the reaction $^{16}O + {}^{16}O$, for example, the desired system is one which scissions into two fragments of equal mass; hence, the proper choice of the mass ratio parameter is $z_0 = 0$. For $\beta_0 = 0$ and x = 0, the initial density is that of a spherical ^{32}S nucleus; as β_0 increases from 0 to 1/3, the compound system deforms to a prolate spheroid. By fixing $\beta_0 = 1/3$ and varying x from x = 0 to x = 1, a neck is formed between the two clusters until, at x = 1 the density distribution is that ot two barely touching spheres. The separation distance R from Eq.(55) is then the half-density overlap radius $R_{1/2}$. Figure 3 shows selected contours from the sequence of half-density contours used in calculating the cluster potential for $^{16}O + {}^{16}O$, with the values of R for that contour.

In the case of a mass-asymmetric system like $^{12}C + \alpha$, a non-zero value of z_0 is used in order to obtain the proper ratio of mass in fragment A_1 to that in fragment A_2; otherwise, the change from a one-cluster initial distribution to the two-cluster form in which one cluster has A = 4 and the second has A = 12 would not connect smoothly at $R_{1/2}$.

For cluster separations greater than $R_{1/2}$, the initial density distribution is obtained by using the two-cluster distribution. As mentioned above, this is just two single-cluster distributions, superposed and shifted to give the desired separation. It is possible to allow each cluster to have a deformed (and necked) half-density contour. However, the choice of the parameter set (β_0, z_0, x) supposes that one knows the shapes of the clusters during scission. Since the fragment shapes during fission or fusion are part of the information available in this study, one cannot choose those

Figure 3. Selected half-density contours for $^{16}O + ^{16}O$. The vertical scales are the radial coordinate, r, in fermi, and the horizontal axes are z, in fermi.

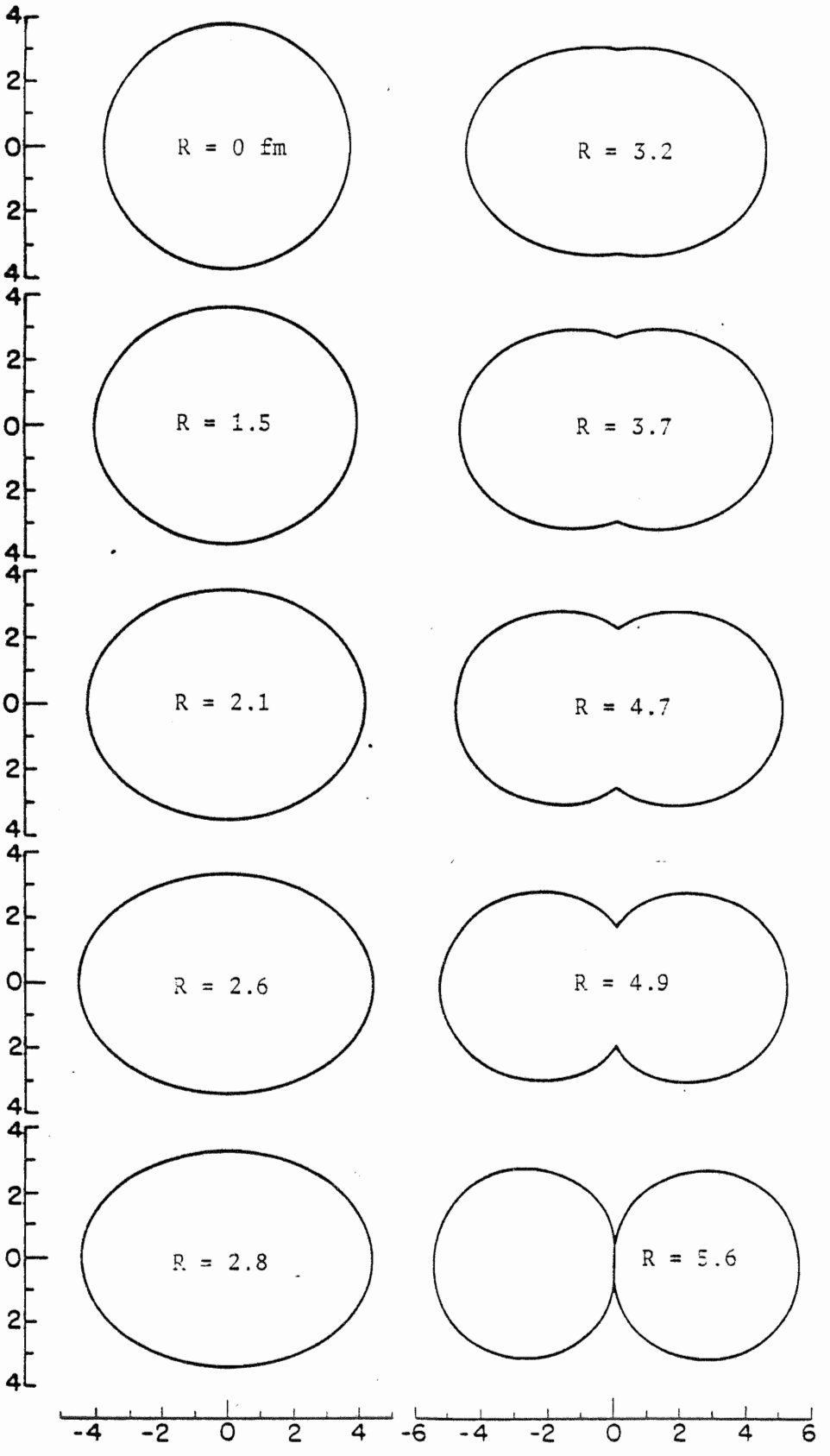
R = 0 fm
R = 3.2
R = 1.5
R = 3.7
R = 2.1
R = 4.7
R = 2.6
R = 4.9
R = 2.8
R = 5.6
4
2
0
2
4
-6
-4
-2
0
2
4
6

shapes a priori; for in making a choice of (β_0, z_0, x), one has chosen a definite path on the potential energy surface. Therefore, spherical clusters are used in constructing the two-cluster distributions.*

Before the initial density is used to calculate the constraint potential and the relative Hamiltonian h_{rel}, it is shifted so that the center of mass of the system is at the origin of coordinates. Hence, the calculations described below are done in the center-of-mass frame.

Procedure for self-consistent iteration.

The calculation of the ion-ion cluster potential begins with the choice of the masses of the cluster pair in the reaction, A_1 and A_2. The initial density distribution for two clusters whose separation R is large enough that they do not overlap is calculated according to the previous sub-section. The density distribution $\rho_0^p(r)$ of the protons is used as input for the calculation of the constraint potentials $\lambda_q v_q(\vec{k}, \vec{r})$ and $\lambda_d z$; the same constraints are used for protons and neutrons in order to simplify the calculation. This causes no difficulty so long as the cluster pair is not very neutron-rich; this condition holds for all reactions in this study.

The first step of an iteration is the calculation of the density dependent matrix elements of h_{eff} for the lowest value of $K = j_z$ to be used in the basis. Because the Hamiltonian matrix is diagonal in K, the $K = j_z$ block can be diagonalized, and the eigenvalues and eigenvectors of that block obtained. These steps are followed for the range of values of K

*This is actually a choice of a path on the potential energy surface which assumes that the two well-separated nuclei are spherical. This is discussed further in Section D below.

determined by Eq. (60) of this section. The resulting set of eigenfunctions ψ_λ^τ (r) satisfy the single-particle Schrodinger equation

$$h_{eff}^\tau \psi_\lambda^\tau = \varepsilon_\lambda^\tau \psi_\lambda^\tau \qquad (76)$$

with eigenvalues ε_λ^τ. The $\{\varepsilon_\lambda^\tau\}$ are the effective single-particle energies for nucleons of kind τ; because h_{eff} contains the constraint potentials, $\{\varepsilon_\lambda^\tau\}$ are the exact single particle energies only for spherical systems, for which $v_q(r) = 0$.

The eigenvalues ε_λ^τ are next arranged in increasing order; single-particle states with ε_λ^τ less than some cutoff energy (usually 4-10 MeV) are occupied with two nucleons each. The double occupation of a state accounts for the $-j_z$ partners of the j_z states. The 4-10 MeV cutoff is employed to include some continuum states while keeping the set of single-particle states as small as possible. The Fermi energy $\varepsilon_{F\tau}$ from Chapter II is chosen so that the occupation of the states yields the correct particle number N^τ calculated from

$$N^\tau = \int d^3r\, \rho_\tau(r) = \sum_\lambda n_\lambda^\tau \qquad (77)$$

where n_λ^τ is the set of occupation numbers for states ψ_λ^τ, and the sum extends over all states ψ_λ^τ. These occupation numbers are also used in calculating the total density for particles of kind τ,

$$\rho_\tau(r) = \sum_\lambda n_\lambda^\tau |\psi_\lambda^\tau|^2 \qquad (78)$$

The proton and neutron densities are utilized in the next iteration in the density-dependent interaction.

Multipole moments of the total densities are calculated up to order L = 6. The moments of the proton density are used to re-adjust the strengths λ_q, λ_d of the constraint potentials. Also, the fraction of the density to be retained in the next iteration (see Eq. (13)), f, is determined from the

total mass quadrupole moment Q_{2T}:

$$f = f_0 \exp\left(-10 \left| \frac{Q_{2T} - Q^0_{2T}}{Q^0_{2T}} \right| \right) \qquad (79)$$

where f = 0.6. Because $R \propto \sqrt{Q_{2T}}$, Eq. (79) stabilizes the iterations with a cluster separation close to the initial value found from Eq. (55). CHK present a complete discussion of the stabilization of the iterative scheme.

Before the beginning of the next iteration using the new proton and neutron densities and new constraint strengths λ_q and λ_d as input, the cluster potential is calculated as

$$V_{cl} = \sum_{\lambda\uparrow} n^{\tau}_{\lambda} \varepsilon^{\tau\prime}_{\lambda}$$

where

$$\varepsilon^{\tau\prime}_{\lambda} = \varepsilon^{\tau}_{\lambda} - \left(\frac{1}{A} t^{\tau}_{\lambda} + \Delta^{\tau}_{B}(\lambda) - \lambda_q v_{q\lambda} - \lambda_d \langle z \rangle^{\tau}_{\lambda} \right) \qquad (80)$$

The quantities used to find V_{cl} must have the Brueckner rearrangement potential removed and contain no contribution from the quadrupole or dipole constraints, because the cluster potential is defined as

$$V_{cl} \approx H_{TOT} - 2T_{cm} \qquad (81)$$

and the Hamiltonian contains neither Δ_B nor the constraint potentials. After the ion-ion interaction potential V_{cl} has been found, a new iteration begins using the previously calculated neutron and proton densities in the effective single-particle Hamiltonian, with adjusted constraints. This procedure continues until the interaction energy V_{cl} has converged, and the oscillations in the separation distance R have stabilized. For the reaction requiring the largest basis used in this work, $^{16}O + {}^{16}O$ at R = 9.0 fm separation, the cluster potential converged to $\pm$ 0.2 MeV in twenty-five iterations, while the oscillation in R was less than 1%, in agreement with the result of CHK.

The scheme described in the preceding paragraphs pertains to the calculation of V_{c1} for a single given separation distance; to obtain the full curve of V_{c1} vs. R, the procedure listed below is used:

1. For separations $R > R_{\frac{1}{2}}$, the two-cluster initial density distribution is required; V_{c1} is calculated as R is decreased in steps of 0.5 fm;
2. When $R = R_{\frac{1}{2}}$, the one-cluster density distribution is employed; the proper value of the mass ratio parameter z_0 must be used to insure that V_{c1} is continuous at $R_{\frac{1}{2}}$;
3. The parameter set described in the sub-section on initial densities is used for $R \leq R_{\frac{1}{2}}$.

In the parameter set of step 3 above, the last set of contour parameters used is $(\beta_0, z_0, x) = (0, z_0, 0)$, so that the half-density contour is given by

$$\left(\frac{\rho}{s}\right)^2 = 1 - \left(\frac{z}{s}\right)^2 ; \qquad (82)$$

that is, the density distribution for this step is spherical and $R \approx 0$ fm ($Q_{2T} \approx 0$ fm^2). It is obvious from available experimental information that in some reactions $A_1 + A_2$, a spherical density distribution for the fused compound system is not the ground state for that system; for example, in the reaction $^{12}C + {}^{12}C$, the compound nucleus ^{24}Mg is most probably deformed in its ground state. It is likely then that the minimum in some systems may lie at $R > 0$. This is discussed in the next section.

A final topic which merits a brief comment is the technique used to calculate the integrals needed to find the matrix elements of the effective Hamiltonian, and to calculate the density functions. In order for the computer code to be fast and reliable, accurate representations of these matrix elements and functions must be available as finite sums with a small number of terms.

Kolb, Cusson, and Harvey (1973) have investigated this problem, and the fast integration technique is discussed at length in CHK. These authors have used a high-speed Gaussian integration method described by Stroudt and Secrest (1968) to calculate the matrix elements of h_{eff}, as well as the nucleon densities $\rho(r)$. CHK state that these quantities are accurate to one part in one million for an IBM 360-91 in a single precision mode. The accuracy of the calculation discussed in the next section is consistent with their results.

D. Results of the Adiabatic Calculation

In this section, results of the calculation of adiabatic cluster potentials for the reactions $^{4}He + ^{4}He$, $^{12}C + ^{4}He$, $^{14}C + ^{4}He$, $^{16}O + ^{4}He$, $^{12}C + ^{12}C$, and $^{16}O + ^{16}O$ are presented. All of the potentials are shallow (in comparison to, for example, folded potentials (see Chapter VI)) and have a diffuse surface region. Each figure includes a line marking the threshold energy for the reaction, and a curve marked 'V_{CT}'. The threshold is defined as the negative of the sum of the binding energies of the two clusters, determined in separate calculations using the code in a single cluster mode. The curve V_{CT} is the sum of the threshold energy and the Coulomb energy for a system of two point charges Z_1 = number of protons in cluster A_1, and Z_2 = number of protons in cluster A_2, separated by a distance R; that is,

$$V_{CT}(R) = -\left(E_b(A_1) + E_b(A_2)\right) + \frac{Z_1 Z_2 e^2}{R} \qquad (83)$$

Ideally, as the two clusters move sufficiently far apart that the Coulomb and nuclear interactions do not distort them from spherical shape, the cluster potential V_{cl} should merge into V_{CT}. In all of the calculations discussed in this section, V_{cl} and V_{CT} differ by less than 2 MeV for large R. In most cases, the points for large R have errors ($\pm$ 1 MeV) which overlap the V_{CT}

curve; these large error bars reflect convergence problems in the calculations which may be due to limiting the basis size, or (as CHK suggest) may derive from neglecting the exchange part of the center-of-mass kinetic energy. In the present work, the basis size is not varied to improve convergence; rather, it is noted that in the smallest (^{4}He + ^{4}He) and largest (^{16}O + ^{16}O) systems considered, $V_{CT} - V_{cl} \leq 0.5$ MeV for large R. The curves for V_{cl} have been drawn merging smoothly into V_{CT} at large R and points with error bars are not shown except in the case $^{12}C + {}^{12}C \rightleftharpoons {}^{24}Mg$.

The potential is given as a function of the cluster separation R defined in Eq. (55). The sequence of initial density configurations discussed in Section C above has as one of its members the parameter set (β_0, z_0, x) = (1/3, z_0, 1); the value of R at the final iteration using this initial contour is defined as the half-density overlap radius, $R_{1/2}$. The overlap radius is indicated on all the following figures for V_{cl} vs. R. The error bars on $R_{1/2}$ are included to account for the residual oscillations in R and because the two clusters in the half-density contour may overlap slightly, as in Figure 2. Also shown in the figures is the strong absorption radius, R_{SA}. For this work, $R_{SA} = R_{1/2} + 2.5$ fm is used. This definition is not derived from experimental results; it is included to indicate a strong-absorption region (hence the error bars) in which the nuclear interaction begins to dominate the Coulomb forces.

The cluster potential V_{cl} is obtained by using the sequence of contour parameters discussed in Section C up to $R_{1/2}$, then switching to the two-cluster initial density for $R_{1/2}$; a smooth curve is drawn through these points. Some of the figures for V_{cl} include a point with error bars to indicate the typical error in determining V_{cl}. In all cases, the range of V_{cl} depicted by the error bars results from a slow oscillation of the potential about an average value, due to a slow periodic change in the constraint potential. Rather than perform

a larger number of iterations in an effort to decrease the oscillation in V_{cl}, small variations (usually less than 0.2 MeV) are accepted.

The remainder of this section contains the results of the adiabatic calculation for the six reactions included in the study. Wherever possible, the present work is compared to that of other authors.

$^{8}Be \rightleftharpoons {}^{4}He + {}^{4}He$

Figure 4 shows the cluster potential calculated for the adiabatic breakup of ^{8}Be into two α-particles. This system is included in the study to point out possible shortcomings in the adiabatic cluster potentials and to compare to the $^{8}Be \rightleftharpoons \alpha + \alpha$ curve from CHK.

The most obvious discrepancy between the V_{cl} results in Figure 4 and known experimental results is the position of the binding energy of ^{8}Be relative to the calculated $\alpha + \alpha$ threshold energy. The experimental binding energy of ^{8}Be is 56.502 MeV, while twice the experimental binding energy of an α-particle is $2 \cdot (28.297)$ MeV = 56.594 MeV; thus, ^{8}Be is underbound by 92 keV relative to breakup into two α-particles. The apparent overbinding of ^{8}Be in the calculation is due to underbinding of ^{4}He, for which $E_b(^{4}He)$ = 26.83 MeV is found in a separate calculation. This value is similar to that obtained by CHK (26.7 MeV); the small difference can be attributed to the inclusion of the spin-orbit density dependent term in the present work. Relative to the calculated $\alpha + \alpha$ threshold of -53.66 MeV, ^{8}Be appears to be bound by about 2.4 MeV. The quadrupole moment is 42 fm^2, compared to Q_{2T} = 40 fm^2 from Cusson and Lee (1973) and Q_{2T} = 44 fm^2 found by CHK.

At the end of Section B of this chapter, it was predicted that the minimum of V_{cl} should be about 15 MeV deeper than the experimental binding energy of the compound system due to the spurious removal of one kinetic degree of freedom in the single cluster configuration. If the ^{8}Be binding energy discrepancy is removed by shifting the THRESHOLD and V_{cl} curves so

Figure 4. Adiabatic cluster potential for $^{8}Be \rightleftharpoons {}^{4}He + {}^{4}He$ as a function of cluster separation R.

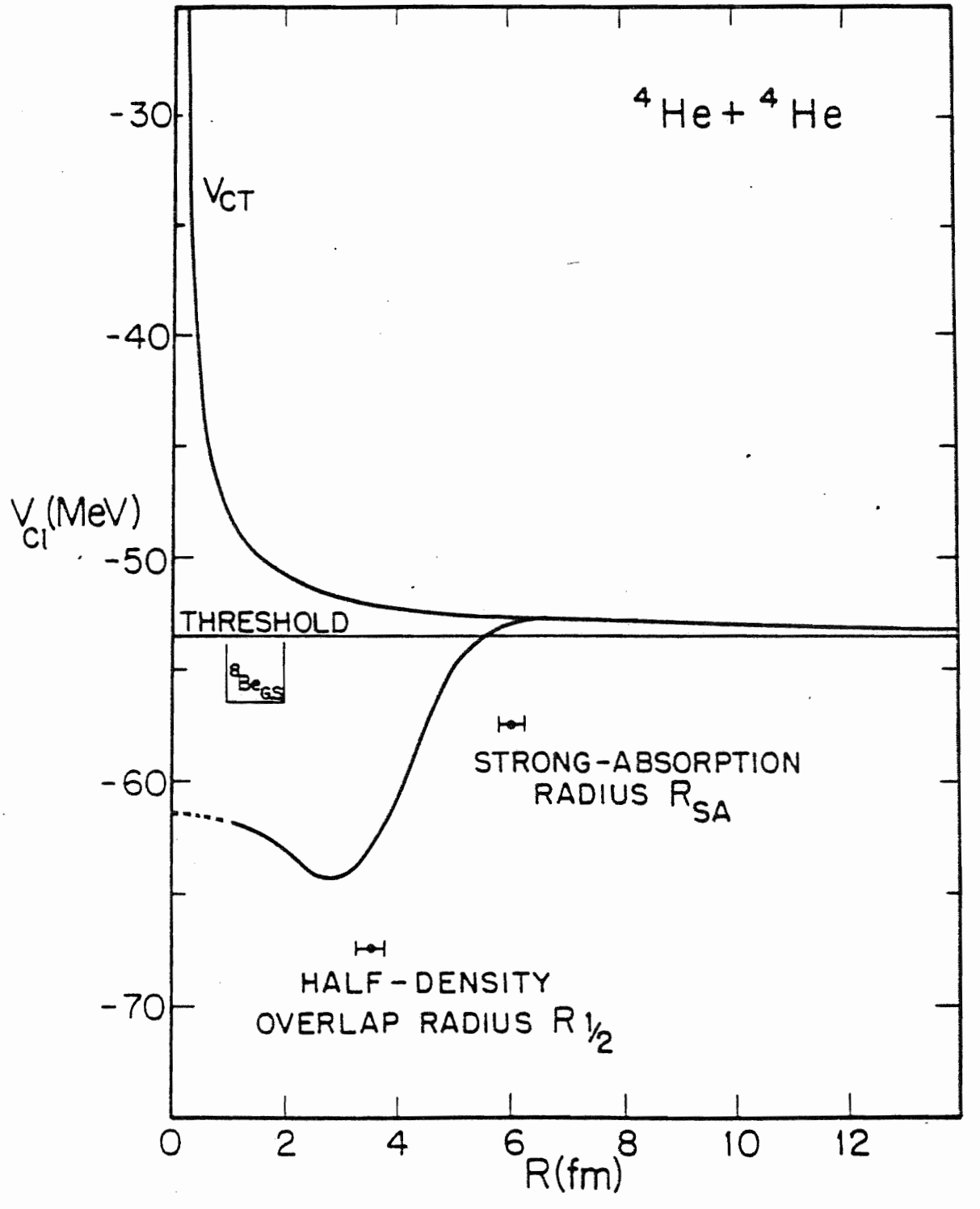
$^4He + ^4He$
V_{CT}
V_{Cl}(MeV)
-30
-40
-50
-60
-70
THRESHOLD
$^8Be_{GS}$
STRONG-ABSORPTION
RADIUS R_{SA}
HALF-DENSITY
OVERLAP RADIUS $R_{1/2}$
0
2
4
6
8
10
12
R(fm)

that THRESHOLD lines up with the ^{8}Be experimental binding energy,* the difference between the minimum of V_{c1} and the ^{8}Be ground state is only about 9 MeV, rather than 15 MeV. This suggests, as noted by CHK, that the subtraction of the spurious kinetic energy should be graduated downward from the predicted 15 MeV for reactions whose fused ground state is not spherical. (The "missing" degree of freedom is only "partially missing.") While several other authors use this method with apparent success, the full subtraction of 15 MeV is retained here for simplicity. This is required to give good agreement between the cluster potential and V_{CT} in the nuclear surface, which is the experimentally accessible region of the nucleus (see discussion in Chapter VI on optical potentials). Further comment on the spurious kinetic energy problem can be found in the summary at the end of this section.

The dashed portion of the curve for V_{c1} indicates that the iterative scheme could not be stabilized in this region, and the dashed line is included to suggest the possible behavior of V_{c1} for a system whose experimental ground state is highly deformed.

$^{16}O \rightleftharpoons {}^{12}C + {}^{4}He$

The results of the calculation for the system $^{12}C + {}^{4}He$ are shown in Figure 5. The initial densities of ^{12}C and ^{4}He in the two-cluster distribution are assumed to be spherical. From earlier Brueckner-Hartree-Fock calculations. (CHK, 1976), the nucleus ^{12}C should be slightly oblate with Q_2 (protons) = -0.16 barns. The spherical minimum in V_{c1} was found by CHK to be a fraction of an MeV higher in energy, with no barrier separating the two shapes (see Figure 2 of CHK). Rather than a somewhat arbitrary choice of the initial

---

*That is, assume that the calculated binding energy of ^{4}He agrees with its experimental value.

Figure 5. Adiabatic cluster potential vs. R for $^{16}O \rightleftharpoons {}^{12}C + \alpha$.

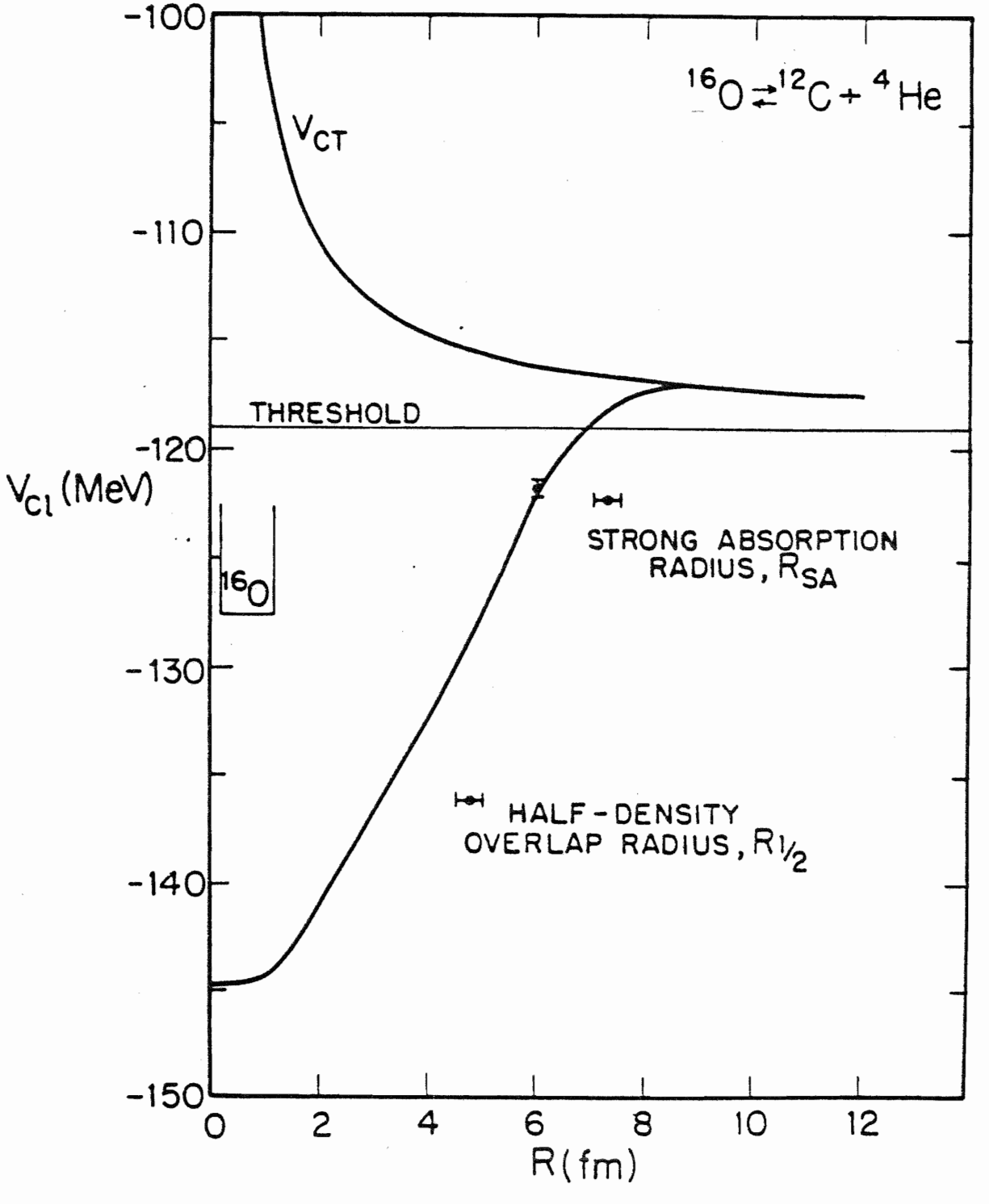
-100
-110
-120
-130
-140
-150
0
2
4
6
8
10
12
R(fm)
V_{cl} (MeV)
$^{16}O \rightleftarrows {}^{12}C + {}^{4}He$
V_{CT}
THRESHOLD
^{16}O
STRONG ABSORPTION RADIUS, R_{SA}
HALF-DENSITY OVERLAP RADIUS, $R_{1/2}$

quadrupole moment for ^{12}C, a spherical shape is imposed in the present work. The total binding energy of ^{12}C is $E_b(^{12}C) = 92.23$ MeV; this value is to be compared to the experimental value of $E_b^{exp}(^{12}C) = 92.17$ MeV, The 60 keV overbinding obtained here contrasts sharply with the difference between $E_b^{exp}(^{12}C)$ and the binding energy found by CHK, $E_b^{CHK}(^{12}C) \approx 82$ MeV. Because the chief difference between the present model and that used by CHK is the spin-orbit density dependent term in the central nuclear potential, the improvement in the binding energy of the light nucleus ^{12}C argues for the use of this div J term in all other systems in this work. The threshold in Figure 5 is -119.06 MeV, nearly 9 MeV deeper than the threshold of CHK.

This shift of the threshold also provides an opportunity to test the effect of the spin-orbit density dependent potential on a spherical closed-shell nucleus, for which the div J contribution should vanish. In their work, CHK report that the experimental binding of ^{16}O is about 17.5 MeV above the minimum of the $^{12}C + \alpha$ cluster potential (close to the 15 MeV difference predicted above). In the present calculation the threshold is some 9 MeV deeper than their value; if the potential found in this work were obtained by merely shifting the entire CHK curve to the -119.06 MeV threshold found here, then the minimum of V_{cl} in Figure 5 would fall at about -153 MeV. This shift would make the difference between $E_b^{exp}(^{16}O)$ and the minimum more than 25 MeV, considerably more than the 17.5 MeV of CHK or 15 MeV expected from previous arguments. However, Figure 5 shows that the minimum of V_{cl} occurs at -145 MeV, exactly as it did in the CHK work. The conclusion is that the div J term has no effect on the closed shell compound nucleus ^{16}O and becomes important only when ^{16}O begins to break up into $^{12}C + \alpha$, thereby allowing a smooth transition from the correct minimum energy to V_{CT}, which has a lower threshold. Additional evidence for $\langle \text{div } J \rangle = 0$ in ^{16}O is provided in the discussion of the $^{16}O + \alpha$

Figure 6. Total density profiles along the z-axis for $^{12}C + \alpha$. Each profile is labelled by the corresponding cluster separation.

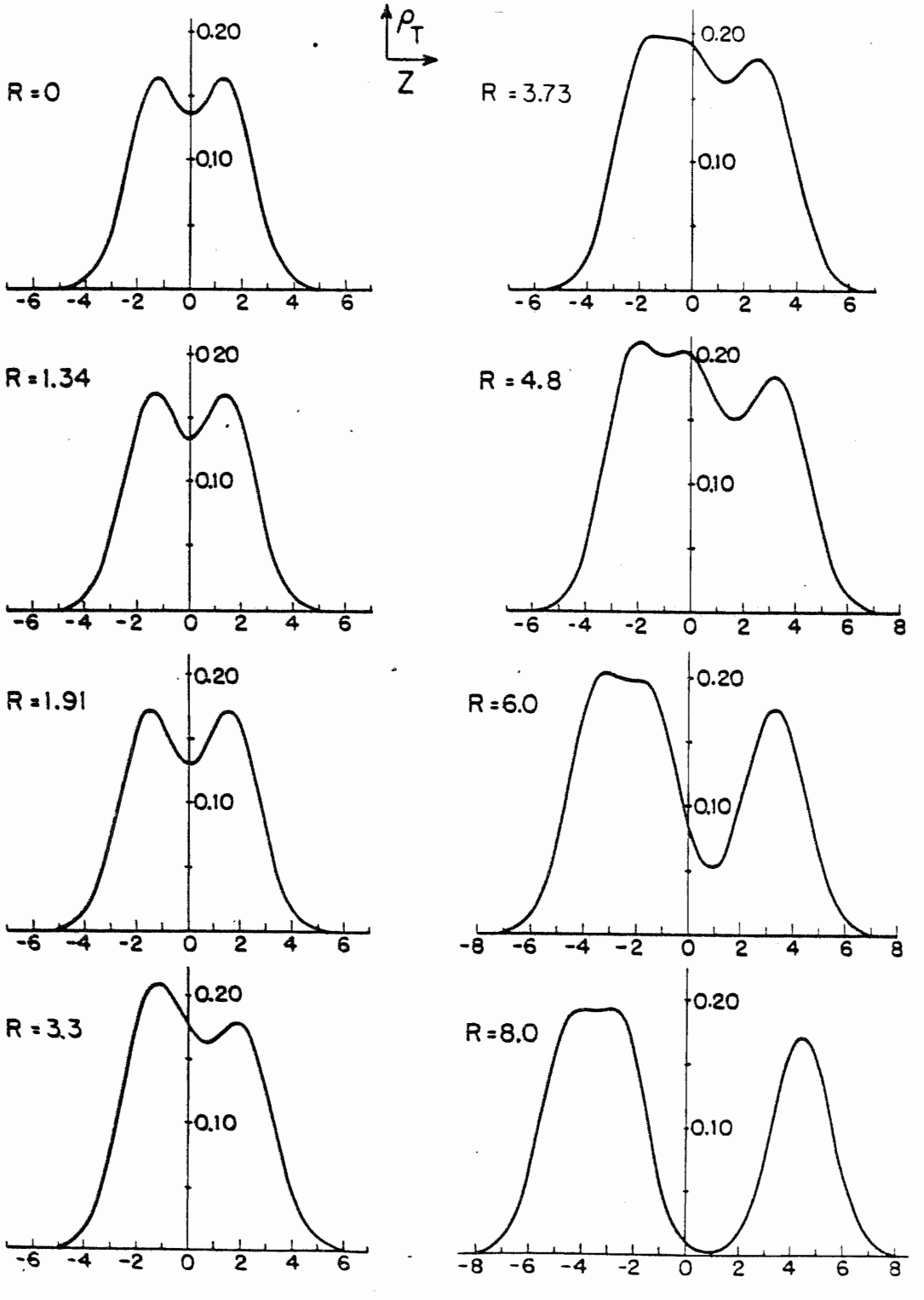
ρ_T
Z
R = 0
R = 1.34
R = 1.91
R = 3.3
R = 3.73
R = 4.8
R = 6.0
R = 8.0
0.20
0.10
-6 -4 -2 0 2 4 6
-8 -6 -4 -2 0 2 4 6 8

cluster potential, where the binding energy of a spherical ^{16}O nucleus is given as $E_b(^{16}O)$ = 129.4 MeV, the same as that obtained by CHK with no div J term in the Hamiltonian.

The other features of the $^{12}C + \alpha$ V_{cl} curve are quite similar to those of the CHK curve. V_{cl} varies smoothly from R = 0 fm to R = 8 fm, where $V_{cl} \approx V_{CT}$. One point with error bars, at R = 6.0 fm, is included to indicate the typical convergence error in the calculation of V_{cl}. The potential is somewhat more diffuse than the CHK curve because the improved binding energy of the ^{12}C fragment pulls the threshold down, while the minimum remains fixed at -145 MeV. This leads to the major difference between Figure 5 and the same potential from CHK: the position of the half-density overlap radius $R_{1/2}$ moves from 4.2 fm in CHK to 4.8 fm in this work.

A series of density profiles for the $^{12}C + \alpha$ reaction are shown in Figure 6. Each of the curves is the total mass (neutron plus proton) density from a cut taken along the z-axis of the system; each profile is labelled by the cluster separation for that profile. The profile for R = 0 shows that R = 0 does not imply two unperturbed clusters have been placed at the origin; the central density is 0.14 nucleons/fm^3, while the maximum density at the symmetrical peaks is $\lesssim$ 0.17 nucleons/fm^3. This is the density distribution corresponding to the minimum in V_{cl} and is obtained from (β_0, z_0, x) = (0, 0.18, 0). The next profile, for R = 1.34 fm, resulted from the initial contour parameter set (0.1, 0.18, 0). The symmetrical deformation (x = 0) of ^{16}O continues for the R = 1.91 fm point where β_0 = 0.2. The fourth profile, for R = 3.3 fm, is from the deformed parameter set (1/3, 0.18, 0.4). The center of mass of this distribution is located at the origin; the smaller peak on the right is the α-particle, and the ^{12}C distribution has a central density ~0.21 nucleons/fm^3. This is an unusually large central density for ^{12}C relative to

the value of 0.155 nucleons/fm^3 used to parameterize the code (Cusson, et al., 1976). The same central density is found for ^{12}C fragments emerging from ^{24}Mg, discussed later in this chapter. The progression of curves in Figure 6 allows one to follow the adiabatic breakup of ^{16}O into $^{12}C + \alpha$, where the final curve at R = 8.0 fm shows the two fragments well separated. The central density of the ^{12}C cluster is now ~0.19 nucleons/fm^3.

$^{18}O \rightleftharpoons {}^{14}C + {}^{4}He$

Figure 7 shows the cluster potential energy V_{cl} for ^{18}O breaking up into $^{14}C + \alpha$. The curve depicts a spherical ^{18}O compound system with the minimum of V_{cl} at -160 MeV. The experimental binding energy of ^{18}O is $E_b^{exp}(^{18}O)$ = 139.8 MeV, slightly more than 20 MeV above the minimum. From the argument in the discussion of $^{8}Be \rightleftharpoons \alpha+\alpha$, a potential leading to a spherical ground state is expected to give a difference $E_b^{exp}(^{18}O) - V_{cl}$ of 15 MeV. The 20 MeV difference found here suggests that V_{cl} is too deep and might actually be better represented by a potential with a deformed ground state, as in the $^{8}Be \rightleftharpoons \alpha+\alpha$ potential. In fact the spherical ground state of ^{18}O has been obtained using a pairing gap Δ_0 =6.0 MeV, instead of Δ_0 = 0.12 MeV used in the adjacent $^{16}O \rightleftharpoons {}^{12}C + \alpha$ system. This large Δ_0 was chosen to obtain an ^{18}O ground state with $Q_{2T} \sim 0$, primarily because the ground state quadrupole moment of ^{18}O is not well established experimentally. While the two neutrons outside the ^{16}O core might be expected to give some non-zero deformation, the small electric quadrupole moment Q_2/e = -0.026 barns suggests only a slight oblate shape for the protons. In the absence of better evidence for a non-zero value of Q_{2T}, and assuming that the proton and neutron density distributions are qualitatively similar, a spherical ^{18}O was used in this calculation. No further study of the dependence

Figure 7. Adiabatic cluster potential vs. R for $^{18}O \rightleftharpoons {}^{14}C + \alpha$.

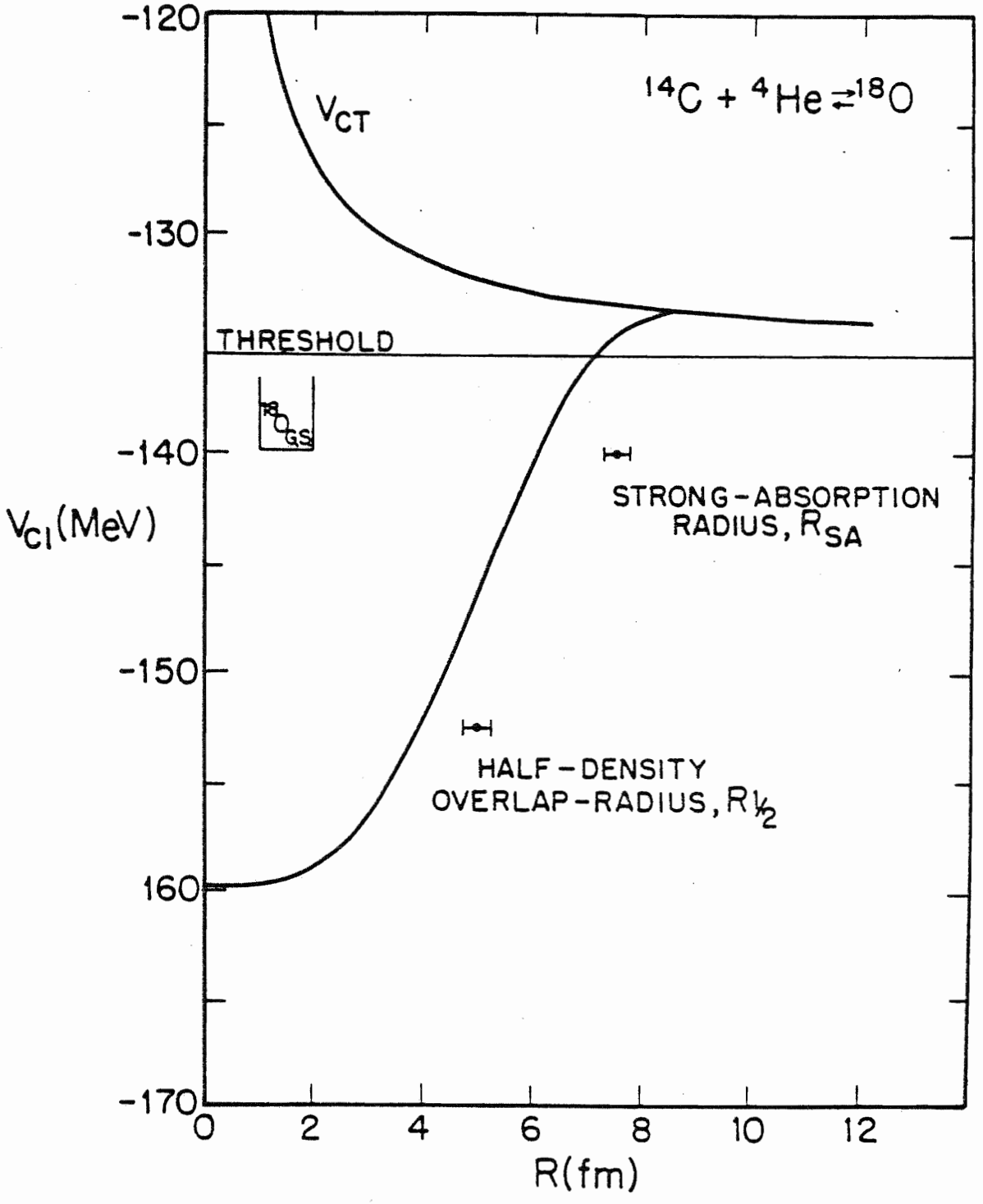
-120
-130
-140
-150
160
-170
0
2
4
6
8
10
12
R(fm)
V_{CI}(MeV)
V_{CT}
$^{14}C + {}^{4}He \rightleftarrows {}^{18}O$
THRESHOLD
$^{18}O_{GS}$
STRONG-ABSORPTION RADIUS, R_{SA}
HALF-DENSITY OVERLAP-RADIUS, $R_{1/2}$

of the ground state deformation on the pairing gap Δ_0 was performed.

The half-density overlap radius at $R_{1/2}$ = 5.0 fm is only slightly larger than that of the $^{12}C + \alpha$ system. This difference can be accounted for completely by the difference in radii of ^{14}C and ^{12}C obtained from the liquid drop formula $R = 1.25\ A^{1/3}$. Once again, the strong absorption radius falls in the region where V_{cl} begins to deviate from V_{CT}.

$^{20}Ne \rightleftharpoons {}^{16}O + {}^{4}He$

Figure 8 contains the adiabatic cluster potential for ^{20}Ne breaking up into two asymptotically spherical clusters ^{16}O and ^{4}He. The mass asymmetry ratio parameter is z_0 = 0.23 for the proper ratio of the masses of the separating fragments.

The minimum in V_{cl} corresponds to a prolate ground state for ^{20}Ne, with $Q_{2T} \approx 83\ fm^2$. This value of Q_{2T} compares favorably to the values obtained previously using similar models ((CHK, 1976), (Lee and Cusson, 1972)). In Figure 9 a plot of the total interaction energy of the system V_{cl} vs. β_2(protons) shows the minimum at -175 MeV for β_2(protons) $\approx$ 0.34. For negative values of β_2(protons) less than β_2 = -0.1, there is a second minimum in the potential surface. This could suggest an excited state of ^{20}Ne which is slightly oblate, or that the ground state of ^{20}Ne has a non-axial shape with a minimum in the potential energy surface for $\gamma \neq 0$ in the β-γ plane of deformation angles. This argument, advanced by CHK to explain an oblate second minimum for ^{24}Mg, is a possible explanation of Figure 9. It is also possible that the second minimum represents an excited state of ^{24}Mg.

The threshold energy of the present calculation is -156.23 MeV, from $E_b(^{16}O)$ = 129.4 MeV and $E_b(^{4}He)$ = 26.83 MeV. The binding energy of ^{16}O agrees very well with the value extracted from Figure 4 of CHK and is slightly greater than the experimental value of 127.62 MeV. Also, in CHK the difference

Figure 8. Adiabatic cluster potential vs. R for $^{20}Ne \rightleftharpoons {}^{16}O + \alpha$.

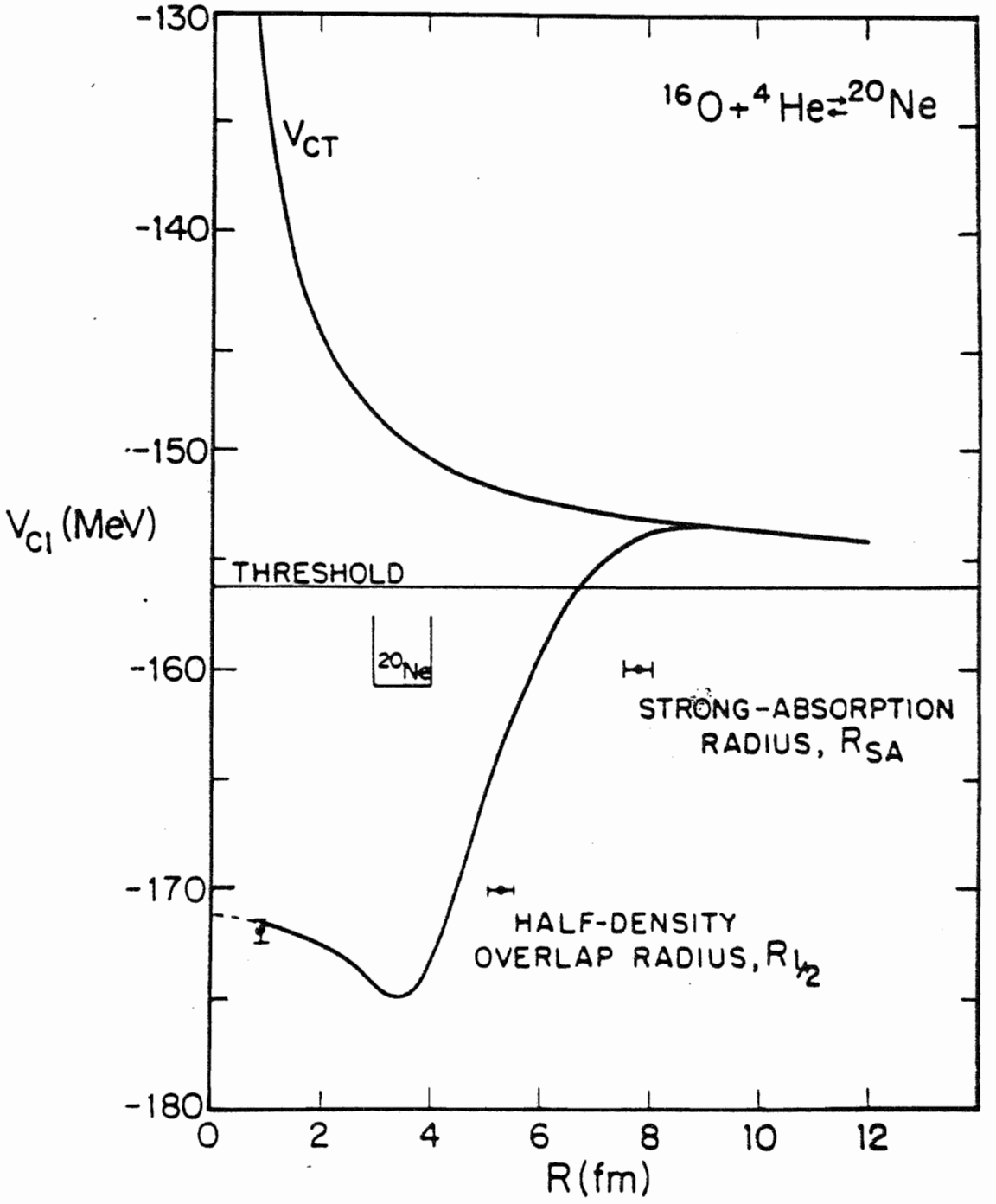
$^{16}O+^{4}He \rightleftarrows ^{20}Ne$
V_{CT}
V_{Cl} (MeV)
THRESHOLD
^{20}Ne
STRONG-ABSORPTION RADIUS, R_{SA}
HALF-DENSITY OVERLAP RADIUS, $R_{1/2}$
-130
-140
-150
-160
-170
-180
0
2
4
6
8
10
12
R(fm)

between $E_b^{exp}(^{20}Ne)$ and the minimum of V_{cl} is only about 8 MeV. The same quantity for the present calculation is 14 MeV. In the discussion of the $^8Be \rightleftharpoons \alpha+\alpha$ potential, it was suggested that a system whose ground state is deformed should have a graduated amount of the spurious 15 MeV relative motion kinetic energy removed, depending upon the deformation of the compound system. The 8 MeV difference found by CHK supports this argument,* while the present work requires the subtraction of nearly 15 MeV from $E_b^{exp}(^{20}Ne)$ to obtain the minimum of V_{cl}. This does not agree with the result from the $\alpha + \alpha$ reaction. Further comment on this problem will be given in the summary at the end of this chapter. The change in the depth of V_{cl} from -170 MeV with the CHK model to -175 MeV in the present model is due to the spin-orbit density dependent term in the Hamiltonian. This provides further evidence that the div J term becomes important in non-closed-shell nuclei for determining correct ground state energies.

The other features of the curve are similar to the CHK results. The half-density overlap radius is about $R \simeq 5.3$ fm, and $R_{SA} \simeq 7.8$ fm, which is once again in the region where $V_{cl} \simeq V_{CT}$. The diffuseness of the potential is decreased compared to the CHK curve because the potential in Figure 8 is deeper than the CHK cluster potential, while the thresholds are nearly equal in the two cases. The error bar at R = 0.9 fm indicates some instability in the convergence of the iterative procedure. The dashed part of the curve is included in the figure to suggest the form of V_{cl} for $R \lesssim 0.9$ fm, although no data is available in this region. An attempt to calculate V_{cl} with $(\beta_0, z_0, x) = (0, 0.23\ 0)$ gave an oblate shape for

---

*CHK explain this apparent underbinding of ^{20}Ne as partly due to a zero-point rotational energy of the deformed compound state. The binding energy calculated here is $E_b = 158.5$ MeV, while $E_b^{exp}(^{20}Ne) = 160.7$ MeV.

Figure 9. Total interaction energy, V_{c1}, vs. β_2(protons) for $^{20}Ne \rightleftharpoons {}^{16}O + \alpha$.

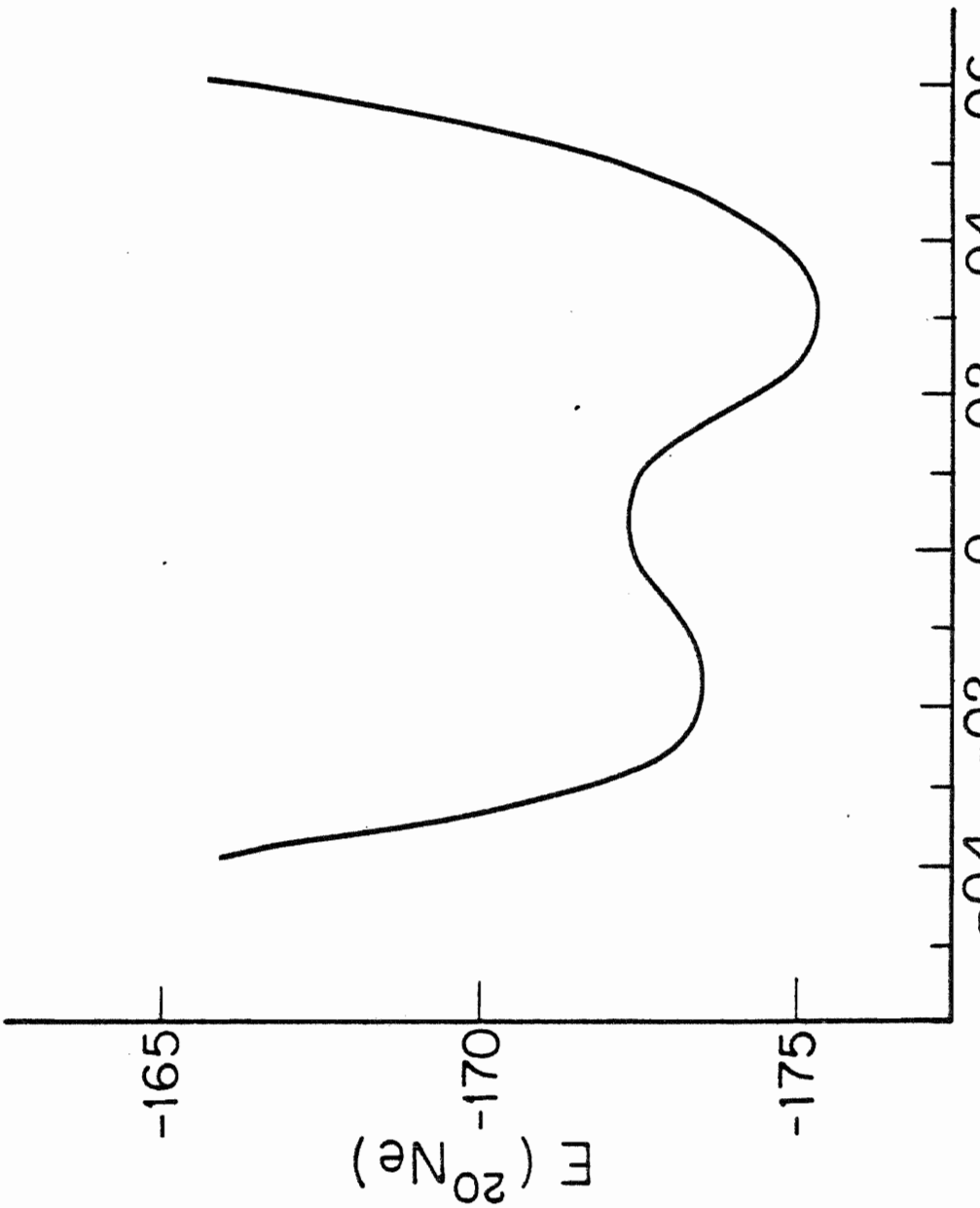
-165
-170
-175
E (^{20}Ne)
-0.4
-02
0
0.2
0.4
0.6
β_2 (protons)

^{20}Ne for which $R = \sqrt{Q_{2T}/2\mu}$ is not defined. The calculated value of the cluster potential for this initial contour parameter set is V_{cl} = -172.4 MeV, with β_2(protons) = -0.02. This point is on the shoulder of the V_{cl} vs. β_2(protons) curve in Figure 9.

$^{24}Mg \rightleftharpoons {}^{12}C + {}^{12}C$

In the calculation of the adiabatic cluster potential for $^{24}Mg \rightleftharpoons {}^{12}C + {}^{12}C$ shown in Figure 10, two spherical ^{12}C clusters are used as input densities for large R. The curve does not merge completely into V_{CT} in the strong absorption region, as in previously discussed cases, but falls about 1 MeV below V_{CT}. Calculations with a larger basis have failed to resolve this problem; another possible source of the disagreement is the neglect of the exchange term of the relative motion kinetic energy (see CHK).

The minimum of V_{cl} occurs at R = 3.0 fm, corresponding to Q_{2T} = 108 fm^2. This is somewhat smaller than the values found by CHK and by Lee and Cusson (1972); the reason for the smaller value is discussed below. The threshold is about 20 MeV deeper than the CHK threshold due to the improved binding energy in ^{12}C. This shift eliminates from the present work the underbinding of ^{24}Mg seen by CHK. The difference between the minimum in V_{cl} and $E_b^{exp}(^{24}Mg)$ is $\sim$ 17 MeV. CHK obtained a value of $\sim$5 MeV for this quantity. The 17 MeV difference strengthens the conclusion reached for the $^{16}O + {}^{4}He$ reaction that the cluster potential overbinds the compound system by about 15 MeV.

The cluster potential of the deforming ^{24}Mg compound system is shown in Figure 11 as a function of the quadrupole deformation parameter of the proton density, β_2(protons). The prolate minimum is located at β_2(protons) = 0.38; an oblate second minimum is found at β_2(protons) = -0.25,

Figure 10. Adiabatic cluster potential vs. R for $^{24}Mg \rightleftharpoons {}^{12}C + {}^{12}C$.

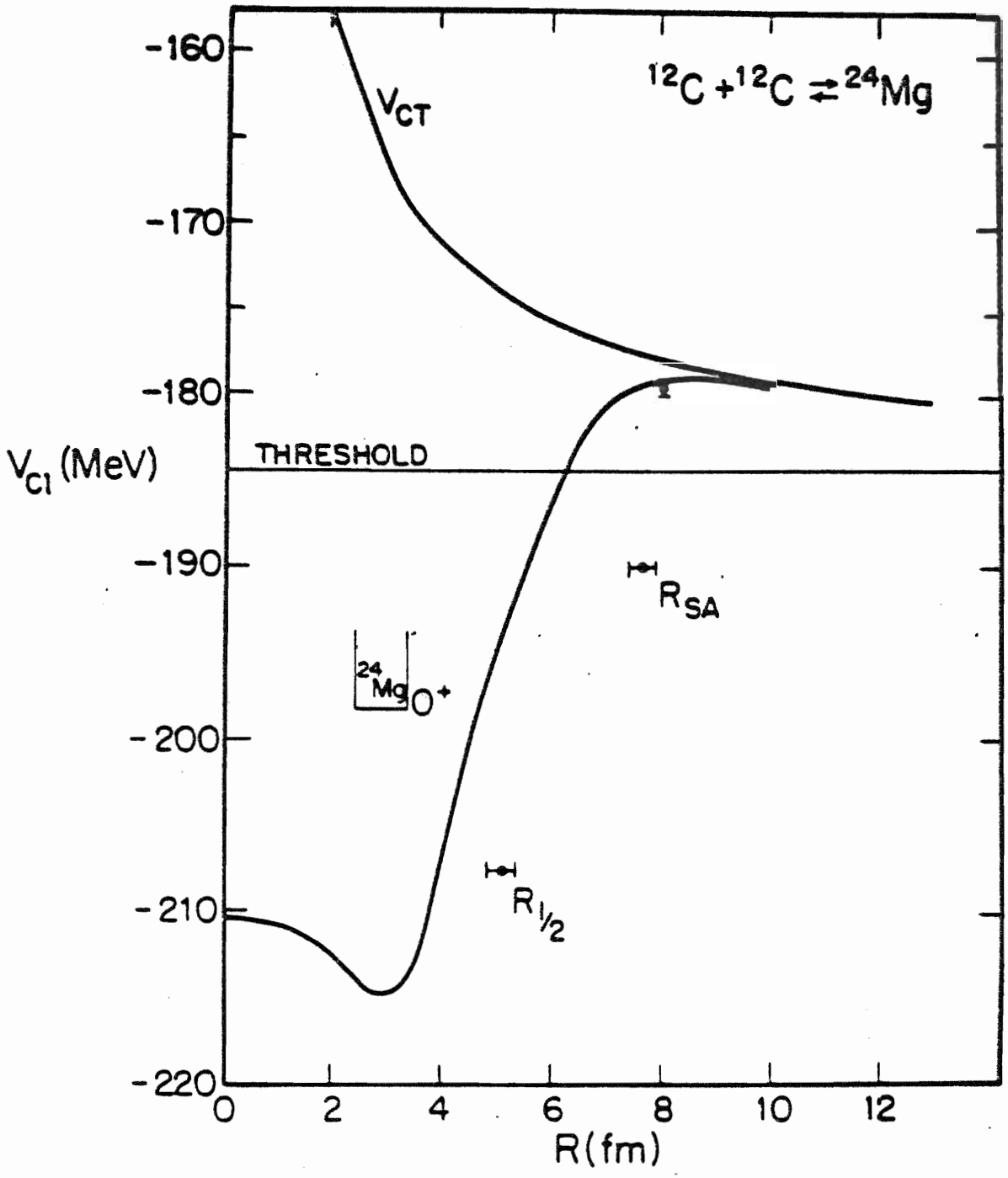
-160
-170
-180
-190
-200
-210
-220
V_{C1} (MeV)
V_{CT}
$^{12}C + ^{12}C \rightleftarrows ^{24}Mg$
THRESHOLD
R_{SA}
^{24}Mg 0^+
$R_{1/2}$
0
2
4
6
8
10
12
R(fm)

about 4 MeV above the prolate minimum. This is quite similar to the result obtained by CHK. Therefore, the present result is consistent with the conclusion by Cusson and Lee (1973) on the non-axial nature of the ^{24}Mg ground state.

A final point of comparison between the V_{cl} in Figure 10 and the same quantity from CHK lies in the agreement of the points "extracted from experiment" and supplied to CHK by G.R. Satchler of Oak Ridge National Laboratory. These points give the real part of the optical potential found in fitting experimental data (see Figure 5 of CHK). CHK state that their cluster potential is about 0.8 fm too large in radius in the tail region compared to Satchler's optical potential. This large difference in the radius of the potential would lead to poor fits to data when used in an optical model. CHK state that the rms charge radius of each of the ^{12}C clusters is about $r_{ch} = 2.75$ fm, compared to the experimental value of $r_{ch}(exp) = 2.45$ fm; they conclude that the 0.6 fm error in the rms charge radii for the two nuclei might explain most of the 0.8 fm shift needed to match Satchler's curve. In the present work, the rms charge radius of ^{12}C is $r_{ch} = 2.49$ fm, so that difference in twice the calculated rms charge radius and twice the experimental value is just 0.08 fm! A visual comparison of the slopes of V_{cl} from Figure 10 and Satchler's optical potential from CHK shows that the present result agrees well with the experimentally derived optical potential, especially in the tail region. If the points of Satchler shown in Figure 5 of CHK are renormalized by setting the CHK threshold equal to the present threshold, very good agreement between V_{cl} and the optical potential is found throughout the region $4.0 \text{ fm} < R < R_{SA}$.*

---

*It is assumed here that Satchler's data are normalized to the CHK V_{cl} curve by setting $V_{opt}(R_{SA}) = V_{CT}$.

Figure 11. Total interaction energy, V_{c1}, vs. β_2(protons) for $^{24}Mg \rightleftharpoons {}^{12}C + {}^{12}C$.

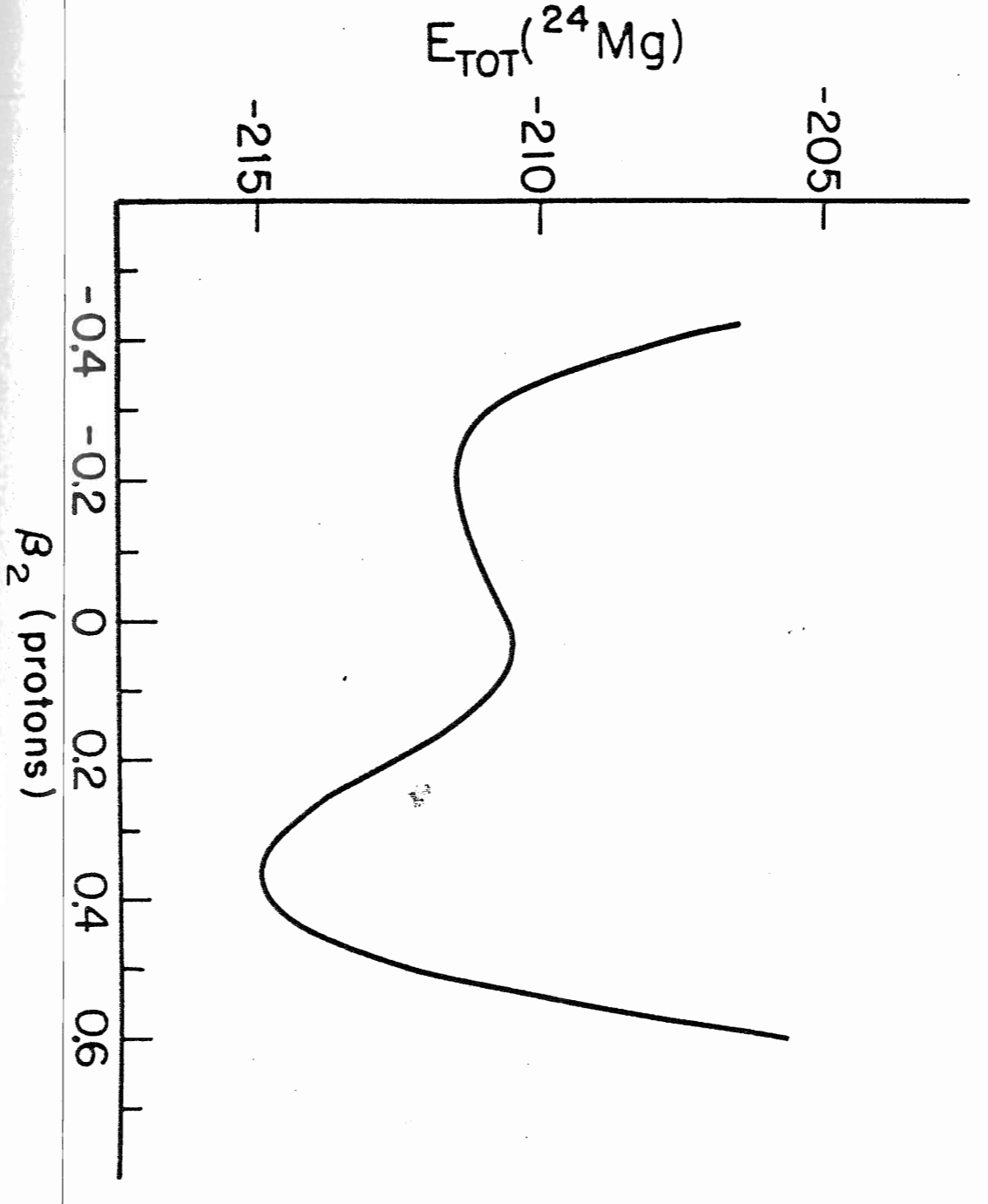
$E_{TOT}(^{24}Mg)$
-215
-210
-205
-0.4
-0.2
0
0.2
0.4
0.6
β_2 (protons)

$^{32}S \rightleftharpoons {}^{16}O + {}^{16}O$

Figure 12 is a plot of the adiabatic cluster potential vs. R for the break-up of ^{32}S into two spherical ^{16}O clusters. The threshold energy in the figure is -258.8 MeV; this is slightly deeper than the value obtained by CHK. The increased over-binding of the two ^{16}O clusters is due to the inclusion of the spin-orbit density dependent potential.

The most dramatic difference between the present result and that obtained by CHK is that the minimum in V_{cl} now occurs at R = 0, whereas CHK found that V_{cl} was a minimum at R = 2.5 fm. The discrepancy between the two curves may be explained by the remark of CHK that their curve probably corresponds to an excited band rather than the ground state of ^{32}S. The present curve is believed to be that for fusion of two ^{16}O ions into the ground state of the compound ^{32}S system. Further discussion of the minimum of V_{cl} is given below.

The occurrence of the second minimum at R $\simeq$ 4.5 fm in Figure 12 agrees with the results of CHK as well as other authors (Zint and Mosel, 1976). The remark by CHK that the height of the barrier between the ground state minimum and the second minimum is sensitive to the pairing gap parameter Δ_0 is born out in these results. The barrier shown here is really just a shoulder, whereas CHK report a barrier height of about 1 MeV. As observed in many other reports (CHK, (Zint and Mosel, 1976), (Zint and Mosel, 1975), (Krieger and Wong, 1972)), the second minimum results from crossings of the single-particle levels as the two ^{16}O ions approach and finally fuse into ^{32}S.

The cluster potential energy is shown as a function of the quadrupole deformation parameter for protons β_2(protons), in Figure 13. The shoulder of the second "minimum" occurs at β_2(protons) = 0.6 - 0.7, indicating a highly deformed configuration. CHK report that their results suggested that the

Figure 12. Adiabatic cluster potential vs. R for $^{16}O + {}^{16}O \rightleftharpoons {}^{32}S$.

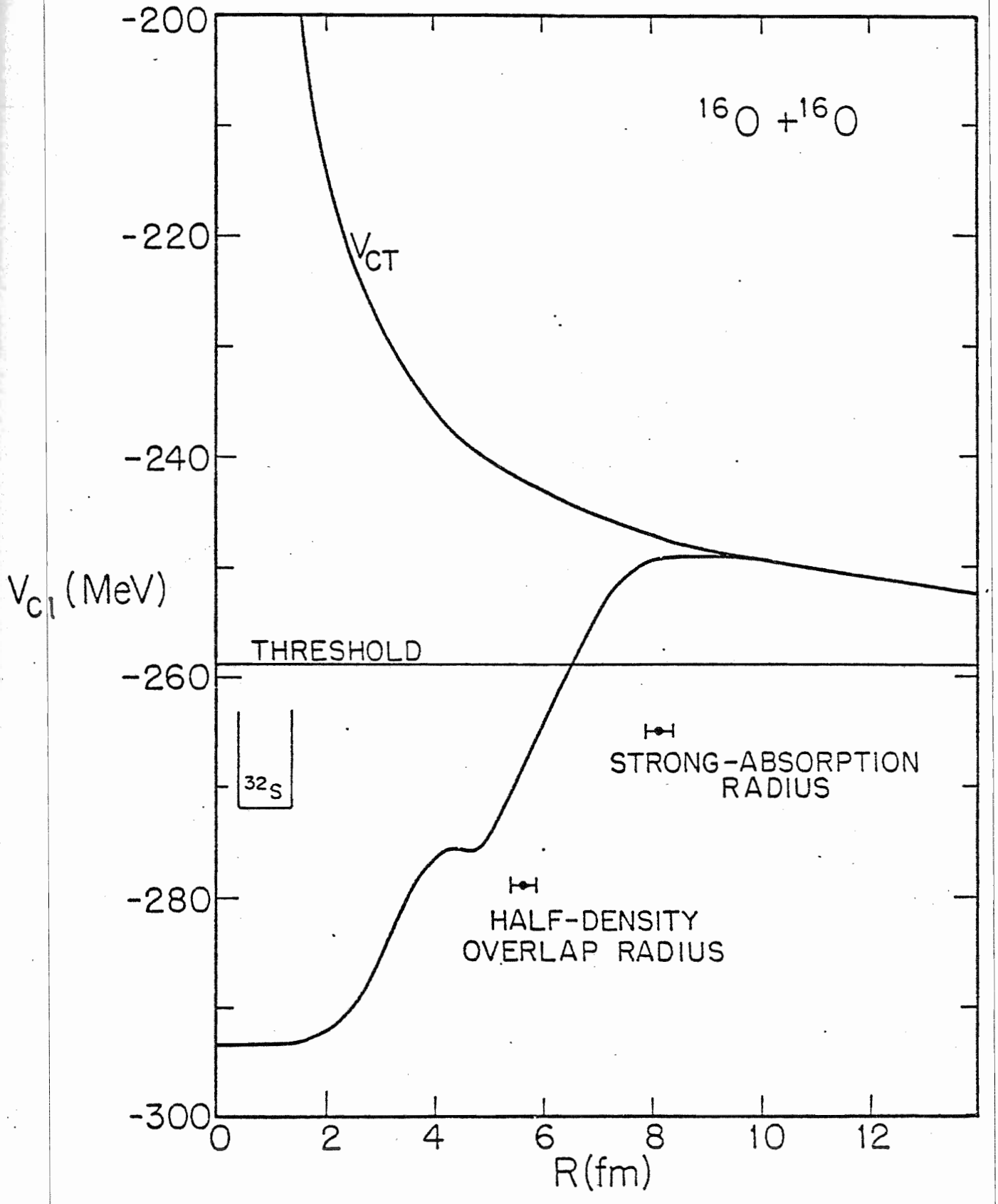
-200
-220
-240
-260
-280
-300
0
2
4
6
8
10
12
R(fm)
V_{cl} (MeV)
$^{16}O + ^{16}O$
V_{CT}
THRESHOLD
^{32}S
STRONG-ABSORPTION RADIUS
HALF-DENSITY OVERLAP RADIUS

Figure 13. Total interaction energy, V_{c1}, vs. β_2(protons) for $^{32}S \rightleftharpoons {}^{16}O + {}^{16}O$.

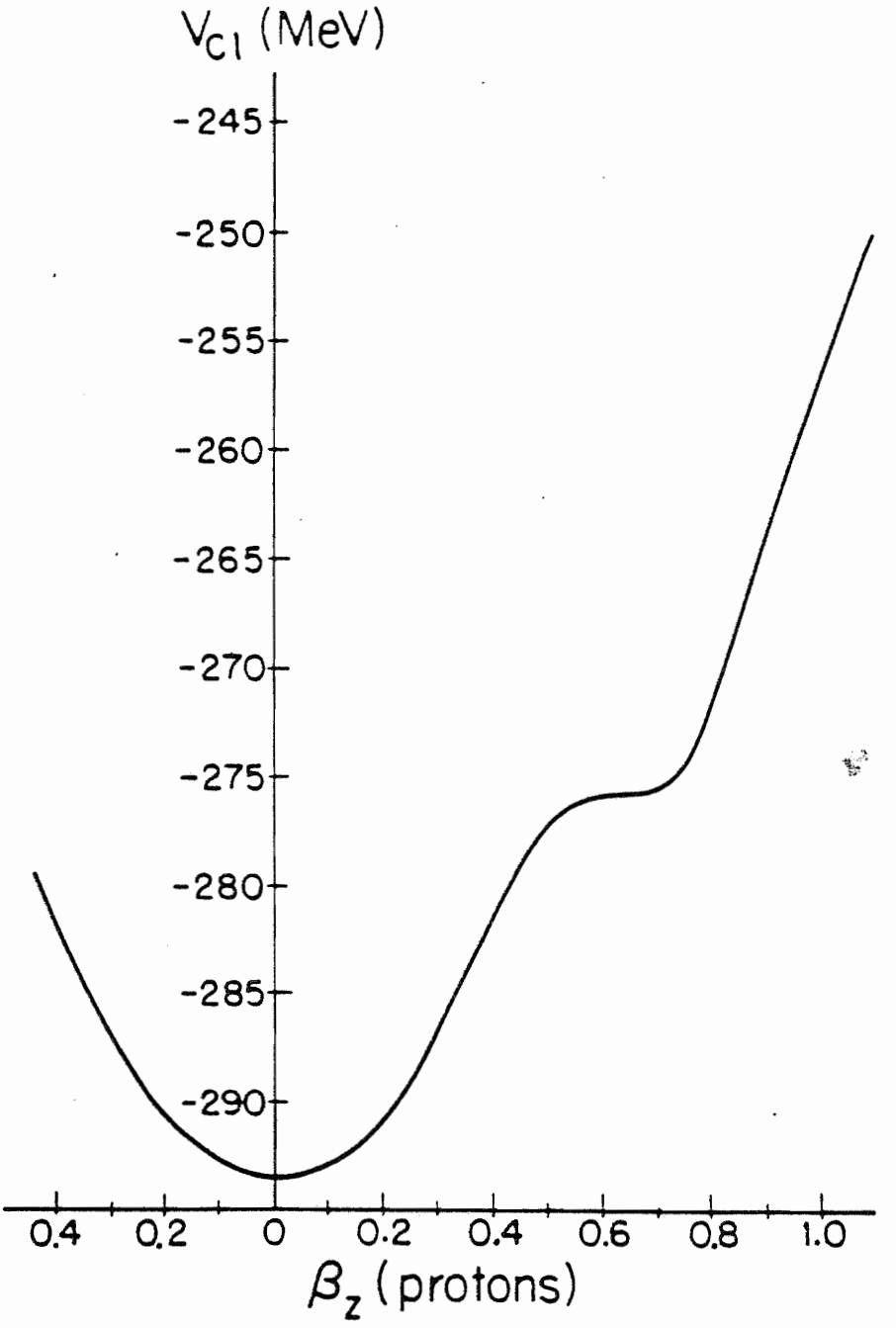
V_{C1} (MeV)
-245
-250
-255
-260
-265
-270
-275
-280
-285
-290
0.4
0.2
0
0.2
0.4
0.6
0.8
1.0
β_z (protons)

ground state of ^{32}S was slightly oblate, in agreement with the previous Hartree-Fock calculation of Cusson and Lee (1973). The $\beta_2 < 0$ portion of the V_{cl} vs. β_2 curve was not explored in detail, but the minimum of V_{cl} clearly occurs for β_2(protons) = 0 . The cluster potential energy as a function of the quadrupole deformation parameter was not studied; however, an inspection of the neutron density distribution shows no deformation of the density and therefore, the ground state of the system is assumed to be spherical. It should be noted that the experimental electric quadrupole moment of ^{32}S is about 47 fm^2, in disagreement with the spherical result found here.

The experimental binding energy of ^{32}S lies about 20 MeV above the minimum of V_{cl}. This difference is not inconsistent with the spurious 15 MeV difference expected from previous discussion. The half-density overlap radius lies at $R_{\frac{1}{2}} \simeq 5.6$ fm and $R_{SA} \simeq 8.2$ fm. The cluster potential merges smoothly into V_{CT} in the strong absorption region. The total density distribution (not shown here) for separations $R > R_{SA}$ shows very little deformation.

Summary

Earlier in this chapter, it was pointed out that the removal of the cluster kinetic energy T_{cl} from the total Hamiltonian was unnecessary for completely fused systems. While the removal provides good agreement between V_{cl} and V_{CT} for large values of R, it also causes a shift of the minimum in V_{cl} to values much lower than the experimental binding energy of the compound system. In the case of $^{8}Be \rightleftharpoons \alpha + \alpha$, this spurious shift is only 9 MeV rather than the 15 MeV expected from previous arguments. On the other hand, the results for the deformed cases $^{20}Ne \rightleftharpoons {}^{16}O + \alpha$ and $^{24}Mg \rightleftharpoons {}^{12}C + {}^{12}C$

suggest that the incorrectly removed energy is the full 15 MeV from T_{cl}. CHK conclude from their $\alpha + \alpha$ results that a graduated removal of T_{cl} is necessary for systems whose minimum in V_{cl} corresponds to a deformed system. However, as mentioned previously, Eq. (48) is used to define V_{cl}, and no provision for a graduated removal of T_{cl} is used.

One possible approach to the removal of spurious kinetic energy is that described by Zint and Mosel (1975); they correct the total energy using the expression (in the case of $^{32}S \rightarrow {}^{16}O + {}^{16}O$):

$$T_{corr} = T_{sp}(\infty) \frac{T(R) - T(^{32}S)}{T(\infty) - T(^{32}S)}$$

where T(R) is the total kinetic energy at a cluster separation R, and T_{sp} (∞) is the spurious energy for large separations. $T(^{32}S)$ is the kinetic energy of ^{32}S in its ground state. From the above expression, $T_{corr} = 0$ at that value of R for which $T(R) = T(^{32}S)$. This is commensurate with the observation made above that the minimum is too deep by the (spurious) value $T_{cl} \approx 15$ MeV. If the expression of Zint and Mosel were applied to the deformed cases of ^{20}Ne or ^{24}Mg, then $T(R) = T(^{20}Ne$ or $^{24}Mg)$ for $R \neq 0$, and this prescription would lead to more realistic calculated minima in V_{cl}. The simple prescription of Eq. (48) is used here with the recognition that further corrections to the kinetic energy removal are necessary for small values of R.

Finally, it would be appropriate here to compare the potential energy curves of this section with potentials used to fit experimental data, as in the optical model. However, such a comparison deserves more than a passing comment; Chapter VI is devoted to such a discussion.

CHAPTER V

CALCULATION OF THE SUDDEN POTENTIAL

A. Why Calculate a Sudden Potential?

The calculation of the cluster potential in the sudden approximation is presented in this chapter. The sudden approximation consists in the assumption that the time involved in the collision of the two ions is much smaller than the orbiting time of nucleons in each cluster. The nucleons therefore have insufficient opportunity to rearrange themselves, as allowed in the adiabatic approximation. As in the latter case, the physical situations in heavy-ion collisions to which the sudden approximation applies should be investigated.

The simplest situation to consider is the elastic collision of two heavy ions with large center-of-mass kinetic energy. If the incident energy is large enough, the incident kinetic energy per nucleon t_{inc} can exceed the intrinsic kinetic energy (which averages about 15 MeV (CHK, 1976)) associated with the orbiting nucleons t_{orb}. For $t_{inc} > t_{orb}$, the incident nucleons have time to interact before rearrangement occurs; hence, one expects that the density of the composite system would be nearly the sum of the densities of the separate fragments, provided that the bombarding energy is well above the Coulomb barrier. Because the K-matrix model used here is density-dependent, it is possible for the cluster potential in the sudden approximation to differ greatly from the adiabatic potential; the repulsive short-range terms which arise from the hard-core of the nucleon-nucleon interaction should produce a potential which resembles the Lennard-Jones potential of molecular physics (Slater, 1963). Further changes in V_{cl} are due to the kinetic energy which, in

a Thomas-Fermi approximation increases rapidly as the ions overlap (Fleckner and Mosel, 1977). This problem will be discussed in Section C below. The results of Brink and Stancu (1975) for heavy-ion collisions with $E_{cm} \neq 0$ indicate that a hard or soft core may develop in the interior region of the potential; the slope of the potential near the core radius increases as the center-of-mass bombarding energy increases.

There are of course other reaction channels which might be described in the context of the sudden approximation; however, because this work is limited to a consideration of elastic scattering, discussion of the application of the results obtained here will be restricted to that case. The possible value of the sudden potential in interpreting elastic scattering data at high energies is indicated by Vary and Dover (1974) who point out the increasing importance of the surface and interior region of the target nucleus (and hence, the potential) at higher bombarding energies ($>$ 50 MeV/nucleon), based on their calculation using an impulse approximation.

In the remainder of this chapter, three attempts to calculate the sudden cluster potential are examined. Section B contains a discussion of the two abortive calculations. In Section C, the overlap techniques finally used to produce the potentials presented in Section D are developed.

B. Abortive Attempts to Calculate the Sudden Cluster Potential

The first attempt to calculate a sudden cluster potential was similar to the approach of other authors (Wilets, et al., (1970), Pruess and Greiner, (1970), Brueckner, et al., (1968) and CHK). In earlier calculations, the sudden approximation was realized as a straightforward superposition of

the densities of the colliding fragments,* without provision for rearrangement effects due to local densities exceeding the equilibrium density. In order to implement this type of approximation in the existing deformed BHF code of CHK, the same K-matrix interaction developed for adiabatic calculations (see Chapter II) is employed, but rather than iterate the Hartree-Fock equations to obtain a self-consistent solution, only one iteration is performed. The total energy from this non-self-consistent calculation gives the cluster potential in a "frozen density" approximation. With only one iteration, the Brueckner rearrangement potential Δ_B does not affect the potential in a self-consistent manner. In addition, because the density distribution is not adjusted for a second iteration, the quadrupole constraint potential is irrelevant. The dipole constraint is included to keep the initial density distribution from drifting along the z-axis. The parameters of the K-matrix model given in Section C of Chapter II are used in this calculation.

To test the single-iteration approach to the sudden approximation, the potential for the reaction $^{12}C + \alpha$ was calculated for values of the cluster separation ranging from R = 0.6 fm to R = 9.0 fm. The result of this calculation is shown in Figure 14. The cluster potential given in the figure is similar to the adiabatic cluster potential in Figure 5 of Chapter IV in the interior region $R \simeq 0$ fm. The single-iteration potential has a smaller radius than the adiabatic case and is much less diffuse. The potential increases rapidly as R increases, compared to the adiabatic potential; V_S does not approach V_{CT} for large R. These difficulties are caused by a lack of a

---

*Note that Brueckner, et al.(1968) claim to employ an "adiabatic" approximation in their work. Wilets, et al. (1970) correctly point out that the former's approximation of frozen density distributions is not compatible with an adiabatic limit. In fact, the ansatz of Brueckner, et al. is quite similar to the sudden approximation of Greiner and co-workers (Pruess and Greiner, (1970) and Park, et al., (1972)).

Figure 14. Single-iteration sudden potential for $^{12}C + \alpha$.

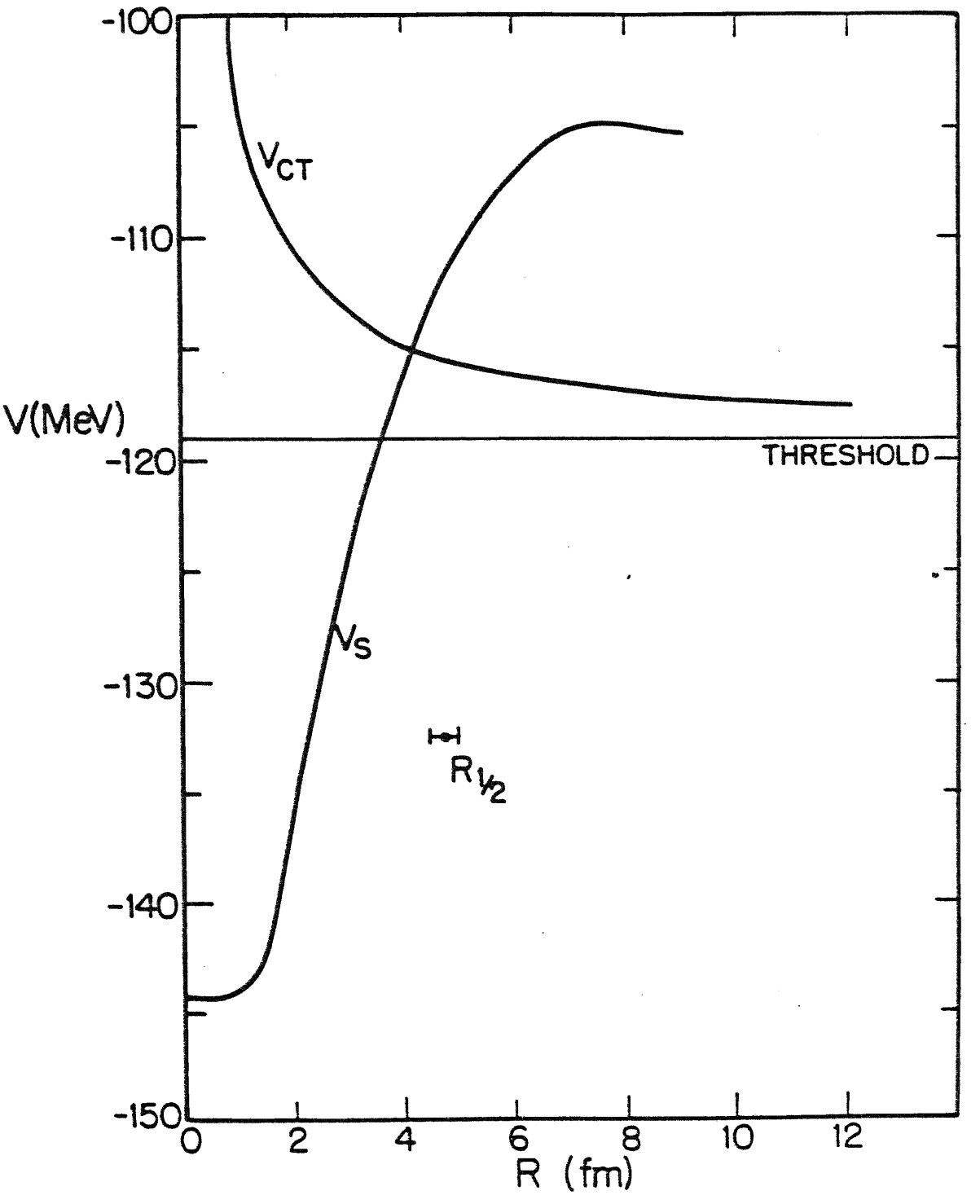
-100
-110
-120
-130
-140
-150
V(MeV)
V_{CT}
V_S
THRESHOLD
$R_{1/2}$
0
2
4
6
8
10
12
R (fm)

constraint potential in this non-self-consistent method. Comparison of the single-iteration case without a constraint and the first iteration of the adiabatic method (using a quadrupole constraint potential) shows that the cluster potential in Figure 14 is too shallow by 5-15 MeV, except for small R. The single-iteration method for calculating a sudden potential failed to produce a potential with a hard or soft core such as that found by Pruess and Greiner (1970). Pruess and Greiner state that the hard-core which they obtain in the case of $^{16}O + ^{16}O$ is due to a compression effect; that is, the rapid increase in the interaction energy is a result of the density exceeding the equilibrium for their model. When this happens in nuclear matter, the increase in the total energy is determined by the compressibility of nuclear matter. While Pruess and Greiner do not describe the stiffness of their shell model with a compressibility, they do indicate that the compression energy for putting ^{32}S into an ^{16}O shell model potential is quite high. The compressibility used in the calculation shown in Figure 14 was 150 MeV (see Section C, Chapter II); this low value of the compressibility, chosen to give good results for the total binding energy in an adiabatic calculation, allows the density distribution for the $^{12}C + \alpha$ single-iteration case with $R \ll R_{\frac{1}{2}}$ to assume a form commensurate with the ^{16}O density. (The density distributions for $^{12}C + \alpha$ in the single-iteration cases are not shown, but are comparable to those shown in Figure 6 for $R \ll R_{\frac{1}{2}}$) One is led to conclude that the successful calculation of the cluster potential in the sudden approximation requires the superposition of the densities of the two interacting clusters such that the total density is equal or nearly equal to the sum of the individual densities. This conclusion, supported by the work of Pruess and Greiner (1970), motivated a second attempt to calculate a sudden potential.

The next approach to calculating a sudden potential was an effort to produce the expected total density distribution described above. Both the initial density $\rho_0(r)$ and the Brueckner-Hartree-Fock Hamiltonian for that density are known; a successful calculation must produce a single Slater determinant for the total wave-function $\Psi(r_1, r_2, \ldots, r_A)$, whose density distribution $\rho(r)$ is the same as the initial density. This total wave-function must also correspond to the minimum in the total energy of the system with that initial density distribution. These conditions are identical to the conditions for which the variational principle of Hohenberg and Kohn (1964) is defined. Usually called the Kohn variational principle, this theorem states that for a given density $\rho(r)$ and Hamiltonian $H(\rho(r), k^2)$, there exists a properly anti-symmetrized wave-function Ψ_{total} constructed from the eigen-functions of H, which reproduces $\rho(r)$, and minimizes the total energy; the proof of this theorem requires the introduction of a constraint potential which is a functional of the density. The constraint functional $v_c([n])$ is included in the Hamiltonian, and an effective single-particle Hamiltonian $\tilde{h}$ is defined such that:

$$\tilde{h}\varphi_\lambda = [h(\rho_0(r), k^2) + v_c(\rho_0(\vec{r}))]\varphi_\lambda = \tilde{\varepsilon}\,\varphi_\lambda \quad (84)$$

where

$$E_{TOT} = \sum_\lambda \tilde{\varepsilon}_\lambda n_\lambda \quad (85)$$

is a minimum. The single particle wave-functions which are the eigenfunctions in Eq. (84) must satisfy

$$\rho_0(\vec{r}) = \sum_\lambda n_\lambda |\varphi_\lambda|^2 \quad (86)$$

in order to reproduce the input density. The application of the Kohn variational principle in a calculation requires the knowledge of the functional form of $v_c([n])$, for any initial density $\rho_0(r)$. In the second approach to

finding the sudden potential, utilizing the variational principle described here, the form of the constraint potential is deduced from arguments presented below.

Consider the superposition of two ^{16}O clusters with a small separation between their centers, for example, R = 2.0 fm. It is clear from the abortive single-iteration method that in a BHF calculation without an initial constraint, the summed density would spread until $\rho(z=0) \simeq \rho_e(z=0)$, the equilibrium density for an adiabatic calculation of ^{32}S. This can be visualized as matter flowing out of the center of the distribution into the surface, thereby increasing the radius of the compound system and decreasing the central density. However, if an external constraint which is attractive in the interior and repulsive outside the surface of the initial, overlapped distribution is applied to the system, the flow of density out of the center would be retarded. This constraint is constructed as:

$$v_c(\vec{r}) = v_c(\rho(\vec{r})) = -V_c\left(\rho_0(\vec{r}) - \rho(\vec{r})\right) \quad (87)$$

Wherever the density $\rho(r)$ found from Eq. (86) is less than the initial density $\rho_0(r)$, $v_c(r)$ is attractive; likewise, if $\rho(r) > \rho_0(r)$, then $v_c(r)$ becomes repulsive. In an iterative scheme similar to that described in Chapter IV, $v_c^i(\vec{r})$ is the new constraint potential for input to the i^{th} iteration; $v_c^i(\vec{r})$ depends upon the density from the (i-1)st iteration,

$$v_c^{i}(\vec{r}) = -V_c\left(\rho_0(\vec{r}) - \rho_{i-1}(\vec{r})\right) + v_c^{i-1}(\vec{r}) \quad (88)$$

Ideally, the constraint would continue to be adjusted in each succeeding iteration until $\rho_0(\vec{r}) \simeq \rho_{i-1}(\vec{r})$; then $v_c^i(\vec{r}) \simeq v_c^{i-1}(\vec{r})$ is the desired constraint potential, and the i^{th} iteration would give a density $\rho_i(\vec{r}) = \rho_0(\vec{r})$. The Kohn variational principle would be satisfied for the final difference potential $v_c^i(\vec{r})$.

A test of the method described above was made for the case of ^{16}O + ^{16}O, with the clusters superposed at a separation of R = 1.0 fm. The quadrupole constraint potential $v_q(r)$ of Chapter IV was turned off to prevent possible interference with the action of $v_c(\vec{r})$. A slight stabilization of the constrained iterations was allowed by using the density updating expression given in Eq. (68). The dipole constraint was retained to eliminate drift of the densities along the z-axis. Finally, to keep the sharp "edges" of the constraint potential from causing unstable oscillations in the density distribution, the constraint was smeared using the folding integral:

$$v_c^i(\vec{r}) = v_c^{i-1}(\vec{r}) - V_c \int d^3r' \, e^{-|\vec{r}-\vec{r}'|^2/b^2} \left(\rho_0(\vec{r}') - \rho_{i-1}(\vec{r}') \right) \qquad (89)$$

Both the constraint strength V_c and the smearing parameter b were varied through a range of values in an effort to parameterize $v_c(\vec{r})$. The results of this test indicates that, for constraint strengths ranging from 0.1 to 1.0 and smearing parameters b = 0.35 and b = 0.6, no stable constraint potential could be constructed. The method was successful in preventing a spreading of the density distribution, but the constraint potential in the central region became deeper with each iteration; hence, the central density increased to values in excess of twice the central density of one ^{16}O cluster. A possible solution to this instability is to introduce a method for modifying the constraint strength after each iteration, in a manner similar to that used by CHK to adjust the quadrupole constraint (see Section C, Chapter IV). The incorporation of such an ad hoc adjustment of V_c was rejected; the Kohn variational principle approach to calculating the sudden potential was abandoned in favor of the formally consistent method described in the next section.

C. Method of Overlapping Clusters

The method described in this section is taken from an early paper by Löwdin (1955) in which the general properties of the density matrix formalism involving two non-orthogonal sets of wave-functions are developed. This approach is well-suited to the calculation of a sudden interaction potential between two superposed clusters; by using Löwdin's formalism, a renormalized total wave-function can be obtained so that Pauli corrections are always included in the calculation. The implementation of Löwdin's formalism to calculate a single Slater determinant wave-function, the resulting total density and the matrix-elements of the Hamiltonian is presented in greater detail below.

The physical situation involved in the calculation is as follows: two clusters, A_1 and A_2, approach each other along the z-axis; the cluster separation R is defined in Eq. (55). The wave-functions describing the two clusters are ψ_{A_1} and ψ_{A_2}, respectively. When R is large enough that the clusters do not overlap at all, the total wave-function of the system is:

$$\Psi_{TOTAL} \approx \psi_{A_1} \psi_{A_2} \tag{90}$$

that is, the antisymmetrization between clusters well-separated in coordinate-space is a small correction to the total wave-function. However, when the two clusters begin to overlap, Pauli correlations require that the exchange of particles between clusters be included explicitly. If the two cluster wave-functions ψ_{A_1} and ψ_{A_2} are constructed of basis states $\{\varphi\}$ such that the sets $\{\varphi_{A_1}\}$ and $\{\varphi_{A_2}\}$ are orthogonal, then the total wave-function is simply,

$$\Psi_{TOTAL} = \frac{1}{\sqrt{A!}} \det\{\varphi_1(1) \cdots \varphi_A(A)\} \tag{91}$$

$$\Psi_{TOTAL} = \frac{1}{\sqrt{A!}} \begin{vmatrix} \varphi_1(1) & \cdots & \varphi_1(A_1) & \varphi_1(A_1+1) & \cdots & \varphi_1(A) \\ \vdots & & & & & \vdots \\ \varphi_{A_1}(1) & & & & & \\ \vdots & & & & & \\ \varphi_A(1) & - - - - & & - - - - & & \varphi_A(A) \end{vmatrix} \quad (92)$$

Unfortunately, the inner product between members of different basis sets used here, expressed as

$$\mathcal{O}_{\lambda\mu} = \int d^3r \, \varphi_{A_1}(\lambda) \, \varphi_{A_2}(\mu) \quad (93)$$

does not result in the required orthogonality. Therefore, the total wave-function for the system is not the simple Slater determinant in Eq. (91); in addition, the expectation values of operators also involve the overlap of non-orthogonal wave-functions. The formalism of Löwdin (1955) provides a straightforward, consistent method for renormalizing the basis wave-functions and the matrix elements of the Hamiltonian, so that the total wave-function of the system is a single Slater determinant, and matrix elements properly include Pauli effects.

The set of basis states for the single Slater determinant (SSD) wave-function for cluster A_1 is written as $\{\varphi_\lambda^{(1)}\}$, $\lambda = 1, 2, \ldots, A_1$, and the basis set for the cluster A_2 SSD is $\{\varphi_\lambda^{(2)}\}$, $\lambda = 1, 2, \ldots, A_2$. The two bases are combined in a direct sum to give $\{\varphi_\lambda\}$, $\lambda = 1, 2, \ldots, A_1, A_1, A_1+1, \ldots, A_1+A_2$. In this notation,

$$\varphi_\lambda = \begin{cases} \varphi_\lambda^{(1)} & \lambda \le A_1 \\ \varphi_\lambda^{(2)} & A_1+1 \le \lambda \le A \end{cases} \quad (94)$$

The renormalized total wavefunction has the same form as the SSD in Eq. (71),

but now contains a normalization factor $\sqrt{N}$:

$$\Psi_{TOTAL} = \frac{1}{\sqrt{N}\sqrt{A!}} \begin{vmatrix} \varphi_1(1) & \cdots & \varphi_1(A) \\ \vdots & & \\ \varphi_A(1) & \cdots & \varphi_A(A) \end{vmatrix} \tag{95}$$

The normalization constant N is determined from the requirement

$$\langle \Psi_{TOTAL} | \Psi_{TOTAL} \rangle = 1 ; \tag{96}$$

this can be re-written as:

$$\langle \Psi_{TOTAL} | \Psi_{TOTAL} \rangle = \frac{1}{N} \frac{1}{A!} \int d^3r_1 \ldots d^3r_A \sum_P (-)^P \prod_{\lambda=1}^{A} \varphi_\lambda^*(\vec{r}_\lambda) \varphi_{p\lambda}(\vec{r}_\lambda) \tag{97}$$

where the integration implicitly includes summations over the spin and isospin quantum numbers of the basis states. The overlap of two basis functions is defined as

$$d_{\lambda\mu} = \int d^3r \, \varphi_\lambda(r) \varphi_\mu(r) \tag{98}$$

and the integration again denotes summation over quantum numbers. The normalization condition in Eq. (97) is now

$$\langle \Psi_{TOTAL} | \Psi_{TOTAL} \rangle = \frac{1}{N} \sum_P (-1)^P \prod_{\lambda=1}^{A} d_{\lambda p\lambda} = \frac{1}{N} \det \{ d_{\lambda\mu} \} \tag{99}$$

where $\{ d_{\lambda\mu} \}$ is the overlap matrix defined above. Combining Eq. (96) and Eq. (99) gives

$$N = \det \{ d_{\lambda\mu} \} \tag{100}$$

so that the renormalized total wave-function is the SSD below:

$$\Psi_{TOTAL} = \frac{1}{\sqrt{A!}\sqrt{\det\{d_{\lambda\mu}\}}} \begin{vmatrix} \varphi_1(1) & \cdots & \varphi_1(A) \\ \vdots & & \vdots \\ \varphi_A(1) & \cdots & \varphi_A(A) \end{vmatrix} \tag{101}$$

The density matrix in coordinate space is defined as:

$$\rho(r,r') = \int d^3r_1 \ldots d^3r_A \, \Psi^*_{TOTAL} \Psi_{TOTAL} \; ; \qquad (102)$$

this can be shown to be of the form (Löwdin, 1955):

$$\rho(r,r') = \frac{1}{det\{d_{\lambda\mu}\}} \sum_{\lambda\mu=1}^{A} \varphi^*_\lambda(r) \varphi_\mu(r') D_{\lambda\mu} \qquad (103)$$

where $D_{\lambda\mu}$ is the minor of the determinant $det\{d_{\lambda\mu}\}$:

$$det\{d_{\lambda\mu}\} = \sum_{\lambda\mu} d_{\lambda\mu} D_{\lambda\mu} \qquad (104)$$

Equation (104) can be used to define the inverse overlap matrix $d^{-1}_{\lambda\mu}$:

$$d^{-1}_{\lambda\mu} = D_{\lambda\mu} / det\{d_{\lambda\mu}\} \qquad (105)$$

From Eqs. (103) and (105), the density matrix can be re-written in the form

$$\rho(r,r') = \sum_{\lambda\mu=1}^{A} \varphi^*_\lambda(r) \varphi_\mu(r') d^{-1}_{\lambda\mu} \; ; \qquad (106)$$

the diagonal form of $\rho(r, r')$ is

$$\rho(r) = \sum_{\lambda\mu} \varphi^*_\lambda(r) \varphi_\mu(r) d^{-1}_{\lambda\mu} \qquad (107)$$

At this point it is convenient to express each single particle wave-function in terms of its expansion in the harmonic oscillator basis used in the BHF computer code. The oscillator basis states $\Psi^{\mu}_{n_z n_r}$ are defined in Eqs. (56-59). Let

$$\varphi_\lambda(r) = \sum_k C^k_\lambda \Psi_k(r) \qquad (108)$$

where k represents a set of quantum numbers (n_z, n_r, μ). (See Section B, Chapter IV.) The expansion coefficients are just the overlap integrals

$$C^k_\lambda = \int d^3r \, \Psi^*_k(\vec{r}) \varphi_\lambda(\vec{r}) \qquad (109)$$

The density distribution $\rho(r)$ becomes

$$\rho(r) = \sum_{kl}\left[\left(\sum_{\lambda\mu} C^{*k}_{\lambda} C^{l}_{\mu} d^{-1}_{\lambda\mu}\right)\Psi^{*}_{k}(r)\Psi_{l}(r)\right] \quad (110)$$

with the bracket in Eq. (110) defined as the renormalized density matrix in the harmonic oscillator basis, ρ_{kl}. This matrix is used to calculate the expectation value of the total energy operator:

$$\langle E\rangle = Tr(\rho H_{rel}) = \sum_{kl} \rho_{kl}\left(t_{kl} + \tfrac{1}{2} v_{kl}\right) \quad (111)$$

where t_{kl} and v_{kl} are matrix elements of the intrinsic kinetic energy and the interaction potential in the oscillator basis, respectively. Replacing ρ_{kl} in Eq. (111) with its definition gives:

$$\langle E\rangle = \sum_{\lambda\mu} d^{-1}_{\lambda\mu} \sum_{kl} C^{*k}_{\lambda}\left(t_{kl} + \tfrac{1}{2} v_{kl}\right) C^{l}_{\mu} \quad (112)$$

Equation (112) represents the form of the expression for the total cluster potential to be calculated in the sudden approximation. The oscillator basis matrix elements are available in the adiabatic version of the computer code, as described in Chapter IV. The remaining terms of Eq. (112), namely the matrix elements of the inverse of the overlap matrix, $d^{-1}_{\lambda\mu}$ and the overlap coefficients C^{k}_{λ}, can be calculated using Eq. (98) and (109), respectively. These calculations have been facilitated by additions to the original adiabatic BHF code, and a new procedure for obtaining the cluster potential developed; these changes are described in subsequent paragraphs below.

Procedure for calculation of sudden potential with the overlap method

The procedure for calculating the sudden potential using the BHF

code is similar to that of a single-iteration adiabatic calculation, except that the information needed to begin the calculation is now a set of initial single particle wave-functions, rather than an initial density distribution. The set of input wave-functions is found in separate adiabatic BHF calculations for clusters A_1 and A_2, where the number of iterations is sufficient to obtain good convergence of the binding energy of that nucleus. The resulting single particle functions are fitted to a power series-times-exponential function on a standard grid, and the coefficients from that fit punched onto cards for later input in the sudden calculation. The K-matrix model, its parameterisation, and the selection of the set of harmonic oscillator basis states are identical to that discussed in chapters II, III, and IV.

The constraint potential of Chapter IV is not included in the single particle Hamiltonian, h_{rel} because the sudden potential is calculated in a non-self-consistent manner; only one iteration is performed in the method described here.

Once the least-squares coefficients of the initial wave-functions are stored in the program, the wave-functions are reconstructed with the origin of each function shifted so that the center-of-mass of the system lies at the origin of coordinates, and the cluster separation found using Eq. (55) corresponds to an input value of $R = R_0$. The overlap coefficients C^k_λ are found using Eq. (109) with the same high-speed Gaussian integration technique described in Section C of Chapter IV. The overlap matrix $\{d_{\lambda\mu}\}$ is calculated from Eq. (98) in a similar manner, and its inverse $\{d^{-1}_{\lambda\mu}\}$ is obtained. The density $\rho(r)$ is found using Eq. (107); multipole moments up to order $L = 6$ are determined. The calculated density is used to construct the matrix elements of the relative single particle Hamiltonian h_{rel} for neutrons and protons.

After the matrix elements of the Hamiltonian in the oscillator basis are found, the sudden potential is calculated as:

$$\langle V_{cl} \rangle = \sum_{\lambda\mu} d^{-1}_{\lambda\mu} \sum_{kl} C^{*k}_{\lambda} \left(\tilde{t}_{kl} + \tfrac{1}{2} v_{kl} \right) C^{l}_{\mu} \qquad (113)$$

where the $\tilde{t}_{kl}$ are matrix elements corresponding to a Hamiltonian

$$H_{TOT} - Z\, T_{cm} \qquad (114)$$

as in the adiabatic calculation.

To find the sudden potential as a function of cluster separation R, the shift of the initial wave-functions is varied by changing the initial separation R_0 between centers of the unperturbed clusters. Because Pauli corrections are included through the renormalization of the total wave-function, the density $\rho(r)$ in the composite system is not just the sum of the separate densities of clusters A_1 and A_2, separated by R_0. The antisymmetrization smears the density somewhat in the region of overlap between the clusters, and the calculated density usually differs from the summed density. Hence, the overlap method given here is not strictly a sudden approximation, as defined by Pruess and Greiner (1970) for their "fast" potentials; it contains Pauli distortion effects. Results of the overlap calculation of the sudden potential for the six reactions $\alpha + \alpha$, $^{12}C + \alpha$, $^{14}C + \alpha$, $^{16}O + \alpha$, $^{12}C + {}^{12}C$, and $^{16}O + {}^{16}O$ are presented in the next section.

D. Results of the Sudden Calculation

The sudden cluster potentials for several reactions are discussed in this section. The curves for V_s vs. R are presented in a format similar to that used for the adiabatic cluster potentials of Chapter IV. Each figure contains the THRESHOLD and V_{CT} curves, and the adiabatic potentials V_A are included for comparison with the sudden results. With the exception of the

reactions $^{12}C + \alpha$ and $^{14}C + \alpha$, the V_s curves contain a hard core, or steep rise, in the interior region; the radius of this core is around 1.5 - 2.0 fm. In comparison with the adiabatic potentials, the sudden potentials have a smaller radius so that the tail of the potential V_s occurs at smaller values of R; this will be discussed in the context of the optical model in Chapter VI.

$^4He + ^4He$

Figure 15 contains the sudden potential for the overlap calculation of the reaction $\alpha + \alpha$. The potential rises sharply, with a hard core of radius $R_{core} \approx 2.0$ fm. The minimum in the sudden curve is around V_s -59.5 MeV at R = 3.0 fm. The tail of the potential lies at smaller values of R compared to the adiabatic result $V_A(R)$. The good agreement between V_s and V_{CT} for R = 6.0 fm provides an upper bound for the range of Pauli effects in this reaction. Once R > 6.0 fm, the antisymmetrization between clusters is not important; the total interaction energy is nearly equal to the total binding energy of the separate clusters, plus Coulomb energy, in the strong absorption region.

Figure 16 is a graph of the inverse overlap matrix elements $d^{-1}_{\lambda\mu}$ for the overlap of the $1s_{\frac{1}{2}}$ proton wave-function from one cluster with itself, d^{-1}_{11}, and the overlap of the $1s_{\frac{1}{2}}$ proton wave-function from cluster A_1 with the $1s_{\frac{1}{2}}$ function from cluster A_2, d^{-1}_{12}. As the d^{-1}_{12} curve indicates, the two $s_{\frac{1}{2}}$ wave-functions in different clusters do not overlap strongly until R $\leq$ 3 fm. Up to this point d^{-1}_{11} is about unity; it begins to grow as the clusters overlap because the off-diagonal matrix elements d_{12} and d_{21} contribute to the overlap matrix. When the overlap matrix is inverted, the non-zero value of overlap integrals between different clusters affects the diagonal elements of the

Figure 15. Sudden cluster potential vs. R for $\alpha + \alpha$.

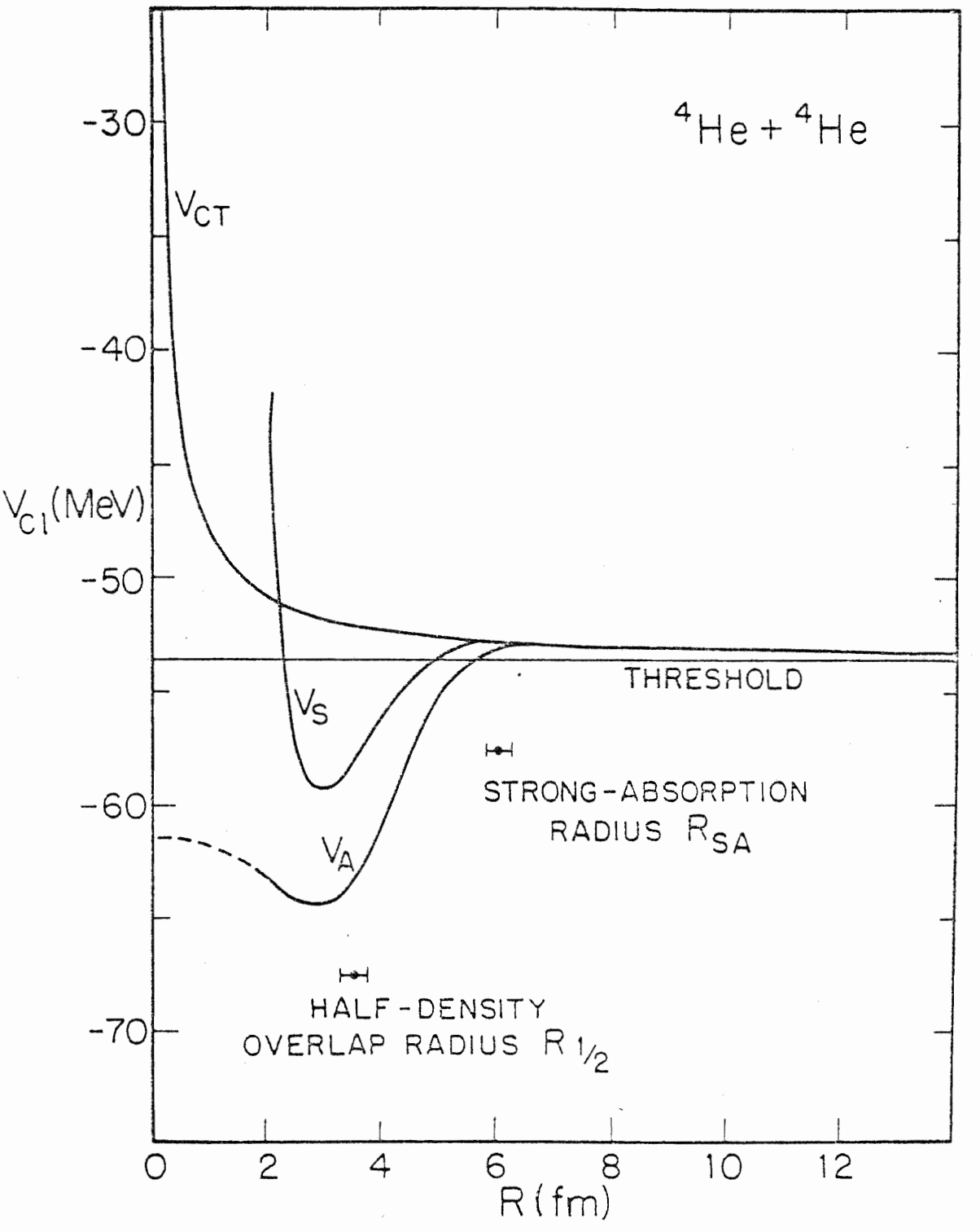
$^4He + ^4He$
V_{CT}
V_S
V_A
THRESHOLD
STRONG-ABSORPTION
RADIUS R_{SA}
HALF-DENSITY
OVERLAP RADIUS $R_{1/2}$
V_{Cl}(MeV)
-30
-40
-50
-60
-70
0
2
4
6
8
10
12
R(fm)

Figure 16. Inverse overlap matrix elements for protons vs. R for the sudden approximation of the $\alpha + \alpha$ reaction.

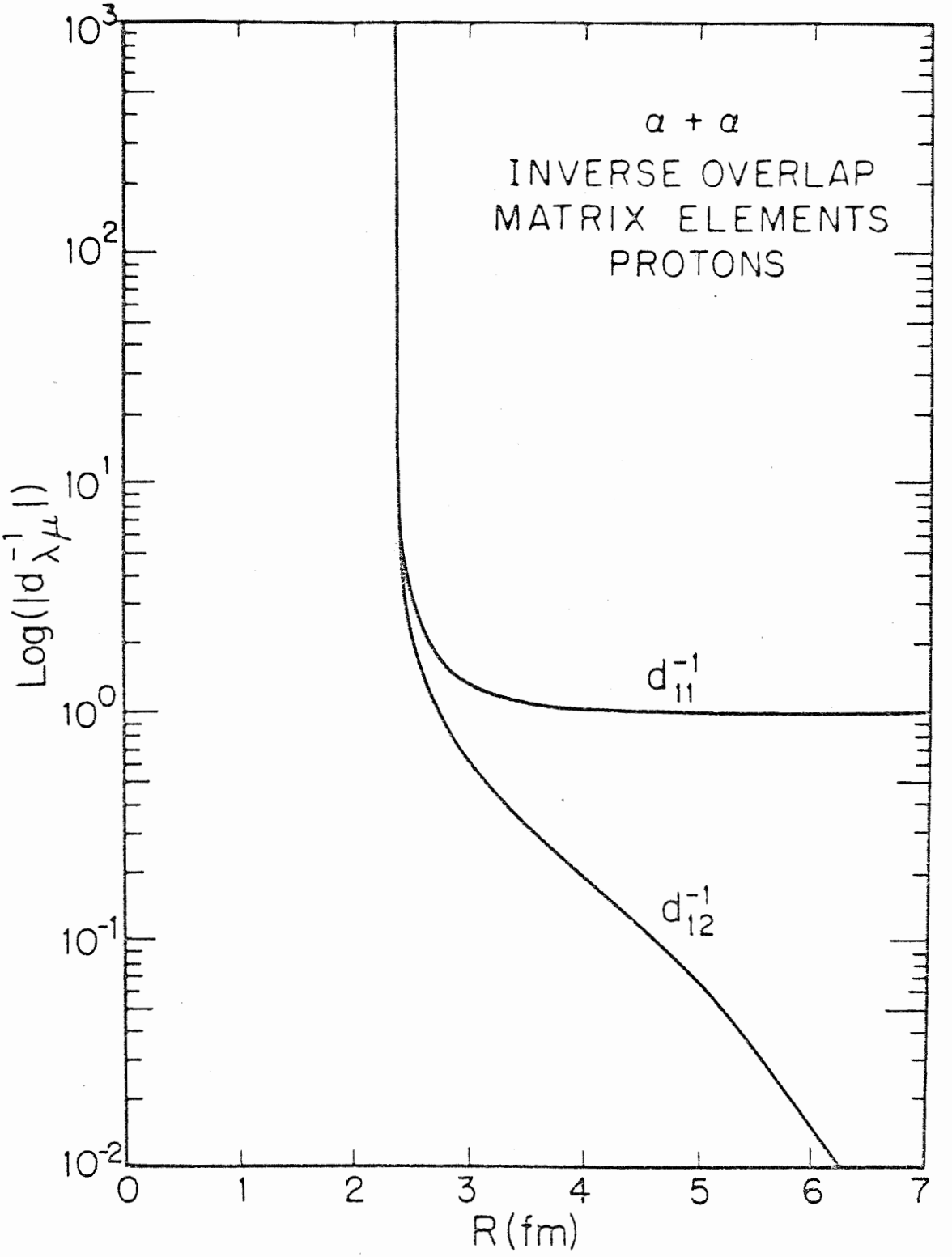
α + α
INVERSE OVERLAP
MATRIX ELEMENTS
PROTONS
d_{11}^{-1}
d_{12}^{-1}
10^3
10^2
10^1
10^0
10^{-1}
10^{-2}
Log(|$d_{\lambda\mu}^{-1}$|)
0
1
2
3
4
5
6
7
R(fm)

inverse of the overlap matrix. Both d_{12}^{-1} and d_{11}^{-1} increase rapidly as the overlap between clusters increases; for R = 2.3 fm, $d_{11}^{-1} \approx 4 \times 10^4$, and $d_{12}^{-1} \approx -4 \times 10^4$. The neutron single particle wave-functions have similar inverse overlap matrix elements.

$^{12}C + \alpha$

The sudden potential calculated for the $^{12}C + \alpha$ reaction, shown in Figure 17, differs greatly from the $\alpha+\alpha$ potential in Figure 15. There is neither a hard nor soft core in the potential at small values of R, although the minimum of V_S is about 11 MeV above the minimum for V_A. The sudden potential has a form similar to that of the $\alpha + \alpha$ curve for R > 4.0 fm, with a smooth, diffuse surface region. The potential falls off more rapidly as R increases than the adiabatic curve also shown in the figure.

The lack of a hard or soft core in V_S is due to the relatively slow increase in the inverse overlap matrix elements $d_{\lambda\mu}^{-1}$ as R approaches zero. Figure 18 is a plot of $d_{\lambda\mu}^{-1}$ for several proton wavefuntions for $^{12}C + \alpha$. While the d_{11}^{-1} elements increased rapidly in the $\alpha + \alpha$ case (see Figure 16 and note that the scale of the ordinate is logarithmic), the largest value of d_{11}^{-1} for $^{12}C + \alpha$ is $d_{11}^{-1} \approx 12$ at $R \approx 0.8$ fm. The notation for d_{13}^{-1} is the inverse overlap matrix element for the overlap of the $1s_{\frac{1}{2}}$ proton wave-function from one cluster with the $1p_{\frac{1}{2}}$ proton wave-function from the same cluster. The d_{13}^{-1} curve shows clearly the influence of the renormalization of the total wave-function on the calculation of matrix elements of h_{rel}. Usually the $1p_{\frac{1}{2}}$ and $1s_{\frac{1}{2}}$ functions from the same cluster are exactly orthogonal, and lead to $d_{13} = 0$. However, as the figure shows, $d_{13}^{-1} \neq 0$ until the clusters A_1 and A_2 are well-separated (as determined by the condition $d_{\lambda\mu} = 1$, that is, when the normal-

Figure 17. Sudden cluster potential vs. R for $^{12}C + \alpha$.

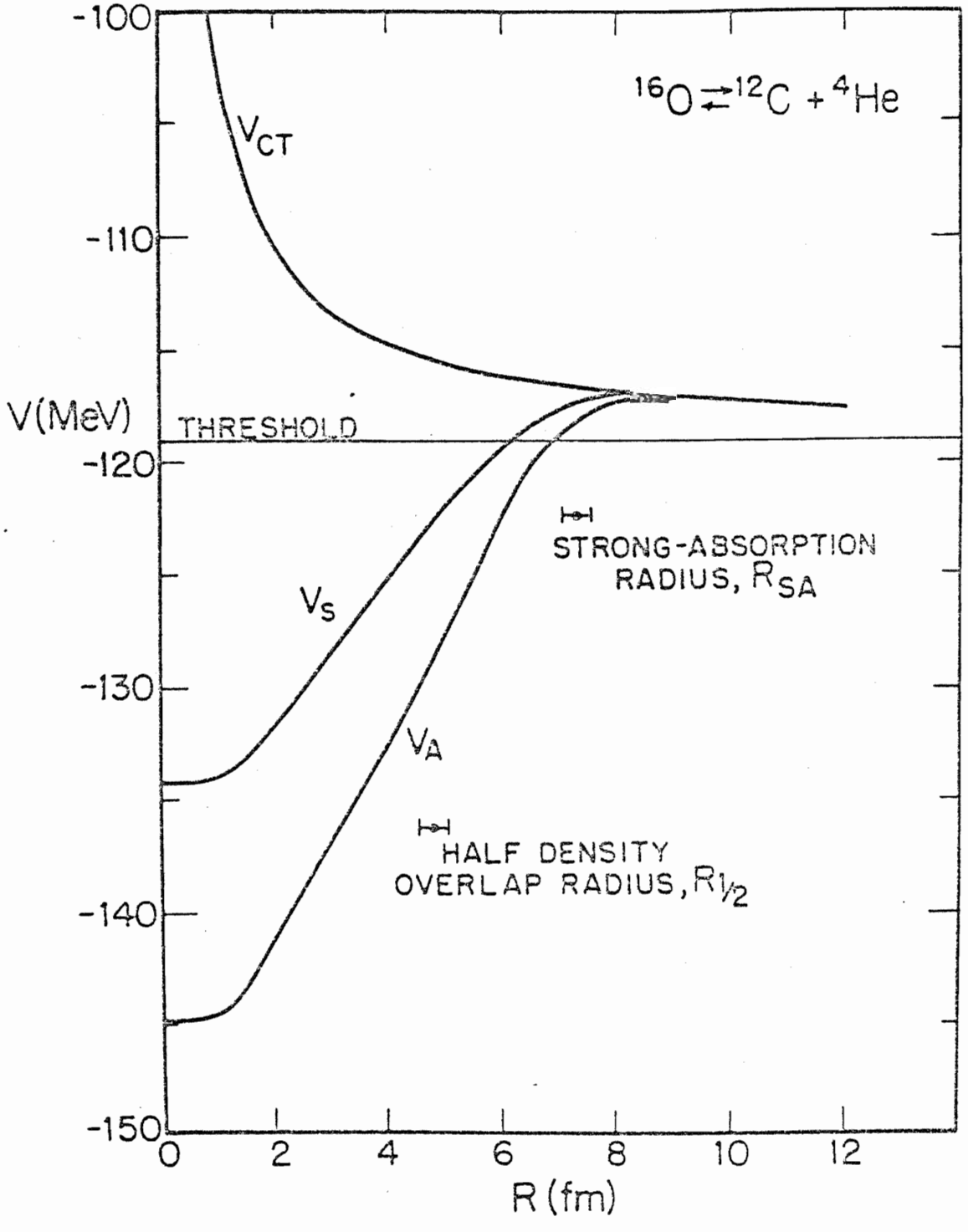
-100
-110
-120
-130
-140
-150
V(MeV)
$^{16}O \rightleftarrows ^{12}C + ^{4}He$
V_{CT}
THRESHOLD
V_S
V_A
STRONG-ABSORPTION
RADIUS, R_{SA}
HALF DENSITY
OVERLAP RADIUS, $R_{1/2}$
0
2
4
6
8
10
12
R (fm)

Figure 18. Inverse overlap matrix elements for protons in the $^{12}C + \alpha$ reaction.

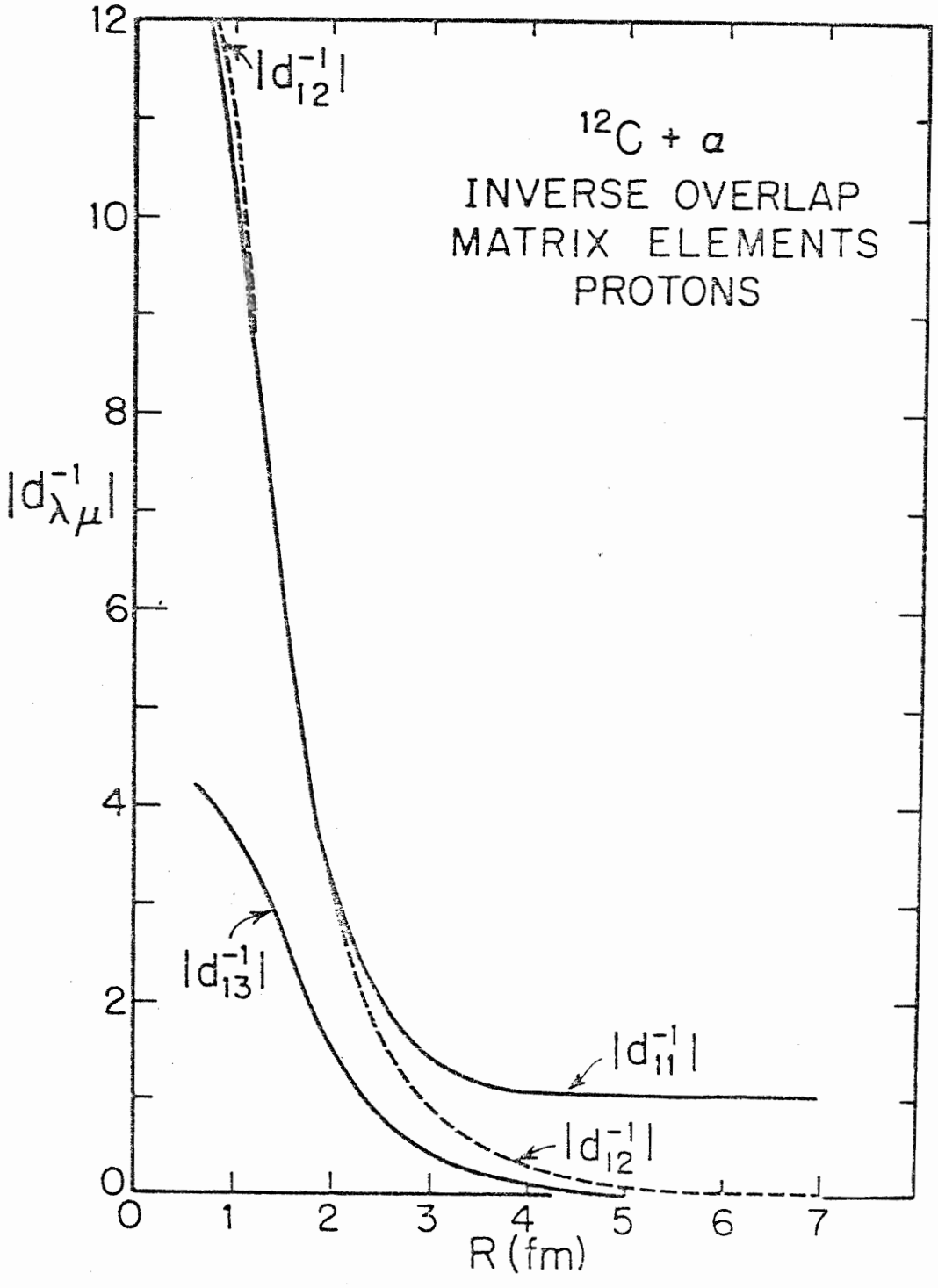
$^{12}C + \alpha$
INVERSE OVERLAP
MATRIX ELEMENTS
PROTONS
$|d^{-1}_{12}|$
$|d^{-1}_{13}|$
$|d^{-1}_{11}|$
$|d^{-1}_{12}|$
$|d^{-1}_{\lambda\mu}|$
R (fm)
0
1
2
3
4
5
6
7
0
2
4
6
8
10
12

ization of a single-particle state returns to its asymptotic value). The behavior of the inverse overlap matrix elements for neutrons (not shown here) is similar to that in Figure 18 for protons.

A physical argument for the absence of a hard or soft core in V_s can be offered. While $\alpha+\alpha$ system yields a ^{8}Be compound system, $^{12}C + \alpha$ leads to the doubly-magic nucleus ^{16}O. Because doubly-magic nuclei are tightly bound relative to non-magic nuclei, it is energetically favorable for the α-particle to be strongly absorbed by ^{12}C, which has an open p-shell for both protons and neutrons. The resemblance of $^{12}C + \alpha$ at small R in the overlap approximation to ^{16}O could be shown by diagonalizing the Hamiltonian $\langle\lambda|H_{rel}|\mu\rangle$, and finding the new eigenvectors $|\lambda'\rangle$; by calculating the overlap of the new eigenvectors with the states of ^{16}O (obtained in a separate adiabatic BHF calculation), the ^{16}O-like character of the $^{12}C + \alpha$ compound system would be revealed. The shell effect observed here indicates the success of the prescription for including both shell effects and bulk properties (such as binding energies) in the K-matrix model of Chapter II. The proper consideration of shell corrections has been shown to be essential in calculating the potential energy surface for fission of heavy ions (Mosel and Schmitt, 1971).

$^{14}C + \alpha$

The sudden potential for $^{14}C + \alpha$ is shown in Figure 19. In the surface region, it is similar to the V_s curves for $\alpha+\alpha$ and $^{12}C + \alpha$; however, for $R < 4$ fm, the potential energy curve has a behavior intermediate to the $\alpha+\alpha$ and $^{12}C + \alpha$ curves. It does not exhibit a hard core as in the $\alpha+\alpha$ case, but the potential does increase for small R so that the minimum of V_s lies at $R \approx 3.5$ fm. The potential has a very soft core. An extension of the discussion of the preceding paragraph shows why this occurs.

Figure 19. Sudden cluster potential vs. R for $^{14}C + \alpha$.

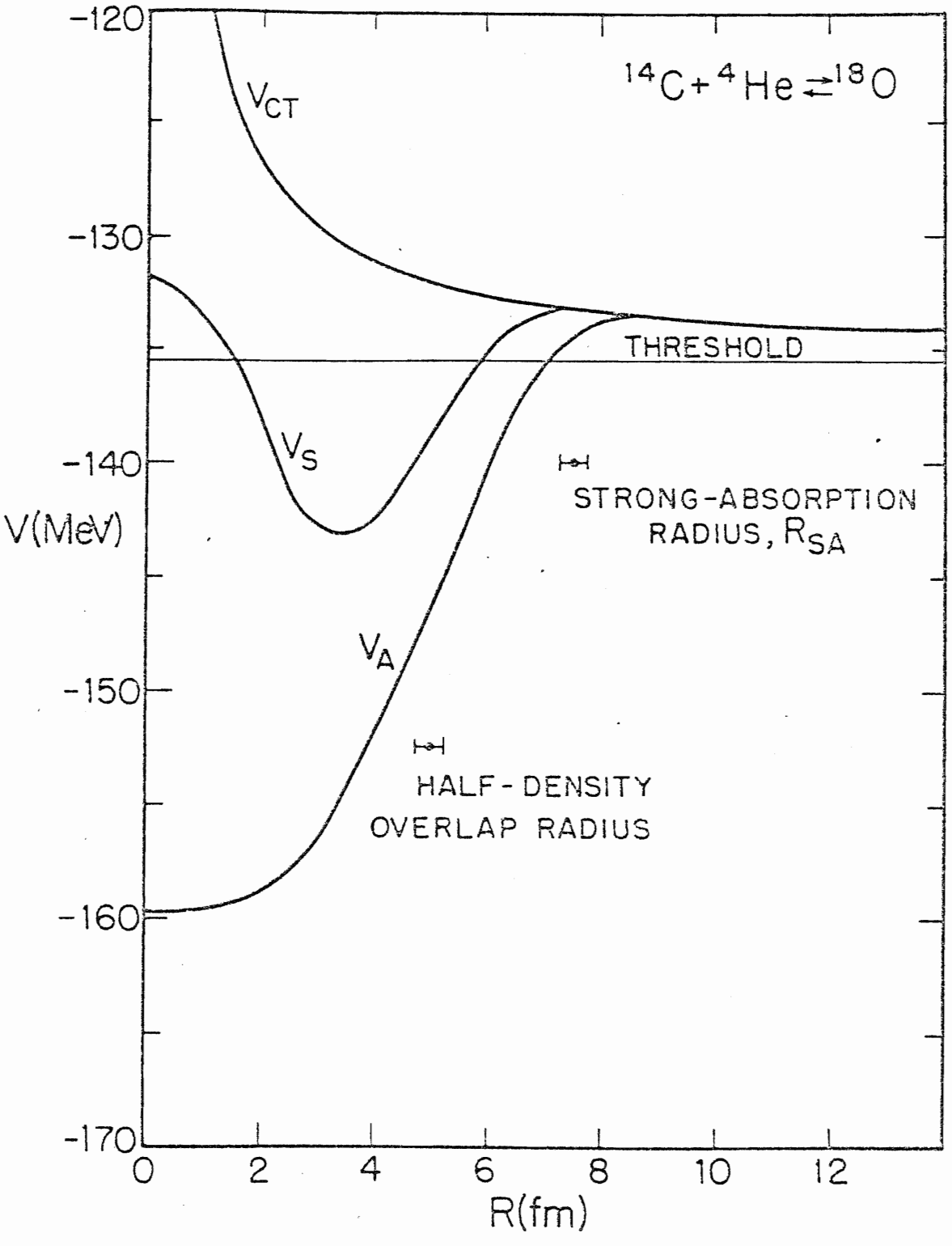
$^{14}C + ^{4}He \rightleftarrows ^{18}O$
V_{CT}
V_S
V_A
THRESHOLD
STRONG-ABSORPTION RADIUS, R_{SA}
HALF-DENSITY OVERLAP RADIUS
V(MeV)
R(fm)
-120
-130
-140
-150
-160
-170
0
2
4
6
8
10
12

Figure 20. Inverse overlap matrix elements for neutrons in the $^{14}C + \alpha$ reaction.

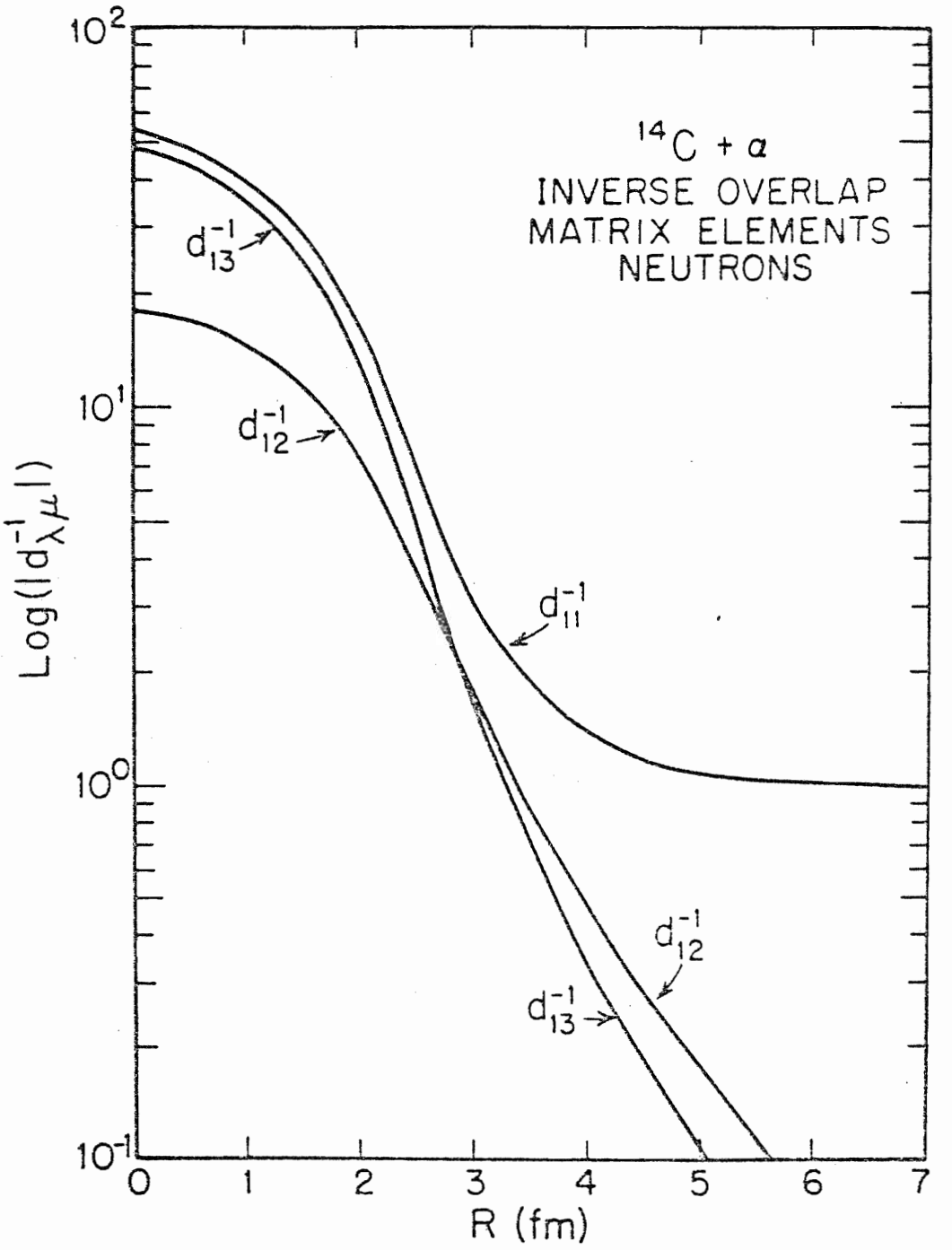
$^{14}C + \alpha$
INVERSE OVERLAP
MATRIX ELEMENTS
NEUTRONS
d_{13}^{-1}
d_{12}^{-1}
d_{11}^{-1}
d_{12}^{-1}
d_{13}^{-1}
10^2
10^1
10^0
10^{-1}
Log($|d_{\lambda\mu}^{-1}|$)
0
1
2
3
4
5
6
7
R (fm)

For the $^{12}C + \alpha$ case, there is no hard or soft core because the ^{12}C nucleus absorbs the α-particle to form ^{16}O; the open proton and neutron shells are filled by the nucleons from the α-particle. However, for $^{14}C + \alpha$, there is only an open proton shell, while the neutron shell closes with N = 8, a magic number. Following the reasoning presented above, the neutrons of the α-particle should not be as strongly absorbed as in the $^{12}C + \alpha$ reaction; the protons from ^{4}He would fill the open proton p-shell in ^{14}C and should be strongly absorbed. The behaviour of the inverse overlap matrix elements for protons in the reaction $^{14}C + \alpha$ (not shown here) is quite similar to that in Figure 18 for $^{12}C + \alpha$. This is not too surprising because the Brueckner-Hartree-Fock proton wave-functions for ^{14}C and ^{12}C are similar. However, the curves for $d^{-1}_{\lambda\mu}$ for neutrons, shown in Figure 20, indicate that the inverse overlap matrix elements for small R are much larger than in the $^{12}C + \alpha$ system. One is led to expect that the total energy for the neutrons will increase the total energy in the interior of the composite system, relative to the V_s curve for $^{12}C + \alpha$. Figure 19 exhibits this expected change. The total neutron energy increase from V_s (neutrons) ≈ -70 MeV at R = 4.2 fm to V_s (neutrons) $\approx$ -58.4 MeV for R$\approx$0.1 fm, while the total proton energy remains nearly constant around -73 MeV. The response of the nucleons in the α-particle to open and closed shells in ^{14}C and ^{12}C clearly demonstrates the inclusion of shell effects in the model interaction of Chapter II.

$^{16}O + \alpha$

The result of the overlap calculation of the $^{16}O + \alpha$ sudden potential is shown in Figure 21. The minimum of this potential is more shallow than the minimum in the adiabatic potential $V_A(R)$ and occurs near R = 3.8 fm, as in the

Figure 21. Sudden cluster potential vs. R for $^{16}O + \alpha$.

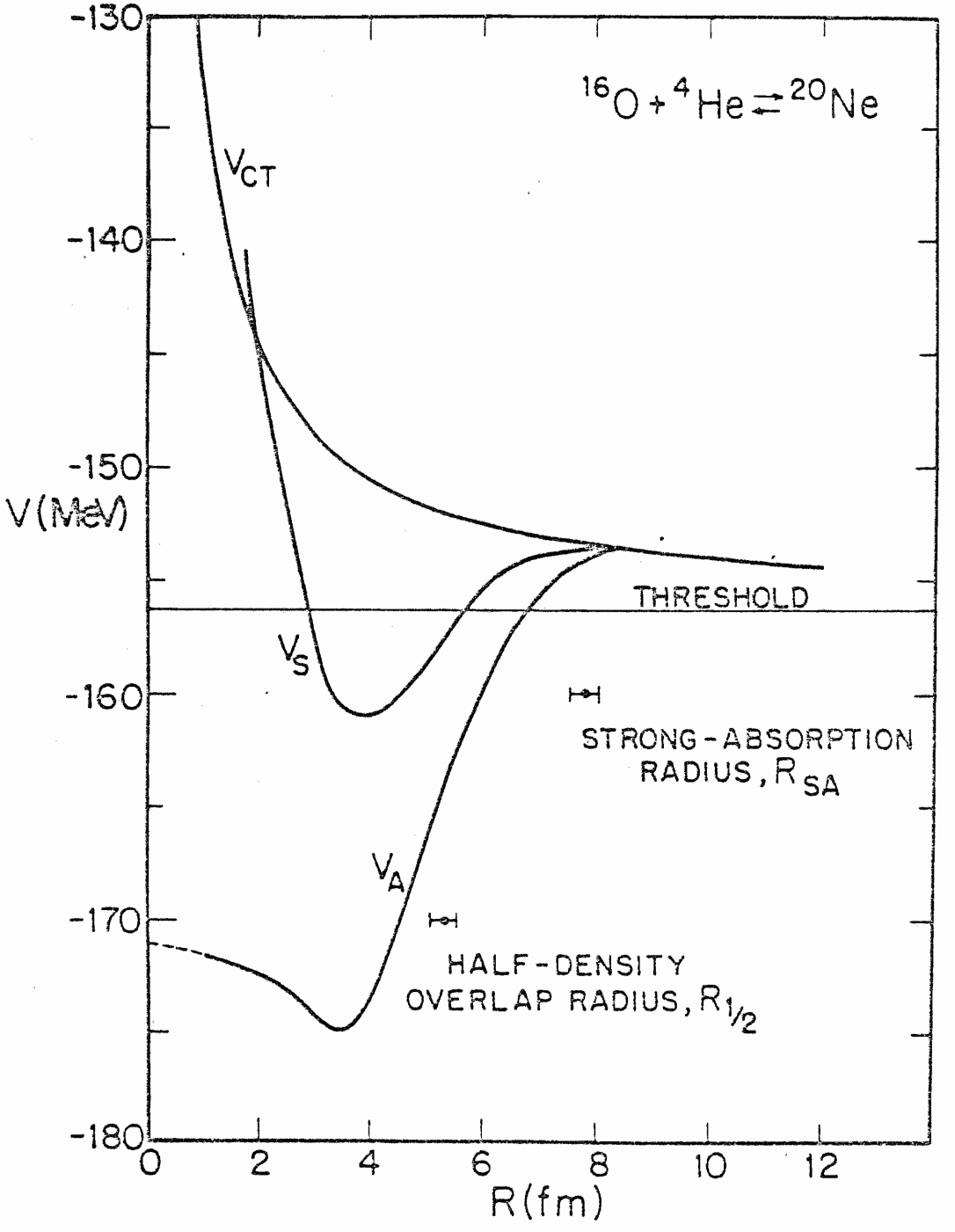
-130
-140
-150
-160
-170
-180
V(MeV)
0
2
4
6
8
10
12
R(fm)
$^{16}O + ^{4}He \rightleftharpoons ^{20}Ne$
V_{CT}
V_S
V_A
THRESHOLD
STRONG-ABSORPTION RADIUS, R_{SA}
HALF-DENSITY OVERLAP RADIUS, $R_{1/2}$

case of the adiabatic potential. For $R < 3.5$ fm the potential rises sharply suggesting a hard core of radius $R_{core} = 1.5$ fm. No points of V_s for $R < 2$ fm could be obtained because the density distribution $\rho(r)$ became oblate for smaller separations. The separation of the clusters defined Eq. (55) is undefined for $Q_{2T} < 0$.

The slope of the potential for $R \simeq 2 - 3$ fm is not as steep as in the $\alpha + \alpha$ case, and it is possible that there exists a soft core (i.e., V_s is finite at $R = 0$) rather than the hard core shown in the figure. This is also suggested by the behaviour of the inverse overlap matrix elements, which increase more rapidly as the clusters overlap than the $^{12}C + \alpha$ quantities, but do not have the singular form of the $\alpha+\alpha$ matrix elements. This possibility could not be investigated further because no data for $R < 2$ fm is available.

$^{12}C + ^{12}C$

The sudden potential V_S in Figure 22 for the collision of two ^{12}C ions is qualitatively similar to the $^{16}O + \alpha$ potential. Once again, there is a sharp rise in V_s for small values of R; the radius of the core is between 1.2 fm and 1.5 fm. The surface region of V_s is nearly 1 fermi smaller in radius than the adiabatic potential also shown in the figure. The minimum of V_s is 15 MeV higher than the V_A minimum and occurs at the same value of R. As in the case of the $^{16}O + \alpha$ system, the total mass quadrupole moment becomes negative near that value of R identified as the core radius, and no further information about $V_s(R)$ can be obtained past this radius. The core radius is estimated from the shape of V_s in the neighborhood of this cut-off. Further comment on the $^{12}C + ^{12}C$ sudden potential will be made in Chapter VI.

$^{16}O + ^{16}O$

The sudden potential for the $^{16}O + ^{16}O$ reaction is shown in

Figure 22. Sudden cluster potential vs. R for $^{12}C + {}^{12}C$.

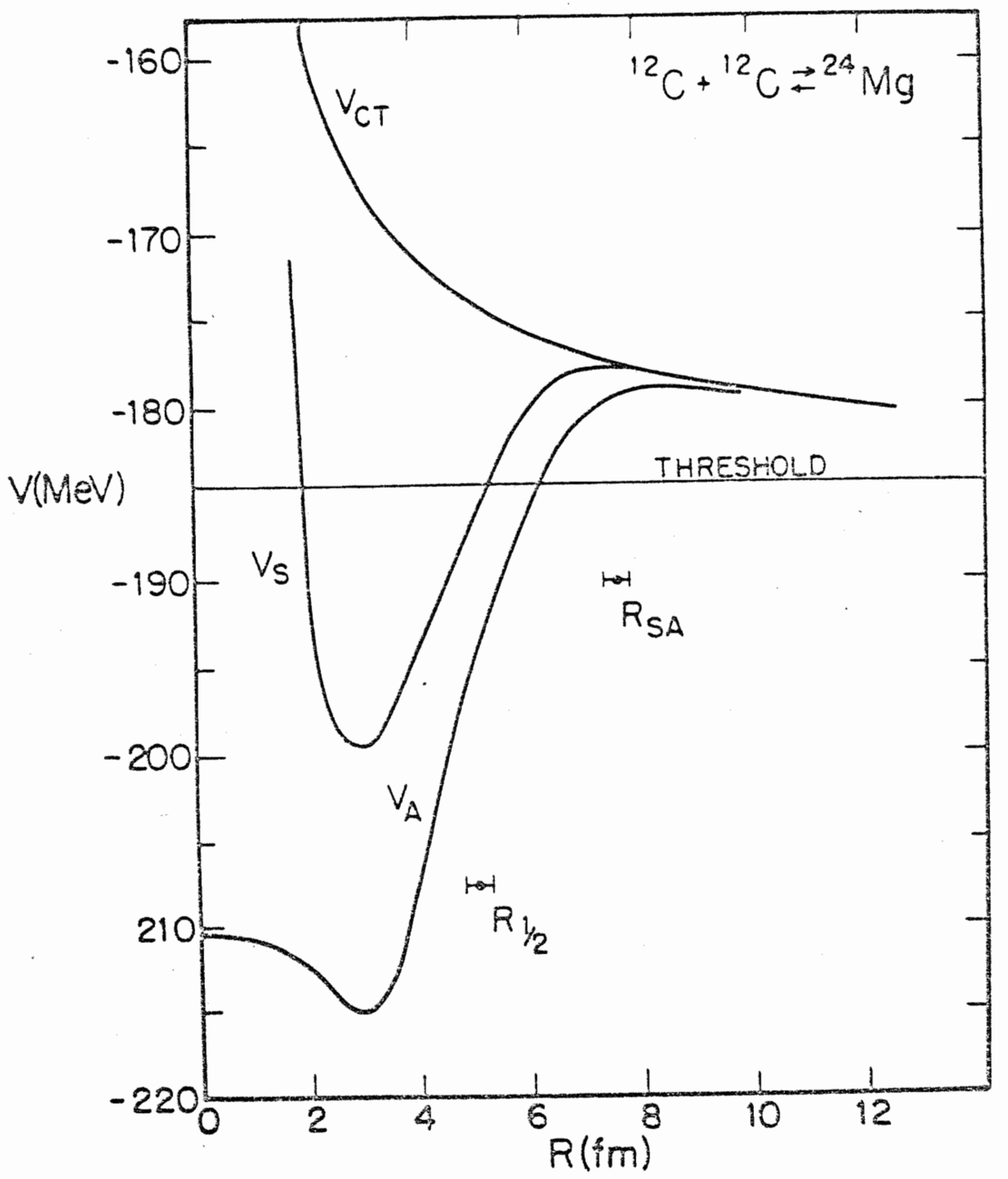
$^{12}C + ^{12}C \rightleftarrows ^{24}Mg$
V_{CT}
THRESHOLD
V_S
V_A
R_{SA}
$R_{1/2}$
V(MeV)
R(fm)
-160
-170
-180
-190
-200
210
-220
0
2
4
6
8
10
12

Figure 23. Sudden cluster potential vs. R for the $^{16}O + {}^{16}O$ reaction.

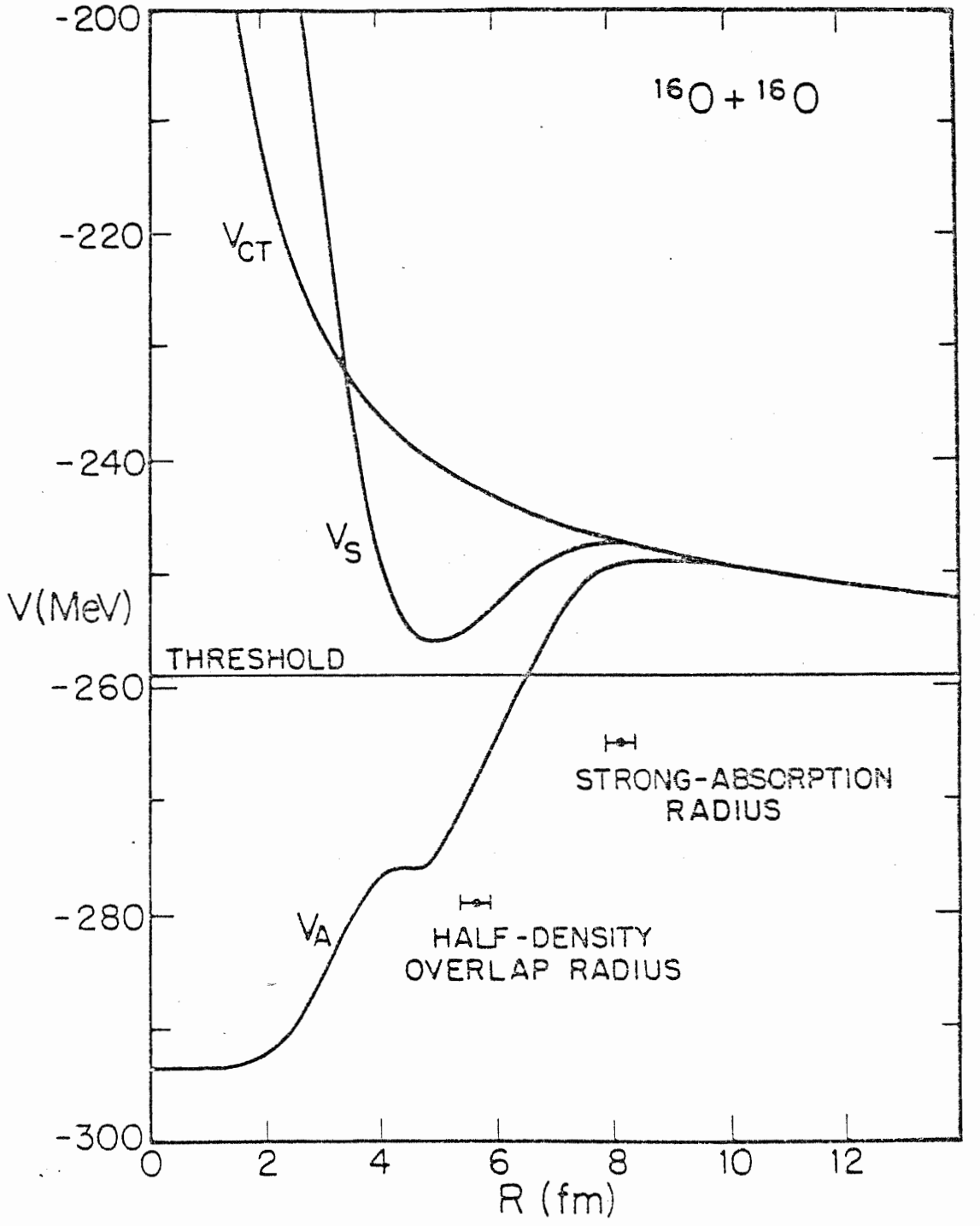
-200
-220
-240
-260
-280
-300
V(MeV)
$^{16}O + ^{16}O$
V_{CT}
V_S
V_A
THRESHOLD
STRONG-ABSORPTION RADIUS
HALF-DENSITY OVERLAP RADIUS
0
2
4
6
8
10
12
R (fm)

Figure 22. This curve differs substantially from previously discussed results in that it predicts an unbound composite system in the sudden approximation; the minimum V_s lies above the threshold energy of the two ^{16}O ions. One would expect from the curve that for a collision of two ^{16}O nuclei in which the overlap calculation is valid (for example, high bombarding energy), the system would only resonate as a bound system, rather than fuse to form ^{32}S, as in the adiabatic calculation.

The potential in Figure 23 exhibits a hard core of radius R_{core} = 2 fm. The potential bears no similarity to the adiabatic curve except in the strong absorption region, where the clusters no longer overlap strongly, and the renormalization of the wave-function (Pauli distortion) is a small correction to the SSD wave-function.

In a recent paper, Fleckner and Mosel have examined several corrections to the ion-ion interaction energy of the $^{16}O + ^{16}O$ system, arising from antisymmetrization requirements. Their calculation is carried out using the Skyrme force to generate an energy-density functional for the system. From this functional they obtain an ion-ion potential in which various sources of Pauli corrections are included in steps. Specifically, the total density is corrected for Pauli distortion and the interaction Hamiltonian matrix elements are calculated in a properly antisymmetrized manner. They also allow for corrections to the intrinsic kinetic energies of the two ions. The calculation is done using a "frozen density" approximation which does not allow the nucleus to rearrange into lower orbits in order to minimize the energy. This is exactly the procedure used in this work, as discussed in Section C. (The intrinsic kinetic energy corrections due to Pauli effects are not included explicitly here.) Therefore, the potential energy in Figure 23

Figure 24. Total density distribution for ^{16}O + ^{16}O along the z-axis for several cluster separations. The cluster separation is noted near each density profile.

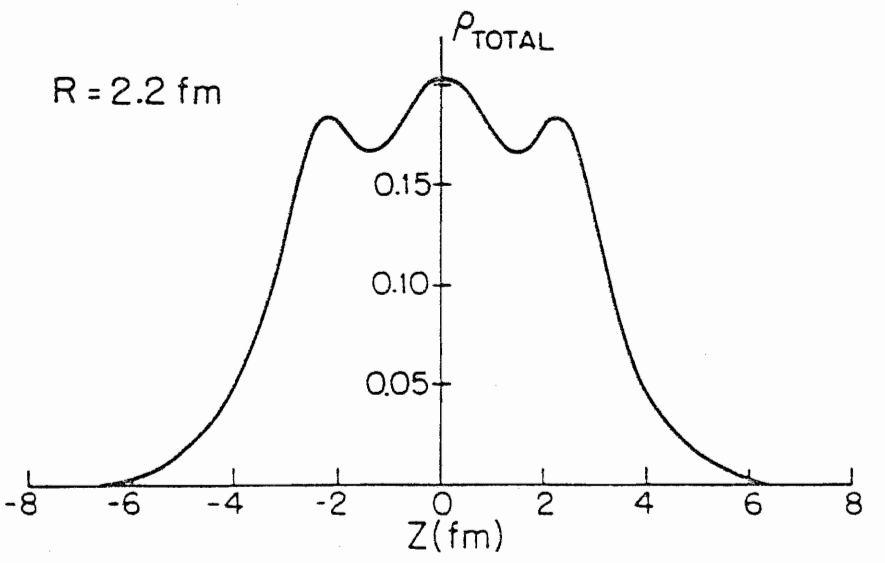
ρ_{TOTAL}
R = 2.2 fm
0.15
0.10
0.05
-8
-6
-4
-2
0
2
4
6
8
Z(fm)

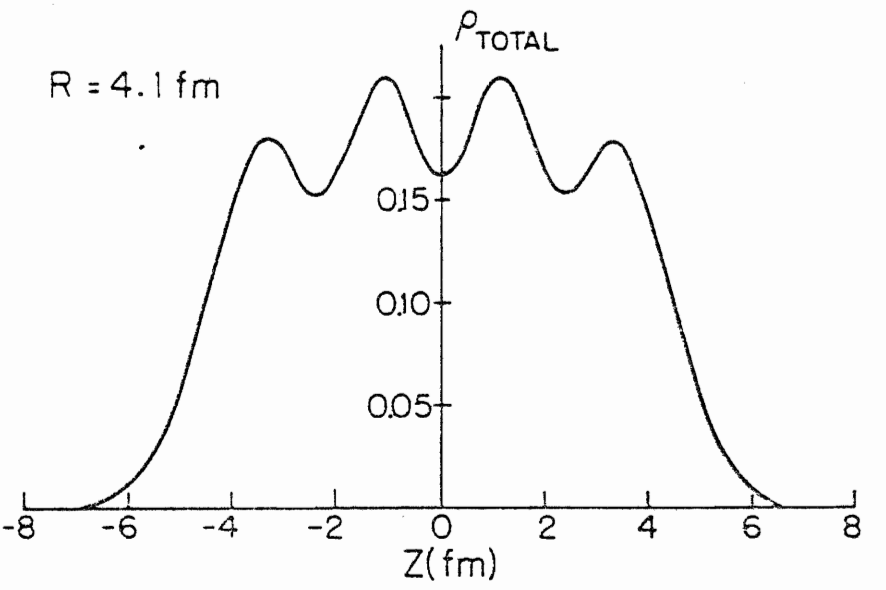
ρ_{TOTAL}
R = 4.1 fm
0.15
0.10
0.05
-8
-6
-4
-2
0
2
4
6
8
Z(fm)

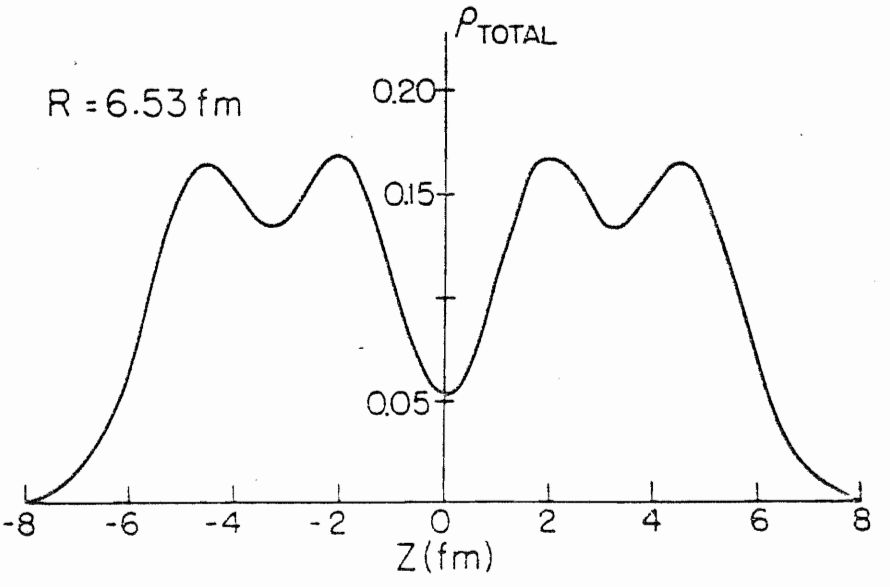
ρ_{TOTAL}
R = 6.53 fm
0.20
0.15
0.05
-8
-6
-4
-2
0
2
4
6
8
Z(fm)

can be compared to the results of Fleckner and Mosel.

Because Fleckner and Mosel use nucleon wave-functions from a harmonic oscillator basis Hartree-Fock calculation for each ^{16}O cluster, it is not surprising that the density profiles of Figure 24 agree well with the curves shown in their Figure 1. In particular, the Pauli distortion indicated in their figure is identical to the spreading shown in Figure 24.

A comparison of the sudden potential in Figure 23 with Fleckner and Mosel's results is difficult because they did not include the Coulomb interaction in their Hamiltonian. However, if the sudden potential is corrected by removing the Coulomb energy for two point charges with Z_1, Z_2 = 8 and separation distance R, a qualitative comparison is possible. Figure 25 shows the curve labelled 'V_{pes}' in Figure 2 of Fleckner and Mosel (1972), and the sudden potential with V_{CT} subtracted from it (the threshold energy is removed because V_{pes} of Fleckner and Mosel is the interaction energy relative to the binding energy of the two ^{16}O ions). Considering the estimates of the Coulomb energy discussed above, the agreement is good. In the interior, i.e. for R $\leq$ 6 fm, the actual Coulomb energy in the present calculation should be lower because the ions are not spherical but are deformed overlapping clusters. A recent study (Sage and Cusson, 1976) indicates that there can be considerable Coulomb distortion of the ions of the order of 0.5 to 1.0 MeV in the strong absorption region where V_s and V_{pes} in Figure 25 have the greatest differences. Therefore, inclusion of the Coulomb interaction in the calculation of Fleckner and Mosel should cause a further distortion of the ions and decrease their potential slightly in the surface region.

Fleckner and Mosel comment that the repulsive core of their potential, beginning around R = 4.0 fm, is wholly due to their frozen density assumption which increases the intrinsic kinetic energy as the ions overlap.

Figure 25. Comparison of the potential energy surface V_{pes} of Fleckner and Mosel (1972) with the sudden potential for $^{16}O + {}^{16}O$ discussed in the text.

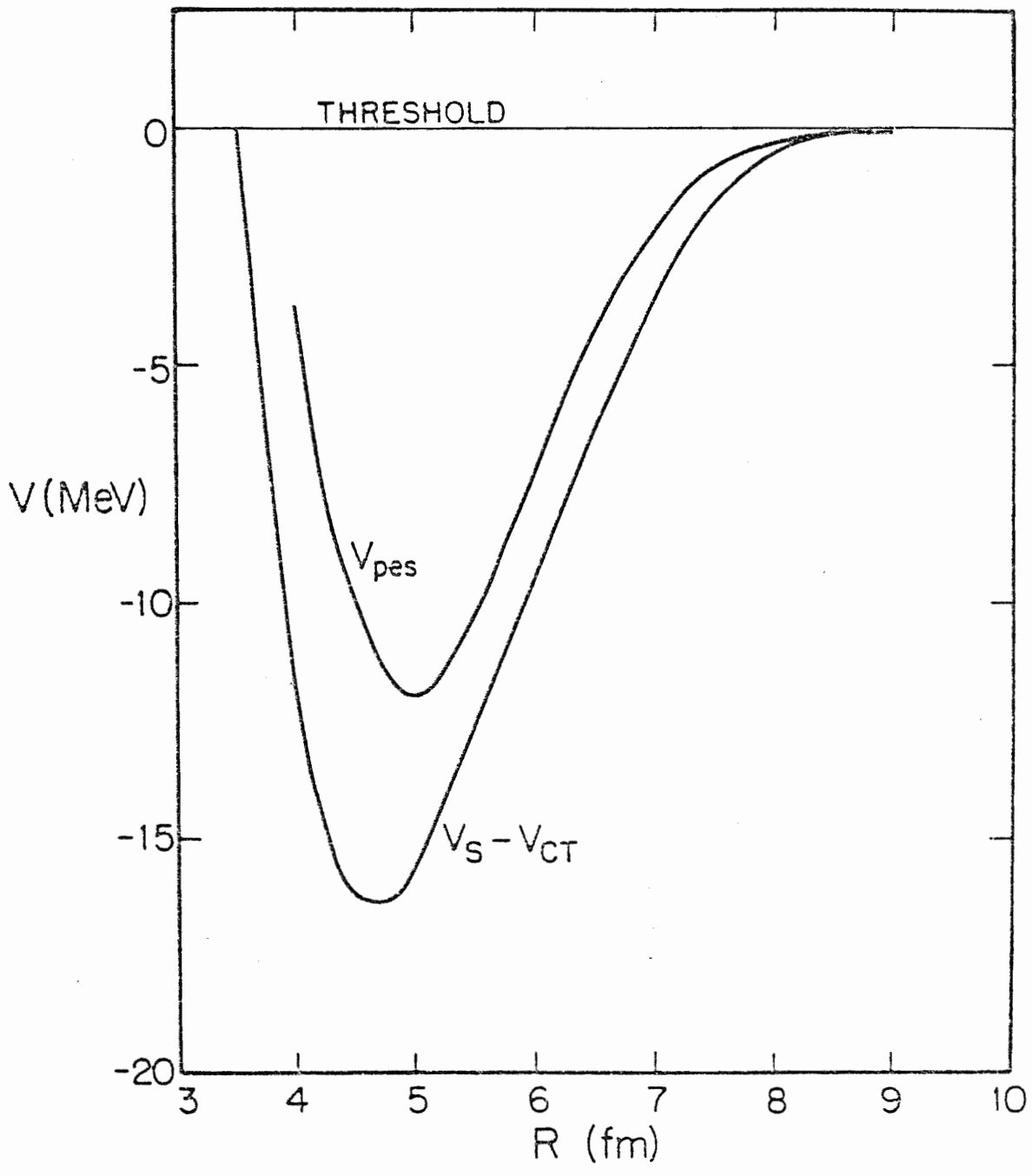
THRESHOLD
0
-5
-10
-15
-20
V (MeV)
V_{pes}
$V_S - V_{CT}$
3
4
5
6
7
8
9
10
R (fm)

However, they dismiss the increase V_{pes} for small R as spurious because the frozen density assumption is not valid for large overlaps in an adiabatic calculation. While this is certainly true, their comment about the repulsive core provides evidence that their potential is physically reasonable, even at small R, in a sudden approximation. Further comparison of V_s and V_{pes} will be made in Chapter VI.

CHAPTER VI

USE OF CLUSTER POTENTIALS IN THE OPTICAL MODEL

A. Use of Optical Potentials in Describing Heavy-Ion Reactions

Most of the recent analyses of experimental data from the elastic scattering of heavy-ions have been based on the optical model (Hodgson, 1971). Among the important considerations of the application of the optical model to the fitting of experimental data is the choice of the real part of the optical potential; while the calculation of the imaginary part of the optical potential has not succeeded from a first-principles approach,* the real part of the potential, V_{real}, has been obtained by several authors using a variety of models ranging from BHF calculations (Zint and Mosel, 1976), to the shell model (Goritz and Mosel, 1976), to the folding method (Vary and Dover, 1974). The value of these theoretical potentials for describing experimental data with the optical model is discussed, and the cluster potentials calculated in Chapters IV and V are compared with other work and with phenomenological potentials. The chapter ends with a comparison of the shallow potentials (such as the cluster potential) with the deep potentials obtained in the folding model.

What regions of the optical potential are important experimentally?

Because potentials from widely different theoretical frameworks can have the same form in a limited region (for example, the surface of the

---

*However, see the work of Fink and Toeppfer (1973).

potential), the question above must be answered before one knows what sort of experiment to perform to distinguish between different models. In order to limit this discussion to coordinate-space, only elastic scattering for head-on collisions (L = 0) is considered; otherwise, the angular momentum barrier present for L ≠ 0 denies access to information about the optical potential for small values of R. For most heavy-ion reactions at energies just above the Coulomb barrier (called 'low-energy' reactions for the remainder of this discussion), only the outer tail of the potential affects the cross section (Zint and Mosel, 1975; Satchler, 1975). Other studies (Vary and Dover, 1974) indicate that the surface and interior regions of the interaction potential become important at higher bombarding energies. Still another complication is the fact that some reaction systems appear to be sensitive to the interior of the potential even at lower energies. (See Zint and Mosel (1975) for their discussion of $^{16}O + {}^{16}O$.) It is also possible that the imaginary part of the optical potential is so large that absorption out of the elastic channel precludes probing of the interior of the target nucleus and hence the real part of the optical potential (CHK, 1976). It is evident though that any reaction system must be sensitive to the strong absorption region of the scattering potential at any bombarding energy. Most elastic scattering experiments cannot distinguish between potentials which are similar in their surface regions.

Cluster potentials as optical potentials. The fact that the functional form of V_{opt} is important only in the surface region for most reactions encourages the comparison of the cluster potentials calculated in the present work with other theoretical optical potentials which are successful in fitting experimental data. If the cluster potentials are similar in form to those

potentials, it is likely that the cluster potential would be equally useful in fitting the same elastic scattering data. Before such a comparison is carried out, two problems mentioned in Chapter IV must be re-examined. In Section B of Chapter IV, the removal of spurious kinetic energy was discussed in detail, and a cautionary note about the use of V_{cl} in a Schrödinger formalism was issued. The method of kinetic energy removal used here should be corrected to account properly for the degree of freedom in the ion-ion separation coordinate R, as described in Section D of Chapter IV. This correction is necessary because the minima of V_A are too deep by values ranging from 9 to 20 MeV. Hence, by using V_A as the real part of the optical potential, one would over-estimate the potential well seen by the projectile in elastic scattering. Fortunately, this difficulty is not very important for the comparison made in the next section because the kinetic energy removal is probably correct in the surface region of V_A (see section D of Chapter IV), which is the experimentally accessible region of the optical potential.

The second of the two difficulties noted above is that elastic scattering of two heavy-ions is neither an adiabatic nor a sudden process; the actual reaction should lie between these two extreme approximations. This problem could be overcome by adjusting the form factor and the depth of the adiabatic potential in a consistent energy-dependent manner. However, there is nothing in the model described in the previous chapters to suggest the form of such an ad hoc potential. A simple choice for an effective optical model potential derived from the adiabatic and sudden potentials is the linear combination

$$V_{opt}(R) = f V_A(R) + (1-f) V_s(R) \qquad (115)$$

where $V_A(R)$ and $V_s(R)$ are the adiabatic and sudden potentials; the fraction $f \leq 1$ of V_A in $V_{opt}(R)$ should be energy-dependent and could be parameterized by fitting experimental data over a wide range of bombarding energies. One expects that $f \approx 1$ for energies very near the top of the Coulomb barrier, and that f should increase with energy.

The energy-dependence postulated above for the factor f results in the inclusion of the hard core of V_s in the optical potential, except for the $^{12}C + \alpha$ and $^{14}C + \alpha$ reactions. Therefore, at the higher energies for which the projectile should penetrate the interior of the target, the hard core occurs in V_{opt}. This implies that a high-energy heavy-ion reaction should provide the information about the existence of such a hard core in the optical potential and about whether the projectile could penetrate the hard core region. However, as Vary (1977) has pointed out, when the relative momenta of the two ions is large, they are well-separated in momentum-space and can overlap in coordinate-space without violating the Pauli principle. Consequently, the Pauli effects which gave rise to the hard core in V_s may not be effective at high bombarding energies. Brink and Stancu (1975) and Flecker and Mosel (1977) also comment on this property of the Pauli corrections to the calculation of the heavy-ion potential.

There is one type of low-energy phenomena in which the hard core may have significant effect. The formation of the resonating molecular (compound) system predicted by Park, Scheid, and Greiner (1974) for $^{12}C + ^{12}C$ may be inhibited when the anti-symmetrization between clusters is properly included. This speculation has not been investigated further; Siemssen, et al. (1967) also comment on this possibility.

B. Comparison of Heavy-Ion Potentials with the Empirical Optical Potential

In this section the cluster potentials of Chapter IV and V are compared

with the real parts of optical potentials determined empirically and with the optical potentials calculated by other workers.

The first reaction considered here is $^{12}C + \alpha$; many experimental investigations of the elastic scattering of α-particles from ^{12}C have been made. For moderate energies (E/A $\leq$ 10 MeV), the depth of the real part of the empirical optical potential used to fit the data is around 100 MeV. The minima in V_A and V_s are -26 MeV and -15 MeV, respectively, with respect to the threshold energy. Figure 26 shows the real part of the Woods-Saxon potential used to fit elastic scattering data for α-particles incident on ^{12}C at E_{lab} = 139 MeV, obtained by S. Smith, et al. (1973). The depth of V_{real} is 108 MeV. The average value of the cluster potentials V_A and V_s are included for comparison. The average is obtained by setting f = 0.5 in Eq. (115) above; the Coulomb energy is removed from $(V_A + V_s)/2$ with the standard optical model Coulomb prescription:

$$V_c(R) = \begin{cases} \frac{Z_1 Z_2 e^2}{2R_c}\left(3 - \left(\frac{R}{R_c}\right)^2\right) & R \leq R_c \\ \frac{Z_1 Z_2 e^2}{R} & R \geq R_c \end{cases} \qquad (116)$$

where the Coulomb cut-off R_c is the usual value found in the optical model. The imaginary part of the optical potential used with the averaged cluster potential was taken to be of Woods-Saxon form. It is obvious from the figure that the extreme differences between the empirical potential and the averaged potential would cause a very poor fit to the scattering data when the averaged potential is used in an optical model calculation. Not only is the depth of the potential too small, but the cluster potential is much too diffuse as well.

The averaged cluster potential was used in an optical model code JUPITOR (written by T. Tamura and supplied to the author by W. J. Thompson) to produce the theoretical angular distribution shown as the solid curve in

Figure 27; the experimental data are represented by the dashed curve. The poor quality of the fit produced by the averaged potential is obvious; variations of the other parameters in the potential such as the depth and diffuseness of the imaginary Woods-Saxon well and Coulomb radius failed to improve the fit. The best value of the χ^2 per degree of freedom obtained was 1600. It is clear that a shallow potential of the form of the averaged cluster potential would not succeed in fitting experimental data for $^{12}C + \alpha$ in this energy region. No attempts to fit lower-energy data were made because the real part of the empirical optical potential is about 100 MeV deep in this regime.

The failure of the cluster potential as the real part of the optical potential for $^{12}C + \alpha$ suggests that one might encounter problems in fitting data for heavier systems. However, de Vries, et al. (1977) observe that there is a transition in the depth of V_{real} in going from light projectiles to heavier ones. Specifically, they notice that while a depth of 150 MeV is needed to fit elastic scattering data for $^{6}Li + ^{28}Si$ at 13 MeV, good fits for $^{12}C + ^{28}Si$ at 24 MeV are obtained for a depth of only 10 MeV. This suggests the possibility of fitting data for $^{12}C + ^{12}C$ and $^{16}O + ^{16}O$ using the shallow potentials obtained in earlier chapters. It should be noted that the depths of the imaginary wells used by de Vries, et al. were 30 MeV for $^{12}C + ^{28}Si$ and 44 MeV for $^{6}Li + ^{28}Si$.

The possibility of fitting elastic scattering data using the cluster potential for $^{12}C + ^{12}C$ was discussed in Section D of Chapter IV in connection with Satchler's empirically-determined potential. No further analysis of that system is made here. However, it is worthwhile to compare the potential for $^{16}O + ^{16}O$ with the potentials calculated by other workers who have used their potentials to fit elastic scattering data.

Figure 26. Comparison of the empirical Woods-Saxon real well used to fit the 139 MeV elastic scattering data for $^{12}C + \alpha$ with the optical potential extracted from the cluster potential.

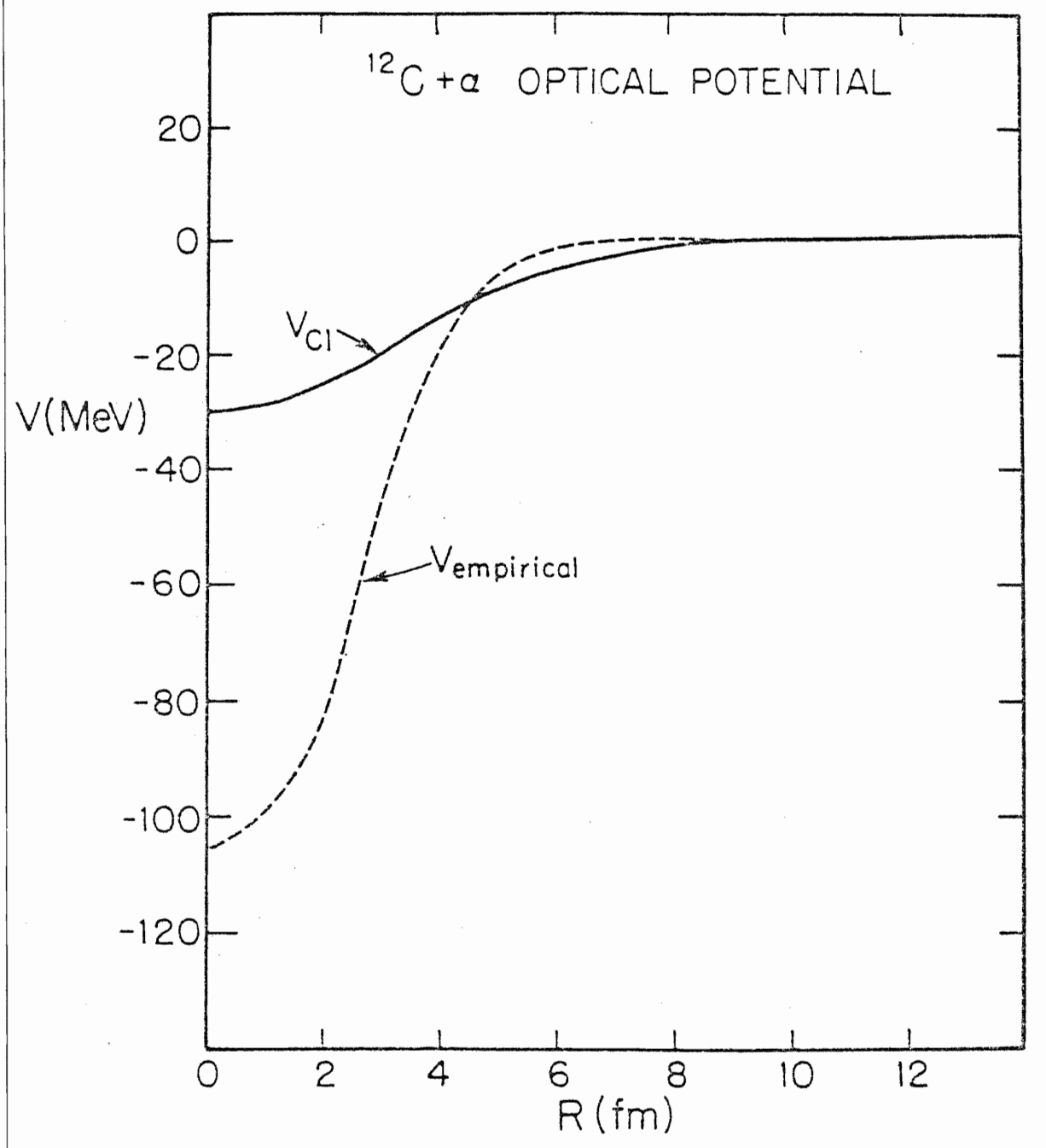
$^{12}C + \alpha$ OPTICAL POTENTIAL
20
0
-20
-40
-60
-80
-100
-120
V(MeV)
V_{C1}
$V_{empirical}$
0
2
4
6
8
10
12
R (fm)

Figure 27. Comparison of the theoretical angular distribution obtained using the averaged cluster potential for $^{12}C + \alpha$ with the experimental data (dashed curve).

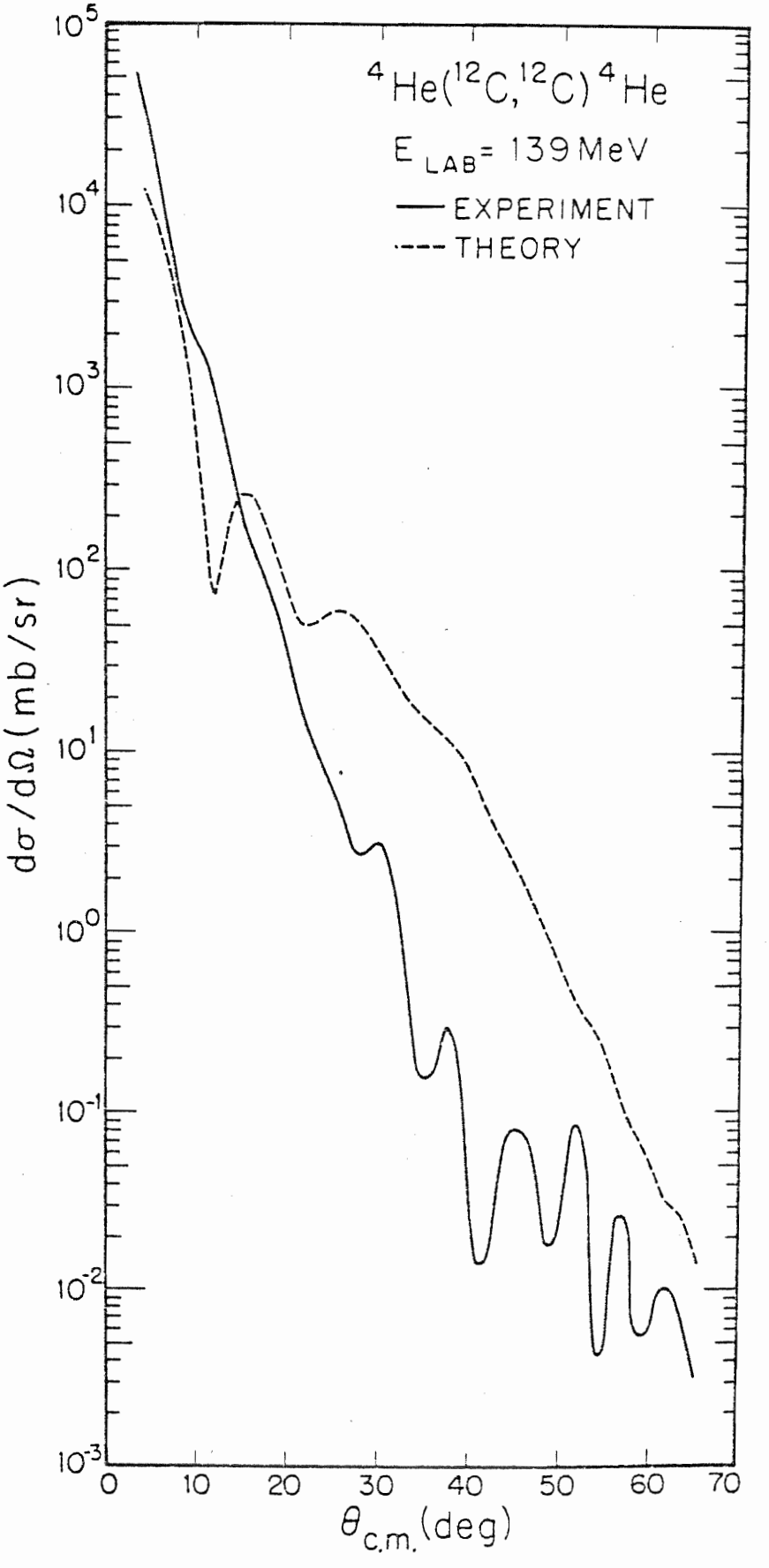
$^4He(^{12}C,^{12}C)^4He$
E_{LAB}= 139 MeV
EXPERIMENT
THEORY
$d\sigma/d\Omega$ (mb/sr)
$\theta_{c.m.}$ (deg)
10^5
10^4
10^3
10^2
10^1
10^0
10^{-1}
10^{-2}
10^{-3}
0
10
20
30
40
50
60
70

The most complete analysis of the low-energy elastic scattering data for $^{16}O + ^{16}O$ using a Woods-Saxon optical potential was made by Maher, et al. (1969). They found that a potential with a real depth of 17 MeV, energy-dependent imaginary depth $W_0 = 0.4$ MeV + 0.1 E_{cm}, radius R = 6.8 fm, and diffuseness a = 0.49 fm gave "surprisingly" good fits for $19 \leq E_{cm} \leq 22$ MeV. The shallow depth of the empirical real part of V_{opt} is encouraging because it is of the same magnitude as the depth of the adiabatic cluster potential of Figure 12.

While an analysis of the data of Maher, et al. was not attempted with V_A from Chapter IV, the work of Zint and Mosel indicates that V_A could be used to fit this data. Zint and Mosel have performed a Hartree-Fock calculation of the cluster potential for $^{16}O + ^{16}O$ using the Skyrme interaction. Their method is similar to that described in Chapter IV, including the use of a quadrupole constraint potential and the stabilization of the iterative scheme using averaged densities from one iteration to the next. Zint and Mosel correct the total energy for the spurious relative motion energy with the interpolation formula given in the summary at the end of Chapter IV. Their $^{16}O + ^{16}O$ cluster potential is quite similar to the adiabatic cluster potential in Figure 12; they have found a second minimum and a rather diffuse surface in their potential, just as in the present work. The threshold energy of V_A in Figure 12 is closer to the experimental value of $2 \times E_b^{exp}$ (^{16}O) than the value found by Zint and Mosel. However, the low value of their threshold energy has no effect on the depth of their extracted optical, taken relative to the threshold. Compared to the Zint and Mosel potential, V_A is too deep in the interior by about 10 MeV, due to the type of kinetic energy correction used here; therefore, the empirical interpolation they have used gives a better value for the minimum of the potential.

Zint and Mosel characterize the results of their optical model fits to the data of Maher, et al as "quite good agreement", where they have used their Hartree-Fock potential as the real part of V_{opt} and used the empirical imaginary form of Maher, et al. The peaks and valleys of the excitation functions which they calculate agree well both in position and magnitude with the experimental data.

The above discussion justifies the use of $V_A(R)$ for the $^{16}O + ^{16}O$ system as the real part of the optical potential. Maher, et al. have also performed a qualitative study of the effect of a repulsive core in the real part of the optical potential on the fit to the experimental excitation function. They found that a repulsive core must have a radius greater than $R_{core} = 1.3$ fm in order to affect this low-energy data. The hard core radius of V_s from Chapter IV was about 2 fm. It is possible then that the sudden potential should be included in V_{real} as in Eq. (115) above in order to fit the data. Goritz and Mosel (1976) and Block and Malik (1967) also obtain repulsive cores in their $^{16}O + ^{16}O$ potentials used in the optical model.

C. Deep vs. Shallow Potentials

For the heavier systems discussed above, the real part of the calculated and empirical optical potential was quite shallow in depth compared to the depths for light projectiles, estimated to be 50 x N MeV where N = number of nucleons in the projectile (Maher, et al., 1969). In contrast, recent additions to the literature on heavy-ion scattering have included calculations of much deeper V_{opt} using the folding method.

The motivation for the folding calculation is a desire to avoid the phenomenological lore required to fit experimental data with standard optical potentials. The folding model attempts to determine an optical potential for scattering of composite particles, utilizing the nucleon-nucleon interaction in a manner which may (one hopes) include many-body corrections (Dover and Vary, 1974). There are two types of folding models used in these calculations. The

first, known as the single folding model, folds the nucleon density of the projectile nucleus P with a nucleon-nucleus optical potential appropriate for the target nucleus A:

$$V_{fold}(r) = V_o \int \rho_P(r') V_{N-A}(\vec{r}-\vec{r}')\, d^3r' \qquad (117)$$

The second method involves convolving the densities of both target and projectile with some effective nucleon-nucleon interaction to obtain the double-folding potential:

$$V_{fold}(r) = V_o \int \rho_P(\vec{r}')\, \rho_A(\vec{r})\, V_{NN}(|\vec{r}-\vec{r}'|)\, d^3r' \qquad (118)$$

The nucleon-nucleon interaction is usually taken to be an effective two-body G-matrix (Dover and Vary, 1974).

Satchler (1975) presents a comparison of the single- and double-folding potentials for several heavy-ion reactions. He argues that the single folding model may over-estimate the depth of the optical potential by as much as a factor of two. Both of these folding models usually produce potentials which are too deep at the strong absorption radius (Zint and Mosel, 1976). Dover and Vary (1974) comment that the folding model is expected to be valid for high energies or for low densities. Therefore, while it is unfair to expect the folding model to succeed in fitting the low energy data of Maher, et al., the model should produce a satisfactory optical potential for reactions where only the surface region (low density) is important. Satchler (1976) reports that a folded potential with real depth of 530 MeV can fit elastic scattering data for $^{16}O + {}^{28}Si$ at E = 215 MeV, which were originally fit by a shallow potential with a real depth of 10 MeV. Satchler concludes that the set of data used in the two analyses is too restricted to allow a distinction between these two vastly different potentials. Other attempts to fit experimental data meet with varying degrees of success. (See Singh, Schwandt,

and Yang, (1975) and Buck, Dover, and Vary, (1975)).

Based on the discussion above and in the previous section, no clear choice between the folding method and the Hartree-Fock method of calculating the real part of the heavy-ion optical potential can be made; both methods are successful in predicting the scattering properties in some reactions. The comments of de Vries, et al. (1977) suggests that the Hartree-Fock approach should continue to be useful as experimental data for heavier systems becomes available. For lighter systems, the folding method provides good agreement with experiment, while the BHF attempts to fit $^{12}C + \alpha$ data were a complete failure. (It should be noted that the BHF method is doomed to failure for very light systems because the "cluster" potential for A + nucleon would be just the separation energy for removing one nucleon from the A + 1 system (Cusson, 1977).) The comparison between the folding method and potentials calculated in the BHF model or two-center shell model is further confused by the necessity of considering numerous corrections to the folding potential (Dover and Vary, 1974). Continued research efforts in both theoretical frameworks, as well as in the extension of experimental data to higher energies and heavier systems, are necessary to determine which approach to the calculation of the heavy-ion interaction is the correct one.

APPENDIX

The calculations discussed here are performed in the center-of-mass frame of the total system. Therefore,

$$\langle R_{cm} \rangle_{cm} \equiv 0, \tag{A.1}$$

and, furthermore,

$$\langle P_T \rangle_{cm} = 0 \tag{A.2}$$

The relation (A.2) is useful in the reduction of the total center-of-mass kinetic energy, T_{cm} into those terms which contribute to the present calculation of $H_{rel} = H_{TOT} - T_{CM}$. The total kinetic energy of the center of mass is

$$T_{cM} = \frac{1}{2mA} \left| \vec{P}_T \right|^2 \tag{A.3}$$

where

$$\vec{P}_T = \sum_{\lambda=1}^{A} \vec{P}_\lambda \tag{A.4}$$

From (A.4),

$$\left| \vec{P}_T \right|^2 = \sum_{\lambda=1}^{A} \vec{P}_\lambda^{\,*} \cdot \sum_{j=1}^{A} \vec{P}_j \tag{A.5}$$

or

$$\left| \vec{P}_T \right|^2 = \sum_{i,j=1}^{A} \vec{P}_i^{\,*} \cdot \vec{P}_j \tag{A.6}$$

The double sum in (A.6) can be split up as

$$\sum_{i,j=1}^{A} \vec{P}_i^{*} \cdot \vec{P}_j = \sum_{i=1}^{A} |\vec{P}_i|^2 + \sum_{i \neq j=1}^{A} \vec{P}_i^{*} \cdot \vec{P}_j \qquad (A.7)$$

$$= [|P_T|^2]_{1\text{-body}} + [|P_T|^2]_{2\text{-body}}$$

The two-body term can be further divided into direct and exchange parts:

$$[|P_T|^2]_{2\text{-body}} = [|P_T|^2]^{D}_{2\text{-body}} + [|P_T|^2]^{Ex}_{2\text{-body}} \qquad (A.8)$$

The form of the direct and exchange components of (A.8) is obtained by re-writing the two-body term as

$$\sum_{i \neq j=1}^{A} \vec{P}_i^{*} \cdot \vec{P}_j = 2 \sum_{abcd} [\langle ab|\vec{p}_1 \cdot \vec{p}_2|cd\rangle (\rho_{ac}\rho_{bd} - \rho_{ad}\rho_{bc})] \qquad (A.9)$$

This expression can be found in any treatment of many-body matrix elements (see, for example, Fetter and Walecka, 1971); the ρ_{ab} are two-body density matrix elements:

$$\rho_{ab} = \binom{N}{2} \int \Psi^{*}(r_1, r_2, \ldots, r_A) \Psi(r_1, r_2, r_A) (d^3r)' \qquad (A.10)$$

where the prime on the differential volume element excludes integration over the coordinates r_a and r_b. The minus sign in the second term in parentheses in (A.9) reflects the explicit inclusion of Pauli effects. The two-body term is then

$$[|P_T|^2]_{2\text{-body}} = 2 \sum_{abcd} \langle ab|\vec{p}_1 \cdot \vec{p}_2|cd\rangle \rho_{ac}\rho_{bd} \qquad (A.11)$$

$$- 2 \sum_{abcd} \langle ab|\vec{p}_1 \cdot \vec{p}_2|cd\rangle \rho_{ad}\rho_{bc}$$

The direct term is

$$\left[|P_T|^2\right]^{D}_{2\text{-body}} = 2\sum_{abcd} \langle ab|\vec{p}_1\cdot\vec{p}_2|cd\rangle \rho_{ac}\rho_{bd}$$

$$= \left(2\sum_{ac}\langle a|\vec{p}_1|c\rangle\rho_{ac}\right)\cdot\left(\sum_{bd}\langle b|\vec{p}_2|d\rangle\rho_{bd}\right) \quad (A.12)$$

$$= 2\langle\vec{P}_T\rangle\cdot\langle\vec{P}_T\rangle = 0$$

where (A.2) is used in the last step. The exchange term is:

$$\left[|P_T|^2\right]^{Ex}_{2\text{-body}} = -2\sum_{abcd}\langle ab|\vec{p}_1\cdot\vec{p}_2|cd\rangle\rho_{ad}\rho_{bc} \quad (A.13)$$

This term, usually estimated using a statistical argument, is neglected here. Therefore, the total kinetic energy of the center of mass is approximately

$$T_{cm} \simeq \frac{1}{2MA}\left[|P_T|^2\right]_{1\text{-body}} = \frac{1}{2MA}\sum_{i=1}^{A}|\vec{p}_i|^2 \quad (A.14)$$

The net kinetic energy appearing in the relative Hamiltonian is found from

$$H_{rel} = H_{TOT} - T_{cm}$$

$$= T + V - T_{cm}$$

$$\simeq \frac{1}{2M}\sum_{i=1}^{A}|\vec{p}_i|^2 + V - \frac{1}{2MA}\sum_{i=1}^{A}|\vec{p}_i|^2$$

so that

$$T_{Rel} \simeq \frac{1}{2M}\left(1-\frac{1}{A}\right)\sum_{i=1}^{A}|\vec{p}_i|^2 \quad (A.15)$$

LIST OF REFERENCES

H. A. Bethe, Phys. Rev. 103 (1956) 1353.

H. A. Bethe, Ann. Rev. Nucl. Sci. 21 (1971) 93.

B. Block and F. B. Malik, Phys. Rev. Lett. 191 (1967) 239.

B. H. Brandow, Lectures in Theoretical Physics, Boulder, Colorado, Vol. XIB, edited by W. E. Britten, et al. (Gordon and Breach, New York, 1969).

D. M. Brink and D. Vautherin, Phys. Rev. C5 (1972) 626.

D. M. Brink and Fl. Stancu, Nucl. Phys. A243 (1975) 175.

K. A. Brueckner, J. R. Buchler and M. M. Kelly, Phys. Rev. 173 (1968) 944.

B. Buck, C. B. Dover and J. P. Vary, Phys. Rev. C11 (1975) 1803.

R. Y. Cusson and H. C. Lee, Nucl. Phys. A211 (1973) 429.

R. Y. Cusson, R. A. Hilko and D. Kolb, Nucl. Phys. A270 (1976) 437.

R. Y. Cusson, private communication, 1976.

R. Y. Cusson, private communication, 1977.

C. B. Dover and J. P. Vary, Brookhaven preprint BNL-19332, 1974.

R. M. Dreizler, H. Galbraith and L. Lin, Nucl. Phys. A234 (1974) 253.

J. M. Eisenberg and W. Greiner, Nuclear Theory, Vol. I, (North-Holland, Amsterdam, 1970).

A. L. Fetter and J. D. Walecka, Quantum Theory of Many-Particle Systems, (McGraw-Hill, New York, 1971).

B. Fink and C. Toepffer, Phys. Lett. 45B (1973) 411.

J. Fleckner and U. Mosel, Nucl. Phys. A277 (1977) 170.

T. Fliessbach, Z. Phys. 247 (1971) 117.

V. Fock, Z. Phys. 61 (1930) 126.

G.-H. Goritz and U. Mosel, Z. Phys. A277 (1976) 243.

D. R. Hartree, Proc. Cambridge Phil. Soc. 24 (1928) 111.

Haxel, Jensen and Suess, Phys. Rev. 75 (1949) 1766.

P. E. Hodgson, Nuclear Reaction and Nuclear Structure (Clarendon Press, Oxford, 1971).

P. Hohenberg and W. Kohn, Phys. Rev. 136 (1964) 864.

H. S. Kohler, Phys. Rep. 18 (1975) 217.

D. Kolb and R. Y. Cusson, Z. Phys. 253 (1972) 282.

D. Kolb, R. Y. Cusson and M. Harvey, Nucl. Phys. A215 (1973) 1.

S. J. Krieger and C. Y. Wong, Phys. Rev. Lett. 28 (1972) 690.

H. C. Lee and R. Y. Cusson, Ann. Phys. 72 (1972) 353.

P. - O. Lowdin, Phys. Rev. 97 (1955) 1474.

J. V. Maher, et al., Phys. Rev. 188 (1969) 1665.

M. - G. Mayer, Phys. Rev. 74 (1948) 235.

M. Mayer and J. H. D. Jensen, Elementary Theory of the Nuclear Shell Model (John Wiley and Sons, Inc., New York, 1955).

H. Meldner, Phys. Rev. 178 (1969) 1815.

U. Mosel, Particles and Nuclei 3 (1972) 297.

U. Mosel and H. Schmitt, Phys. Rev. C4 (1971) 2185.

J.W. Negele and D. Vautherin, Phys. Rev. C5 (1972) 1472.

J. R. Nix, Los Alamos preprint LA-DC-72-769 (1972).

J. Park, W Scheid and W. Greiner, Phys. Rev. C10

K. Pruess and W. Greiner, Phys. Lett. 33B (1970) 197.

K. Sage and R. Y. Cusson, Bull. Am. Phys. Soc.(1976).

G. R. Satchler, Phys. Lett. 59B (1975) 121.

G. R. Satchler, invited paper presented at Symposium on Macroscopic Features of Heavy-Ion Collisions, Argonne, Ill. (1976).

R. H. Siemmsen, et al., Phys. Rev. Lett. 19 (1967) 369.

P. P. Singh, P. Schwandt and G. C. Yang, Phys. Lett. 59B (1975) 113.

T. H. R. Skyrme, Proc. Roy Soc. A, 230 (1955) 277.

T. H. R. Skyrme, Nucl. Phys. 9 (1959) 615.

J. C. Slater, Phys. Rev. 35 (1930) 210.

J. C. Slater, Quantum Mechanics of Molecules and Solids (McGraw-Hill, New York, 1963); Appendix 2.

S. M. Smith, et al. Nucl. Phys. A207 (1973) 273.

A. H. Stroudt and W. J. Secrest, Gaussian Quadrature Formulae (Prentice-Hall, New Jersey, 1968).

W. J. Swiatecki and S. Bjornholm, Phys. Rep. 4C (1972) 326.

H. Trivedi, Duke University Thesis, unpublished (1974).

J. P. Vary and C. B. Dover, Brookhaven preprint BNL-19360 (1974).

J. P. Vary, Comment at 1977 Washington APS meeting (1977).

D. Vautherin, Phys. Rev. C7 (1973) 296.

F. Villars, Nucl. Phys. A285 (1977) 269.

R. M. de Vries, et al., Phys. Rev. Lett. 39 (1977) 450.

L. Wilets, A. Goldberg and I. H. Lewis, Jr., Phys. Rev. C2 (1970) 1576.

P. G. Zint and U. Mosel, Phys. Lett. 58B (1975) 269.

P. G. Zint and U. Mosel, Phys. Rev. C14 (1976) 1488.

BIOGRAPHY

KEITH ALLEN SAGE

PERSONAL: Born August 15, 1950, Newport News, Virginia
Married

EDUCATION: B. S. (physics), Mississippi State University, 1972

POSITIONS: Teaching Assistant, Duke University, 1972-1973
Research Assistant, Duke University, 1973-1977
Research Associate, Catholic University of America, Washington, D. C. 1977-present
Physicist, Office of Marine Technology, National Oceanic and Atmospheric Administration, Riverdale, Maryland, March 1978-present

PROFESSIONAL AFFILIATIONS: American Physical Society
Phi Kappa Phi
Sigma Pi Sigma

PUBLICATIONS: Abstract, Bull. Am. Phys. Soc. 21 (1976) 512.

Abstract, Bull. Am. Phys. Soc. 21 (1976) 973.

Abstract, Bull. Am. Phys. Soc. 22 (1977) 644.

Abstract, J. Acous. Soc. Am. 63 (1978) S11.